UNCLASSIFIED

AD 411820

DEFENSE DOCUMENTATION CENTER

FOR

SCIENTIFIC AND TECHNICAL INFORMATION

CAMERON STATION, ALEXANDRIA, VIRGINIA

UNCLASSIFIED

NOTICE: When government or other drawings, specifications or other data are used for any purpose other than in connection with a definitely related government procurement operation, the U. S. Government thereby incurs no responsibility, nor any obligation whatsoever; and the fact that the Government may have formulated, furnished, or in any way supplied the said drawings, specifications, or other data is not to be regarded by implication or otherwise as in any manner licensing the holder or any other person or corporation, or conveying any rights or permission to manufacture, use or sell any patented invention that may in any way be related thereto.

CATALOGED BY DDC AS AD No. 411820

411820

AFCRL 63-439

ATMOSPHERIC INFRARED OPTICS - FLUX MEASUREMENTS

Merle J. Persky
Block Associates, Inc.
Cambridge, Massachusetts

Contract No. AF 19(628)-210
Research was sponsored by the
Advanced Research Projects Agency
under ARPA Order No. 30-61
and was monitored by AFCRL
Project 4904 Task 49048

FINAL REPORT

May 31, 1963

Prepared for

Air Force Cambridge Research Laboratories
Office of Aerospace Research
United States Air Force
Bedford, Massachusetts

DDC
RELEASED
AUG 6 1963
TISIA A

Block Associates, Inc.
CAMBRIDGE 39, MASSACHUSETTS

NO OTS

AFCRL 63 - 439

ATMOSPHERIC INFRARED OPTICS - FLUX MEASUREMENTS

Merle J. Persky

Block Associates, Inc.
Cambridge, Massachusetts

Contract No.: AF 19(628)-210
Research was sponsored by the
Advanced Research Projects Agency
under ARPA order No. 30-61
and was monitored by AFCRL
Project 4904 Task 49048

FINAL REPORT
May 31, 1963

Prepared for
Air Force Cambridge Research Laboratories
Office of Aerospace Research
United States Air Force
Bedford, Massachusetts

Acknowledgements

The author takes this opportunity to thank Mr. Charles Price and Mr. Leonard Epstein of Northeastern University for the preparation and field service of the telemetry system and gondola used for flight No. 2, and Professors J. Wiren and G. Bartlett, also of Northeastern University, for their aid in reducing the telemetry data for both flights No. 1 and No. 2. In addition, the valuable contributions of Messrs. Karl M. Hergenrother, Alex S. Zachor, and Isaiah Coleman of Block Engineering, Inc., Dr. Andrew Drummond of the Eppley Laboratory, Inc., and Mr. David Murcray of the University of Denver are gratefully acknowledged.

Abstract

The preparation and evaluation of two infrared interferometer spectrometers, Block Associates, Inc., Models I4T and I4TC for the balloon-borne measurement of atmospheric radiance is described.

The flights of 5 April, 1962 and 2 August, 1962 showed agreement with the theoretical data computed from the available temperature, pressure and dewpoint profiles. Auxiliary systems were built, tested and flown in these flights. Comparison spectral runs and evaluations were conducted with independent laboratories. A procedure for calibration was developed and an evaluation of the precision and accuracy of the instrument was undertaken.

Several possible improvements for future measurement programs were evaluated and proposed recommendations are included.

TABLE OF CONTENTS

LIST OF FIGURES

LIST OF SYMBOLS

Symbol	Quantity	Units
λ	wavelength	micron
ν	wavenumber	reciprocal centimeter
f	frequency	cycles per second
B	retardation	micron
x	mirror displacement	micron
T	scan time or	second
T	temperature	degrees Kelvin
γ	solid angle	steradian
p	playback to record ratio	dimensionless
R_ν	spectral radiance	millivolt per microwatt/cm^2-ster-cm^{-1}
V_S	output signal	millivolt
$V_{1\nu}$	output signal corrected for noise at wavelength, ν	millivolt
V_N	noise signal	millivolt
$N_{\nu B}$	detector radiance at wavelength, ν	microwatt/cm^2-ster-cm^{-1}
$N_{\nu S}$	source radiance at wavelength, ν	microwatt/cm^2-ster-cm^{-1}
$\Delta\nu$	resolution	reciprocal centimeter
$\Delta\lambda$	resolution	micron
ϵ	emissivity	dimensionless
α	absorptivity	dimensionless
τ	transmissivity	dimensionless
w	optical mass	centimeter
p	mean pressure	millimeters of mercury
h	altitude	feet
k_λ	absorption coefficient	per centimeter
T_E	earth temperature	degrees Kelvin
T_i	temperature of the i^{th} layer	degrees Kelvin

LIST OF SYMBOLS (CONTINUED)

Symbol	Quantity	Units
P_o	air pressure at sea level	millimeters of mercury
T_o	air temperature at sea level	degrees Kelvin
h_o	observer altitude	feet
ρ_{H_2O}	partial density of water vapor	grams per cubic meter
N_{BB}	black-body radiance	microwatt/cm^2-ster-μ
δ	small value of transmissivity	dimensionless
U	signal - mea red on graphic recorder	units
U_N	noise - measured on graphic recorder	units
$U_{G.O.}$	gain oscillator - measured on graphic recorder	units per millivolt

1.0 Purpose of Contract

This contract was for the study, calibration, and immediate use of Block Associates, Inc. interferometer spectrometers (Model I-4T for the spectral range 1.5 to 15 microns and Model I-4TC for the range 4 to 40 microns) for measurement of the upward and downward radiance of the atmosphere as a function of altitude. Experiments were both ground-based and balloon-borne. From the latter, data was obtained of the flux intensity in the atmosphere from both the nadir and the zenith at altitudes varying approximately from sea level to 55,000 feet. From the experience gained in working with interferometer spectrometers, information on stability, accuracy of radiance measurements, resolution of the spectrum, adequacy of the supporting electronic devices, and the most efficient methods of data reduction were obtained. The interferometer spectrometers were made available for calibration and comparisons both to Block Associates and also to outside groups.

The instruments themselves were provided as Government furnished equipment.

This work continues the extensive Air Force supported interferometer spectrometer development effort. It is expected that two significant "firsts", as far as this type of spectrometer is concerned, will be accomplished as a result of this contract; first, the use of the interferometer for making highly accurate radiance measurements as contrasts with simply identifying emission lines, and second, the use of the instrument in a hostile balloon-borne environment far different from that of the ordinary scientific laboratory.

In addition, the use of the interferometer for balloon-borne atmospheric radiance measurements will produce data covering a

much smaller altitude increment than has been possible in the past, this due to the extremely fast sampling rate. Also, its sensitivity advantage over conventional spectrometers makes possible the measurement of very small radiance increments.

For the purpose of this report the work performed under the contract was divided into six sections.

Section 2 discusses the theory of operation of the interferometer and discusses its advantages over conventional prism or grating spectrometers. Also included is a history of the development of this unique type of spectrometer.

Section 3 describes the auxiliary systems designed and constructed to aid the interferometer in fulfilling the objectives of the balloon borne experiments. In addition, recommendations are made toward improving the instrumentation for future flights.

Section 4 discusses the environmental test program conducted to aid in modifying the interferometers for the balloon flights.

Sections 5 and 6 describe the extensive calibrations conducted, both in-house as well as in conjunction with the Eppley Laboratory, Inc. and the University of Denver.

Section 7 details the two balloon flights themselves and presents the atmospheric data obtained as well as a discussion of the results. The instrumentation for the first flight on April 5, 1962 consisted of the Block Associates I4T interferometer spectrometer, a Perkin-Elmer Model 21 spectrometer operated by the University of Denver and four experimental frost-point hygrometers supplied by Minneapolis-Honeywell. The gondola, telemetry

oscillators and transmitter as well as common battery power supply were also furnished by the University of Denver.

Flight number two on August 2, 1962 utilized both the I4T and I4TC spectrometers as well as improved versions of the frost-point hygrometers flown earlier. For this flight the telemetry system was furnished and operated by personnel from Northeastern University who also fabricated the gondola.

2.0 Description of Interferometer Spectrometer

2.1 Theory of Operation

2.1.1 Introduction

The interferometer spectrometer differs from the more well known prism and grating spectrometers in the manner in which the incident radiation is separated into its component wavelengths.

Both prism and grating spectrometers contain three basic elements: a slit; a dispersing device (prism or diffraction grating) which separates radiation according to wavelength; and a suitable optical system to produce the spectrum lines, which are monochromatic images of the slit.

Interference spectroscopy, on the other hand, uses the principle of constructive and destructive interference of light waves.

The two sections following (Sections 2.1.2 and 2.1.3) discuss the theory of operation of the interferometer so that the development effort under this contract may be better understood.

2.1.2 General Description of System

Figure 1 is a block diagram of the electronic chassis and optical head of the Model I4T Interferometer Spectrometer. The electronics can be divided into three sub-groups: the input regulator and plus and minus 12 volt regulator; the transducer sweep generator and drive amplifier; and the post amplifier. The optical head consists of the optical cube with its associated lenses, mirrors, beamsplitter, and detector together with the preamplifier and detector bias supply.

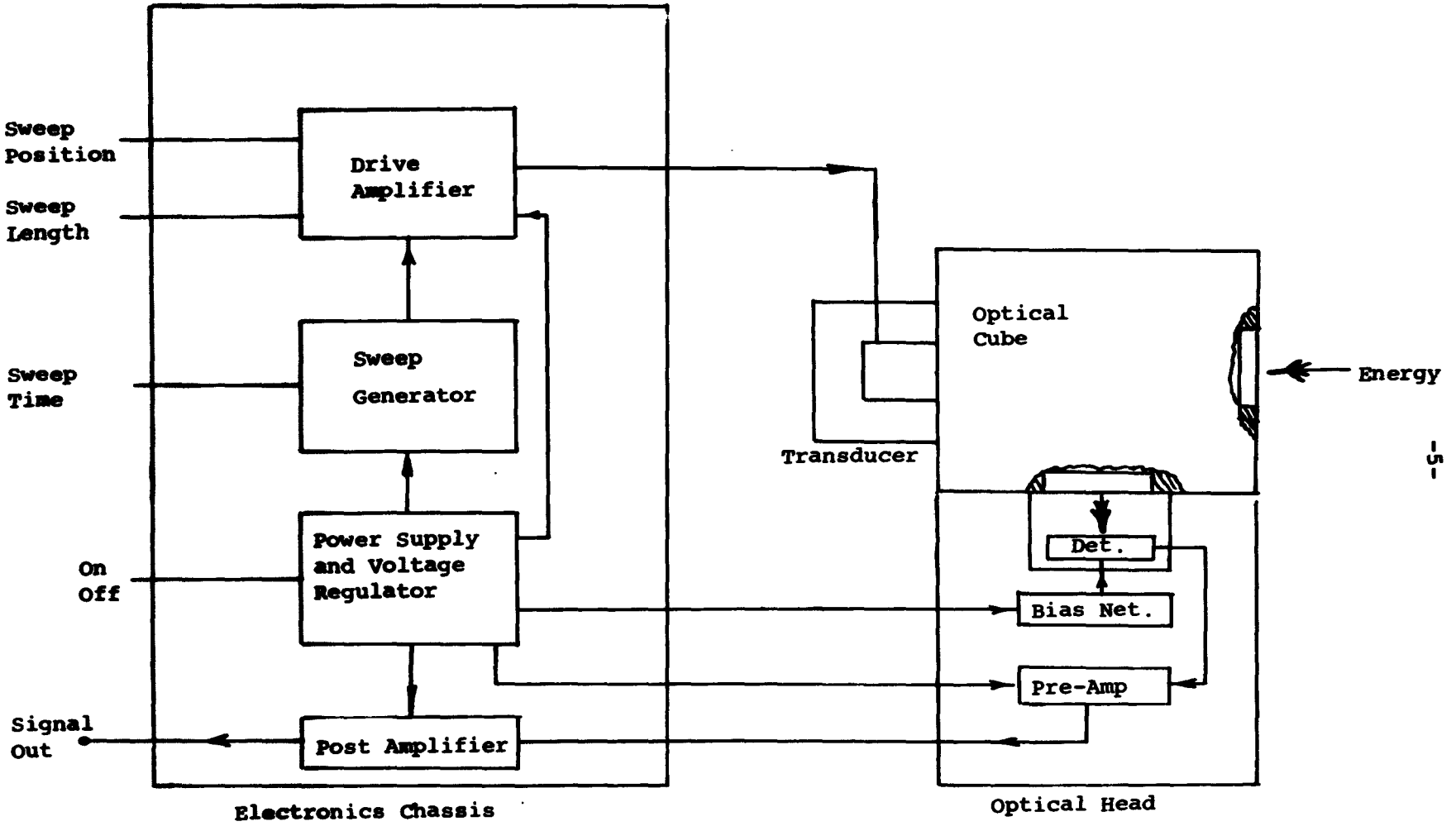

Figure 1.
I4 Block Diagram.

The function of the optical cube is to heterodyne the extremely high infrared frequencies down to audio frequencies for which detectors are available. These audio frequencies are an exact analog of the original light frequencies since the frequency transformation which takes place is linear. The audio frequency spectrum, having been tape recorded, is played back into a narrow-band variable-frequency bandpass filter which is slowly tuned over the appropriate audio frequency range. The result is a record of the amount of energy at each frequency. This data reduction process in effect accomplishes the Fourier transform of the original light spectrum into the amplitude-frequency domain.

2.1.3 Detailed Theory

The interferometer spectrometer built by Block Associates, Inc. utilizes the Michelson optical system. (Optical ray traces are shown in Figure 2). S is a semi-reflective mirror (called a beamsplitter) which reflects 50% of the light which strikes it and permits the other 50% to pass. M_1 and M_2 are mirrors which reflect all the light which reaches them; they are identical except that M_1 can be displaced distance Δx.

If a light beam enters as shown, 50% of it will pass through the beamsplitter and continue toward M_1 while the other 50% will be reflected toward M_2. Upon reaching mirrors M_1 and M_2, each fractional half of the original energy will be completely reflected back toward the beamsplitter. Upon striking the beamsplitter the portion of the light transmitted to the detector and the portion of the light lost from the interferometer depend on the relative phases of the recombined rays in the exit and detector legs of the interferometer. For example, let us determine these phases for the case where the optical distances in legs M_1 and M_2 are equal and

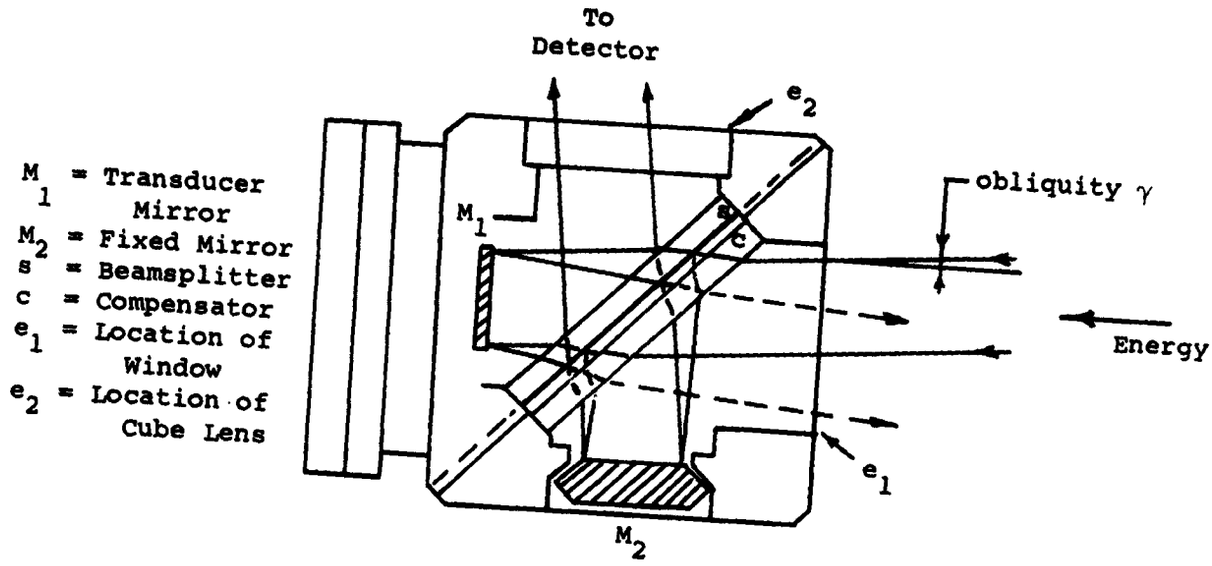

Figure 2a.
Path of an Oblique
Parallel Bundle.

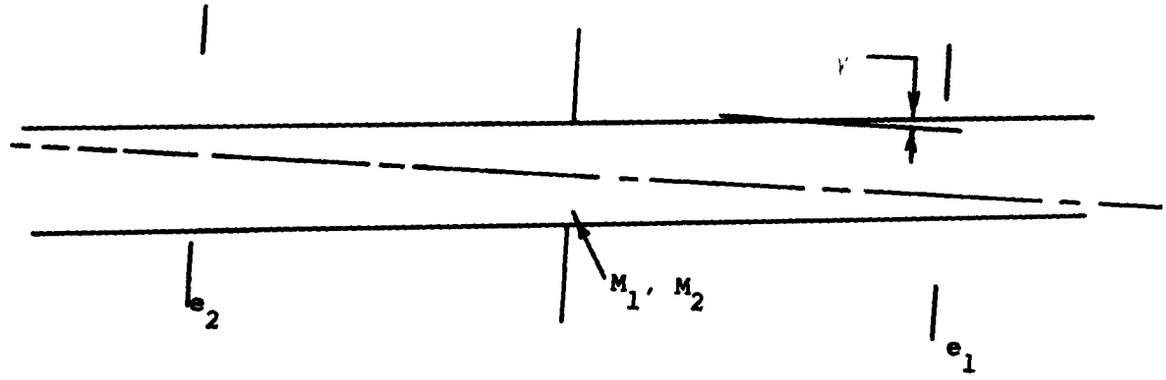

Figure 2b.
Optical Equivalent
to Show Ray Paths.

the splitter is an ideal metal film. When the beam encounters the metal splitter, the reflected ray to leg M_2 is shifted π and the transmitted beam to leg M_1 by $\pi/2$. When the beams return to the splitters, if the light is to be transmitted to the detector, the ray from leg M_2 is transmitted with a shift of $\pi/2$ and the ray from leg M_1 is reflected with a shift of π. The sums of the phase shifts of the rays in both legs are $3\pi/2$ and being equal the waves reinforce each other. On the other hand, the exit ray from the spectrometer requires the ray from leg M_2 to be reflected again with a shift of π and the ray from leg M_1 to be transmitted with a shift of $\pi/2$. The sum of the phase shifts in leg M_2 is 2π and in leg M_1 is π. Since the rays in this case differ in phase by a factor of π, there is destructive interference. The result of this is that all the light entering the spectrometer at zero retardation is transmitted to the detector, thus producing a bright central fringe.

This explanation is somewhat simplified since it does not account for effects such as absorption, but the same general argument holds in a more rigorous treatment. The same treatment is also valid for Michelson interferometers which use dielectric beamsplitters, e.g., a thin germanium film, except that the phase changes are different with the result that the central fringe is black.

In the I4T the beamsplitter's semi-reflective coating is deposited on a sodium chloride plate (cesium iodide is used for the I4TC), which means that a ray traveling the M_1 leg would pass through the plate 3 times while the one traversing leg M_2 would pass through it only once. Because the sodium chloride has dispersion, a compensator plate, c, is needed to insure symmetry (equal optical path length) of the M_2 and M_1 legs.

As we have just seen, when the optical path lengths of the

M_1 leg and the M_2 leg are equal, all of the original light energy which reaches the detector via route M_1 is in phase with that arriving via route M_2. If, however, we cause the M_1 mirror to be displaced an amount Δx, we find that the phase of the light arriving at the detector via route M_1 is retarded by an amount $2\ \Delta x$ from that arriving via route M_2. For monochromatic light of wavelength λ, a displacement $\Delta x = \lambda/4$ will cause a retardation of $2x = 2\lambda/4 = \lambda/2$. The two equal amplitude light fractions will therefore reach the detector 180° out of phase, cancellation will result, and the net signal to the detector will be zero. Detector signal will in fact be zero for all displacements, Δx, which are odd multiples of $\lambda/4$ ($\pm\ \lambda/4$, $\pm\ 3\ \lambda/4$, $\pm\ 5\ \lambda/4$, etc.) and will be equal to the total input energy (minus absorptions) for all even multiples of $\lambda/4$ beginning with zero (0, $\pm\ \lambda/2$, $\pm\ \lambda$, $\pm\ 3/2\lambda$, $\pm\ 2\lambda$, etc.), where the plus and minus signs denote displacements on both sides of zero retardation corresponding to increased or decreased optical path lengths (retardations) respectively.

If the displacement of mirror M_1 is slowly changed, we find that the energy at the detector goes through a series of maxima and minima (light and dark "fringes") as the retardation of the optical path lengths of the two legs differs by integral numbers of wavelengths, according to the expression

$$I = 0.5\ I_o\ (1 + \cos\ 2\pi\ \nu\ Bt/T) \qquad (1)$$

where ν is the wavenumber of the incident radiation in cm^{-1}, and $Bt/2T$ is the instantaneous displacement, x, of the mirror moving a distance $B/2$ in time T. In other words, the frequency of the energy transmitted to the detector is a joint function of the wavenumber of the input radiation and the mirror velocity $B/2T$.

Since the optical retardation, B, is twice the mirror displacement, then,

$$f = 2 \cdot \nu \cdot \frac{B}{2T} = \nu \cdot \frac{B}{T} \qquad (2)$$

Increased mirror velocity yields higher output frequencies.

In the actual I4, the movable mirror is mounted on the armature of an electromagnet and is displaced by changing the d.c. current through the armature. Figure 3a is a plot of the mirror position in time showing the linear mirror displacement.

Clearly, the audio frequency range to which the incident radiation is heterodyned can be changed by varying the sweep rate. For instance, if T is halved while B is kept the same, the resulting audio frequency (for a given monochromatic input) will double. Also, if two (or more) light frequencies are present in the input radiation, there will be corresponding audio frequencies present in the audio output spectrum. The capability of a practical instrument to resolve two neighboring frequencies is specified in terms of the smallest increment of wavelength, $\Delta\lambda$, which can be distinguished at the output (or alternatively, in terms of wavenumber, $\Delta\nu$).

T = Sweep Time

F = Flyback Time

R = Recovery Time

B = Excursion

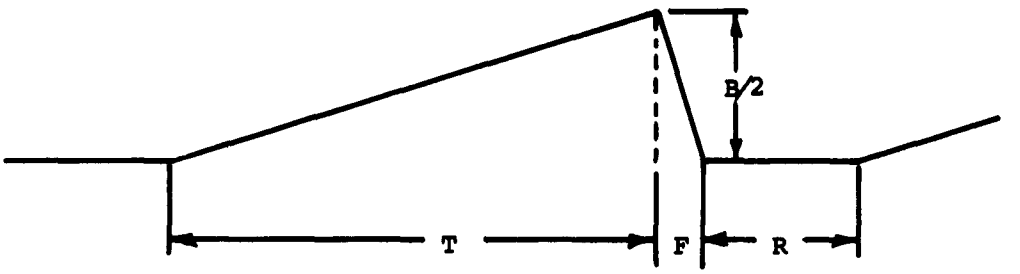

Figure 3a.
Mirror Motion.

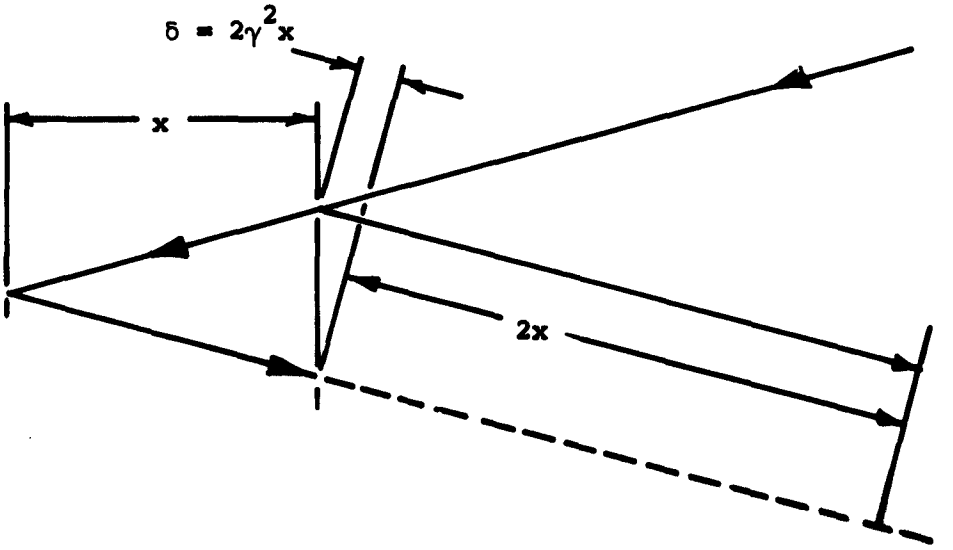

Figure 3b.
Additional Retardation, δ,
Due to Obliquity, γ.

2.2 Instrument Parameters

Before discussing the factors which affect instrument resolution, sensitivity, and field of view, which are all strongly interdependent, it is advisable to speak briefly of the instrument's spectral range. Spectral range is determined by the choice of detector and beamsplitter material which, though they have a tenuous influence on the other parameters, can for our purposes be considered independent of them. The main determinant of spectral range is, of course, the type of detector. However, as mentioned above, the beamsplitter significantly affects the light passing through it, not only by absorption (amplitude effects) but by phase shifts (phase changes), both of which are different for different frequencies.

Spectral resolution ($\Delta\nu/\nu$ or $\Delta\lambda/\lambda$) is a function of three instrument parameters.

a. Linearity of mirror displacement;

b. The solid angle of the energy entering the instrument. (Related to field of view, larger solid angle reduces resolution but increases sensitivity, S/N);

c. Retardation interval (the difference in optical path length of the two legs, $2\Delta x$ or twice the distance B in Equation 1). Larger retardation produces finer resolution.

The easiest of these three factors to understand is the linear velocity requirement of the moving mirror. Clearly, in the light of the $f = \nu B/T$ relationship, a 10 per cent error in mirror velocity will cause a 10% error in the audio output frequencies.

The influence on resolution of the size of the solid angle of the field of view can be understood with the aid of Figure 3b.

As illustrated by the figure, the retardation for a ray entering at a small oblique angle, γ, will be increased (to a first approximation) by $2\gamma^2 x$ over the 2x retardation experienced by a ray entering along the optical axis. If now we imagine an extended monochromatic source large enough to fill the field of view of the instrument however large its angular field of view, it is plain that as γ is increased the radiation contributed by the peripheral region of the field will give rise to output frequencies which deviate substantially from the desired audio frequency (corresponding to the axial ray).

Since field of view to a great extent determines instrument sensitivity, one of the important choices that must be made in the design of an interferometer spectrometer is the trade-off between sensitivity and resolution.

It should be apparent that the degree to which the $2\gamma^2 x$ factor changes the instrument's optical path length will be a constant per cent of the nominal axial path length and independent of frequency. However, the amount of the resulting retardation (frequency) error will be more significant at higher frequencies since a 1% error at say, $\lambda = 8\mu$ is half that at $\lambda = 4\mu$ when expressed in cps.

It is beyond the scope of this report to explain in detail how increasing retardation interval improves resolution. A precise understanding involves the limits of integration of the Fourier integral,

$$F(f) = \int_{-\infty}^{\infty} g(t)\, e^{-i2\pi ft} dt$$

the physical significance of which is associated with the heterodyning operation of the interferometer's moving mirror. In

practice, the validity of the above mathematical expression is circumscribed by the impossibility of realizing physically a mirror drive which will provide an infinite ($-\infty$ to $+\infty$) excursion. Other practical considerations also intervene to restrict the transducer excursion to about 250 microns. It can be shown that the limit of spectral resolution is a constant dependent only on the maximum retardation interval, B, according to

$$\Delta\nu = k/B$$

where k is determined by the amount of refraction at the entrance aperture.

For our instrument, k = 1, approximately, and B = 500 microns so that

$$\Delta\nu = 1/500\mu = 20 \text{ cm}^{-1}$$

In practice, it is just possible to distinguish a dip in the reduced spectrum of about twice this, or $\Delta\nu = 2/B = 40 \text{ cm}^{-1}$.

The frequency resolution required of the spectrum analyzer used in data reduction is given by $\Delta f = \Delta\nu \, B/T = 1.25$ cps. However, it is possible to play the tape recorded data back at some multiple (say four) of the record frequency to match the pass band required to that of the spectrum analyzer used during data reduction, i.e. 4 x 1.25 cps = 5 cps. Otherwise, the resolution limit of the system would be set during data reduction by the excessively wide pass band of the analyzer and information would be lost.

2.3 History of Development and Application of Interferometer Spectrometer.

The rapid advances in development of a practical interferometer spectrometer system are, to a great extent, due to support given this work by a number of Government agencies such as the Geophysics Research Directorate of Air Force Cambridge Research Laboratories, the Jet Propulsion Laboratory, the Naval Ordnance Test Station, and the Army Chemical Center. In addition, continued interest in interferometer spectrometers has encouraged us to continue developments using company funds.

Following Mertz's invention and development of rapid scan interference spectroscopy and its analog transform technique, support was received from the Geophysics Research Directorate of Air Force Cambridge Research Laboratories (under Advanced Research Projects Agency) for applying this basic design to a balloon-borne spectrometer. This work resulted in an instrument known as "Ursa Minor" and was reported in the final report of Contract No. AF 19(604)-2420 (GRD-TR-60-294-4). Additional applications of the interferometer spectrometer to various ground-based field measurements were supported on several AFCRL contracts, including AF 19(604)-7267 and AF 19(604)-7309.

Development of the interferometer spectrometer for space applications was supported under two Jet Propulsion Laboratory contracts for a Mars probe instrument and later under two JPL-sponsored contracts from Texaco Experiment, Inc., for the Surveyor lunar landing program. The application of the interferometer spectrometers to rocket-borne probes to measure target and background radiation was supported by the Naval Ordnance Test Station under ARPA sponsorship.

A contract from Melpar, Inc., under sponsorship of the Army Chemical Center supported development of the interferometer spectrometer for field use in detection of chemical warfare agents.

In addition to the above Government-supported developments of the interferometer spectrometer for various applications, company-sponsored developments continued to improve the reliability, stability, and linearity of the basic elements of the interferometer such as the interferometer construction, the drive mechanism, and certain of the electronic circuits. The results of this work produced off-the-shelf instruments which are available to AFCRL for air-borne measurement programs as well as to other Government agencies such as White Sands Missile Range for range instrumentation.

Thus, it can be seen that the interferometer spectrometer which was used for the measurements described in this report evolved from a variety of developments.

2.4 Data Reduction System

Since the output of the interferometer is in the form of acoustical frequencies, it can conveniently be stored as well as processed using conventional acoustical frequency equipment. For our purposes the interferograms are recorded on magnetic tape using a Magnecord 728 tape recorder. Once the data is recorded on tape the inverse Fourier transform can be taken by means of a Hewlett Packard 302A Wave Analyzer. The output of the wave analyzer is a d.c. level proportional to the amplitude of each of the individual frequencies produced by the interferometer. This d.c. output is recorded on a Varian G-10 graphic recorder.

As can be seen in Figure 4 the frequency selector dial on the wave analyzer is mechanically linked by a chain drive to the paper drive on the Varian. Thus the abscissa on the Varian chart is proportional to electrical frequency while the ordinate is proportional to the amplitude at each frequency. The frequency versus displacement relationship is determined by the ratio of sprocket teeth on the selector dial to the number of teeth on the paper drive bar. In addition, the wave analyzer produces a narrow band signal at zero frequency for reference.

The spectrum to be investigated is recorded on a tape loop whose length is a function of interferogram repetition rate and tape recorder speed. However, in taking the inverse transform the wave analyzer averages the energy in each frequency over all the interferograms on the loop; thus, for the case where the source is not constant, for example, the atmosphere as seen from an ascending balloon, it is desirable to keep the number of interferograms on a loop to a minimum. An additional factor to be

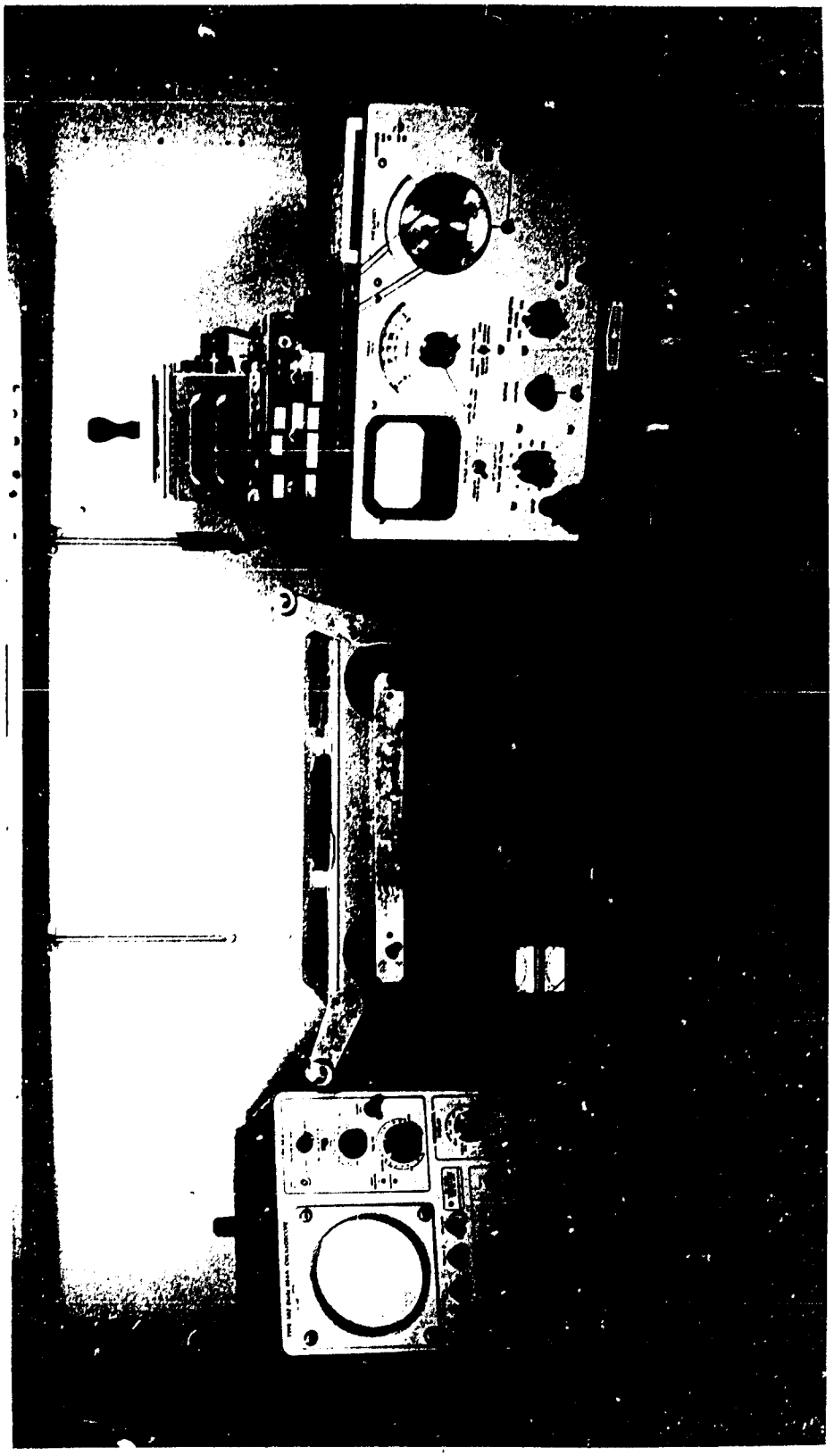

Figure 4.
Data Reduction System.

considered is the fact that since the signal-to-noise ratio of a bit of information increases as the square root of the sampling time, it would be advantageous from the standpoint of the wave analyzer to have a large number of interferograms on a loop. Thus, the number of interferograms recorded is a compromise between these two factors. In order to insure that the spectra will not suffer any loss in resolution, all of the parameters of the data reduction system, tape speed, Varian chart speed, analyzer band width, and Varian time constant are made compatible not only with each other but more importantly with the spectral resolution element of the interferometer.

Although the system in general proved satisfactory, it became evident that it had several limitations. First of all, because of the many possible gain adjustments in the system, it was necessary to superimpose a reference frequency on top of the interferogram and it was necessary to use this signal for every spectrum reduced. Second, great care had to be taken in operating the tape recorder in order to prevent excessive noise from appearing on the reduced spectrum. Third, the speed of the Varian is such that it takes approximately 15 minutes for the wave analyzer to make a complete frequency scan and, thus, the reduction of many spectra takes a relatively large amount of time. And, finally, in order to convert the Varian data into the form of energy versus wavelength, it is necessary to perform six mathematical calculations by hand. For these reasons, it became readily apparent during the course of the program that the data reduction process was a severe limit as far as achieving a high degree of accuracy and precision.

2.5 Computer Adapted Reduction System

Because of the limitations of the tape recorder-wave analyzer-Varian system, an investigation was made into the possible use of high speed computers with the thought that all of the mathematical computations done by hand could be done with much greater speed and accuracy. Figure 5 shows a block diagram of a computer adapted reduction system arrived at after consultation with a data reduction group at Northeastern University as well as several Air Force Cambridge Research Laboratory personnel who were concerned with the same problem.

It should be noted that this system could also be used for reducing the spectral responsivity data during the calibration phase.

It is conceivable that using the system shown in Figure 5 the accuracy of the balloon flight data could be improved to the 1% to 2% limit imposed by the accuracy and repeatability of the FM/FM telemetry system.

Since the cost of writing a computer program is quite high it would be efficient from a cost standpoint to use the system only when two or more flights are planned.

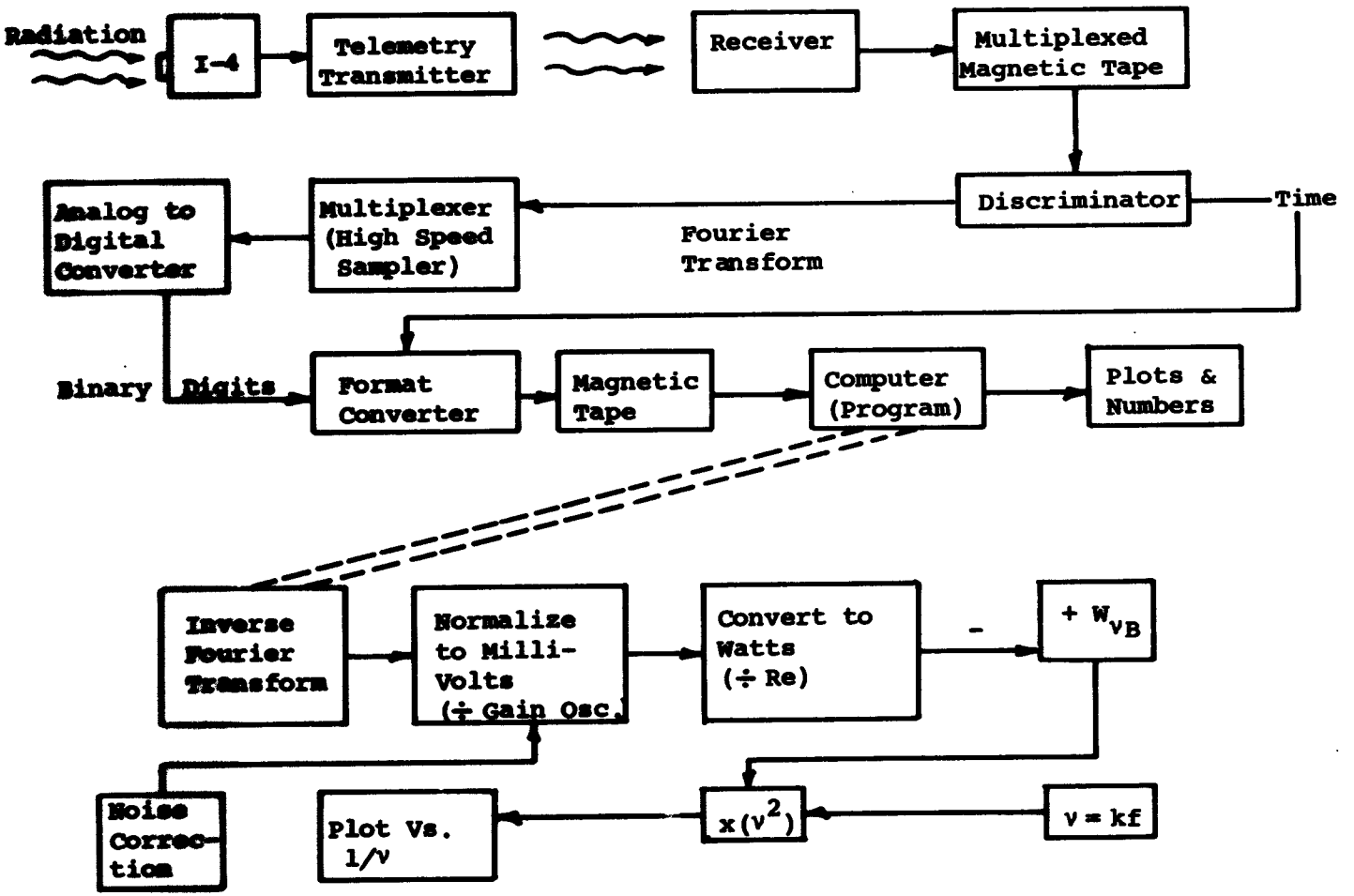

Figure 5. Block Diagram of Computer Adapted Reduction System

3.0 Auxiliary Engineering Systems

3.1 Function of Auxiliary Engineering Systems

The purpose of the two balloon flights was to obtain data on the upward and downward atmospheric radiance as a function of altitude. In order to validate this data it was deemed advisable to monitor the significant supply voltages and component temperatures. This required the design and construction of a motor driven commutator and 26 volt, 400 cps motor power supply for both the I4T and I4TC.

The most important temperature monitored is that of the thermistor bolometer detector. Since the output of the instrument is proportional to the difference in radiance between the source and the detector it is important that the detector temperature be known accurately.

Other temperatures monitored were those of the electronic components and systems where a change in temperature would affect the proper performance of the amplifiers, thus changing the spectral radiance calibration. In addition, during flight #2, the temperature of the electronics chassis and the temperature of the flight box in which it was mounted were monitored in order to make some measure of the overall heat transfer characteristics of the system.

The supply voltages monitored were: battery voltage input to each instrument, +12 volt regulated supply and, -12 volt regulated supply, the latter two being produced by the interferometers themselves.

During flight #1, the 28 volt power required for the I4T was a battery supply furnished by the University of Denver, the same

battery pack that supplied current to all the other systems on board, including the telemetry system, University of Denver spectrometer and Minneapolis-Honeywell frost-point hygrometers. For the second flight separate battery packs were used for each experiment, that is, the telemetry system and the hygrometers each had batteries of their own while three battery packs were used for each of the two interferometers - one supplied power to the interferometer, one to the motor power supply and the third was used for the heating system.

Because both the I4T and I4TC work in a spectral region longer than four microns it was necessary to thermostat the optical heads. This is because the output signal at any wavelength is a function of the difference in radiance between the unknown source and the detector and for wavelengths longer than four microns the blackbody radiance of a detector at room temperature is quite significant. Thus, it is essential to monitor detector temperature. In addition, by maintaining the temperature constant throughout the flight, we can greatly simplify the data reduction process.

For the objectives of flight #2 it was necessary to design and build a system whereby the I4T could look alternately down at the nadir and as close to the zenith as the balloon would allow. The system consists of a mirror which is oscillated from one position to the other by means of a motor driven, Geneva activated gear system, the power for the motor coming from the same motor power supply used for the commutator motor.

In order to make accurate amplitude measurements possible it was necessary to provide a constant, repeatable, reference signal which could be used to correlated the output signals obtained during the flight with the signals produced while looking at known sources

during calibration. The problem here is that the devices which handle the data from the instrument, that is the telemetry system, the tape recorder, wave analyzer and Varian, all have gain adjustments, so the amplitude of the signal in terms of absolute values could be quite arbitrary. However, by superimposing a high frequency electrical signal or so-called gain oscillator on top of the electrical signal from the detector, any gain adjustments which would be applied to the spectral data would also affect the signal from the reference source and, therefore, would be cancelled out.

As a check on the performance of the entire system during the flight a small in-flight blackbody calibration source was used. The radiation from this source, which was periodically inserted into the field of view, follows the same optical and electrical path as does the unknown spectrum.

As a further check on the proper operation of the instrument during flight #2 the output of the sawtooth sweep generator which drives the moving mirror in the optical cube was monitored via a separate telemetry channel.

Figure 6 shows in block diagram form the various elements in the I4 spectrometer system as modified for the balloon flight. Not shown is the alternate-view mechanism used by the I4T during flight No. 2.

The other auxiliary engineering systems necessary to fu fill the objectives of the contract included flight boxes in whic the various systems mentioned above were contained (See Fig. 7), the telemetry system, and the gondola. The flight boxes were designed based on the information gathered during several environmental tests (See Section 4).

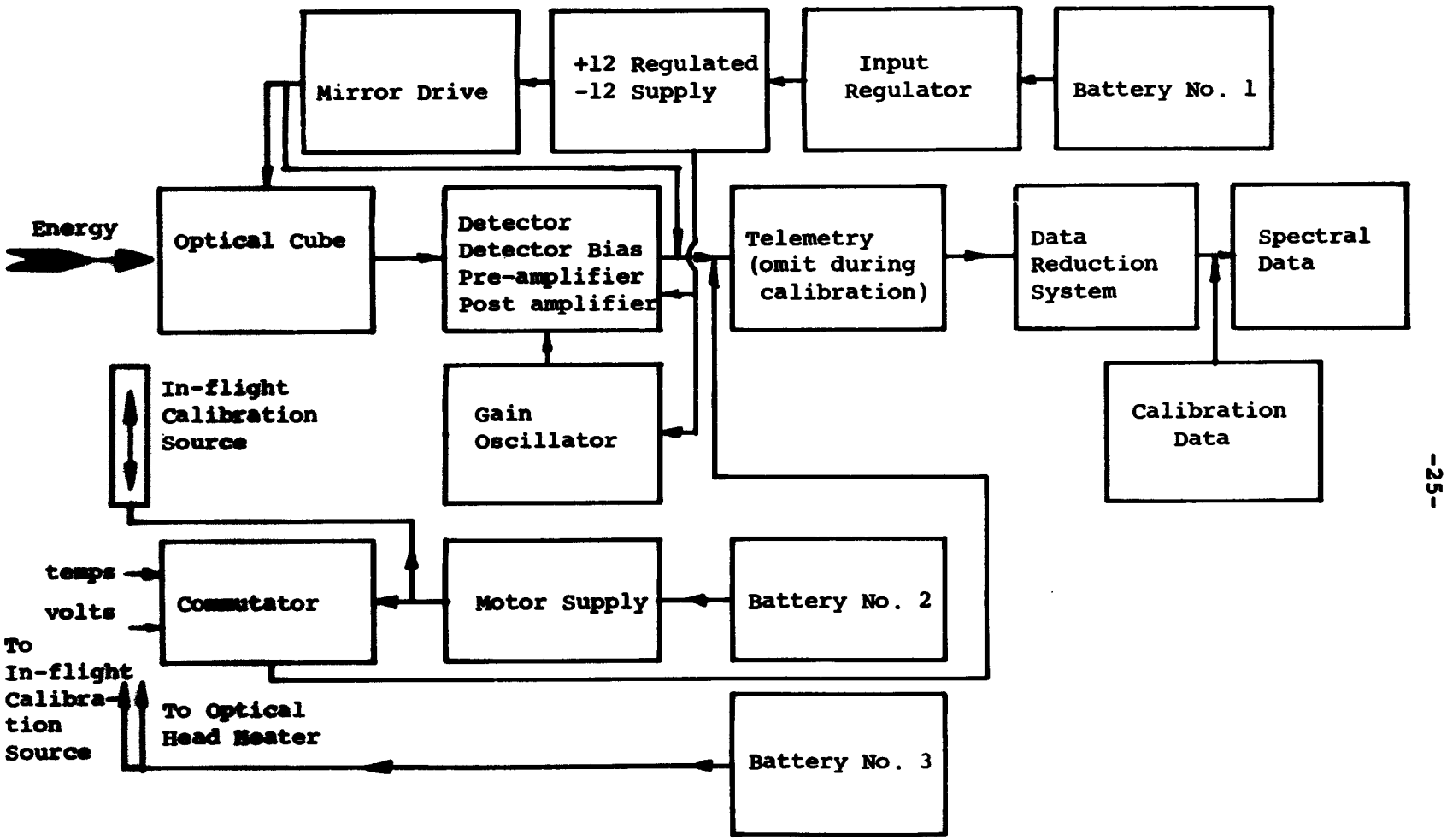

Figure 6.
Block Diagram of
Balloon Equipment

Typical Flight Packaging

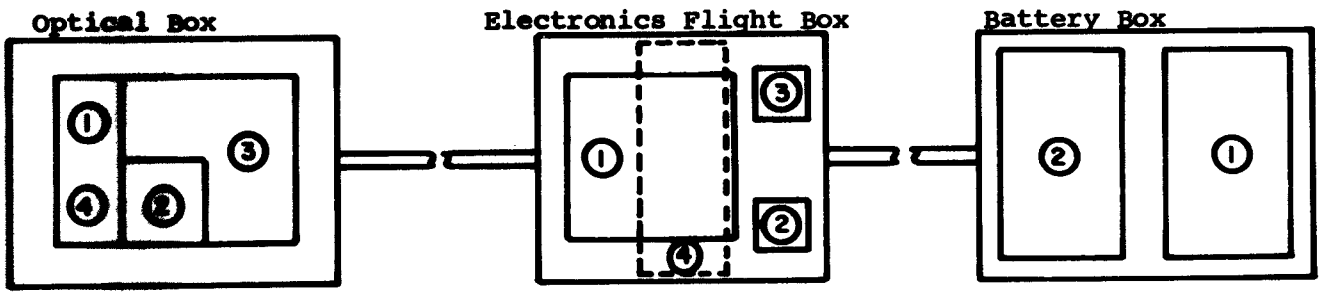

1. In-flight Calibration Source
2. Optical Cube and Detector
3. Pre-amp and Detector Bias
4. Alternate View Mirror Assembly (I4T only)

1. Electronics Chassis (post amp, mirror drive, +12 and -12 regulated supply, input regulator)
2. Commutator
3. Motor Supply
4. Battery No. 1

1. Battery No. 2
2. Battery No. 3

Figure 7.
Block Diagram of
Flight Packaging

3.2 Detailed Description of Auxiliary Engineering Systems

3.2.1 In-flight Calibration Source

The in-flight calibration source used with the I4T is shown in Figure 8. It is identical to that used with the I4TC except for the addition of the alternate-view mechanism (See Section 3.2.2).

The source itself is a ½" thick block of aluminum with a radiating surface, 1 3/4" by 1 3/4", which completely fills the field of view of the I4 when in place. The surface seen by the interferometer is "sawtoothed" and dull black anodized to provide a high emissivity. Two 25 ohm 10 watt resistors were imbedded in the block which was thermally isolated from the rest of the system by means of nylon washers and screws.

The voltage for the resistors was derived from the battery which provides power for the optical head heating. The temperature of the block was maintained at approximately 70°C by the use of a Fenwal thermal switch and the actual temperature was monitored by a Veco 31W1 thermistor bead. Since the calibration source rotated into the field of view rather than oscillating, it was necessary to devise a slip-ring type of arrangement whereby the thermistor bead signal could be fed to the commutator and the resistors could receive power from the battery. Rotary rather than oscillating motion was chosen because of design simplicity. A 26 volt, 400 cps Bendix motor drove, through a step down gear reduction, a Geneva driver which in turn indexed the calibrate source which was mounted on the Geneva. For flight #1 a Schmidt trigger was used to turn the motor on and off. The motor turned on for 33.4 seconds every 2 minutes 52 seconds. Since a four step Geneva was used this meant that the source was in the field of view for 8.4 seconds.

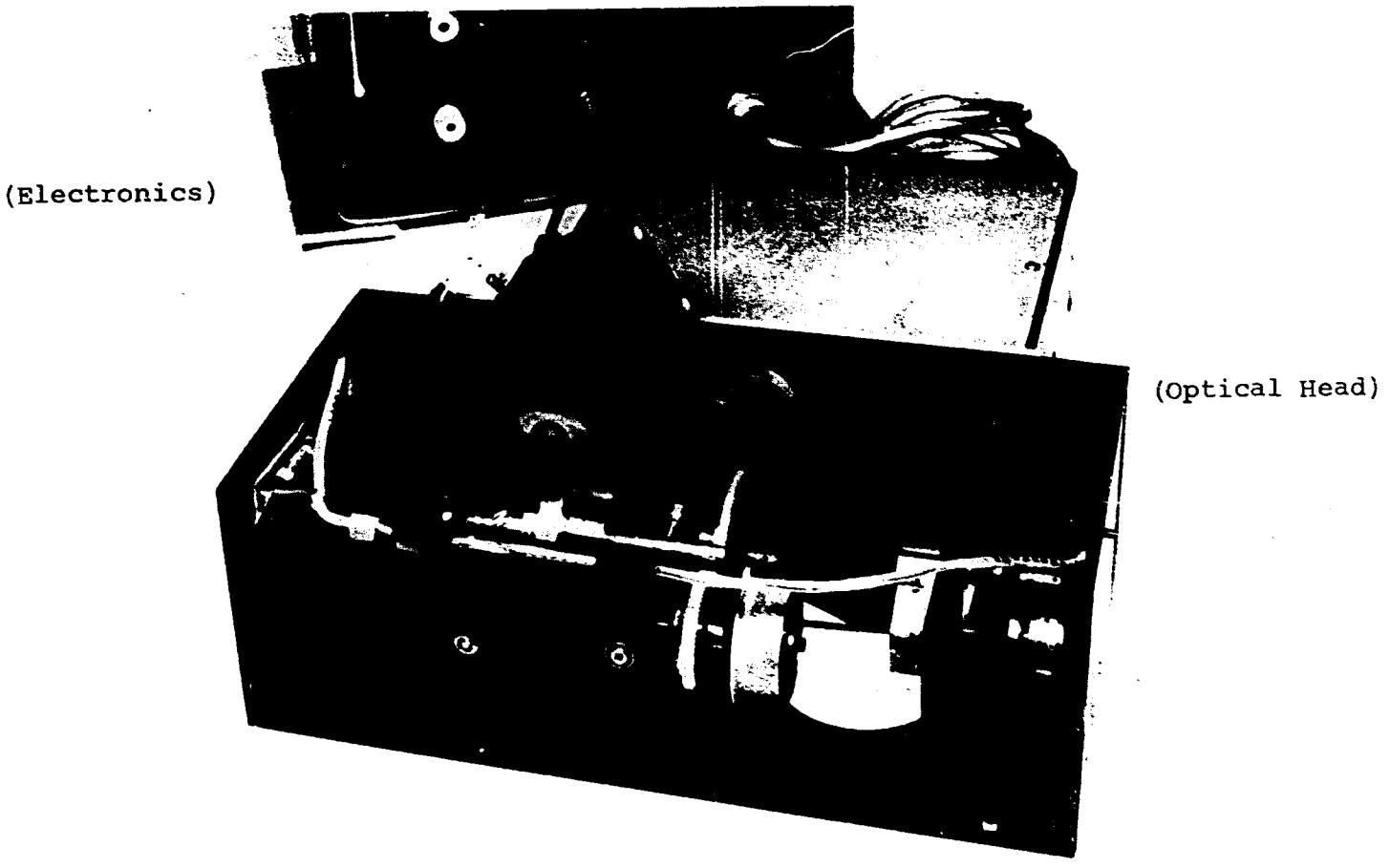

Figure 8.
In-flight Calibration Source
and Alternate-view Mechanism

Because of great difficulty experienced with the Schmidt trigger, it was removed from the system and the motor was allowed to run continuously for flight #2. In addition, the four step Geneva was replaced by a six-step so that the proportion of time spent looking at the atmosphere remained high. With a six step Geneva the source was seen for 30 seconds with a total cycle time of 3½ minutes.

3.2.2 Alternate-view Mechanism

One of the purposes of flight #2 was to compare the radiant flux looking at the nadir with that looking at the zenith, using the I4T. To accomplish this with one instrument it is necessary to oscillate a mirror in front of the unit so as to "bend" the field of view either toward the nadir or toward the zenith. It should be noted that because of the obstruction due to the balloon the zenith angle was limited to 30°.

The system used, shown in Figure 8, makes use of the inherently high duty cycle of a Geneva drive system. The Geneva driver was modified by removal of half of the locking sector. The normal indexing procedure was used to move the mirror from zenith position to nadir position. At the same time, however, a torsion spring was preloaded so that when the driver reached the missing lock sector the mirror was sprung back to the zenith position. Thus the rotation of the motor, which is the same one that drives the in-flight calibration source, is transformed into a combination oscillating and index motion which provides a duty cycle greater than 95%.

The exact position of the mirror at any given time during the flight is noted by use of a potentiometer coupled to the mirror. The regulated 12 volt supply was used to bias the potentiometer so that a change in position created a change in voltage which was monitored by use of the commutator.

3.2.3 Motor Power Supply

The motor power supply (Figure 9) is used to convert 28 volts d.c. to 26 volts at 400 cps for the commutator motors and the in-flight calibration source motors. The power supply used was a Block Associates, Inc. Model E2E motor supply slightly modified by the addition of a thermistor bead for supply temperature monitoring and the substitution of an external fuse holder replacing the missile type soldered fuse.

3.2.4 Commutator

The commutator, shown in Figure 10, can best be described as a rotary switch. Two silver plated, beryllium copper spring fingers are mounted on a motor rotated disk. One finger is in continual contact with a central ring which is in turn connected to the telemetry system. The other finger contacts a second ring which consists of several independent segments each of which represents a specific voltage or temperature. The two fingers are connected to each other by means of a thin copper strip.

In fabricating the commutators, one for the I4T, and a second duplicate for the I4TC, extensive use was made of printed circuit techniques. The desired configuration was photoetched on a copper laminated epoxy board using a photographic negative. This was then plated with a combination of nickel and rhodium to insure that the same commutator could be used for a large number of flights.

The instrument parameters which were monitored during each flight by means of the commutators are tabulated below.

Flight #1 - I4T	Flight #2 - I4T and I4T
1. 1.3 volt mercury battery	1. 1.3 volt mercury battery
2. 2.6 volt mercury battery	2. 2.6 volt mercury battery
3. Input voltage to I4T	3. Interferometer battery voltage
4. +12 volt regulated power supply	4. +12 volt regulated power supply voltage

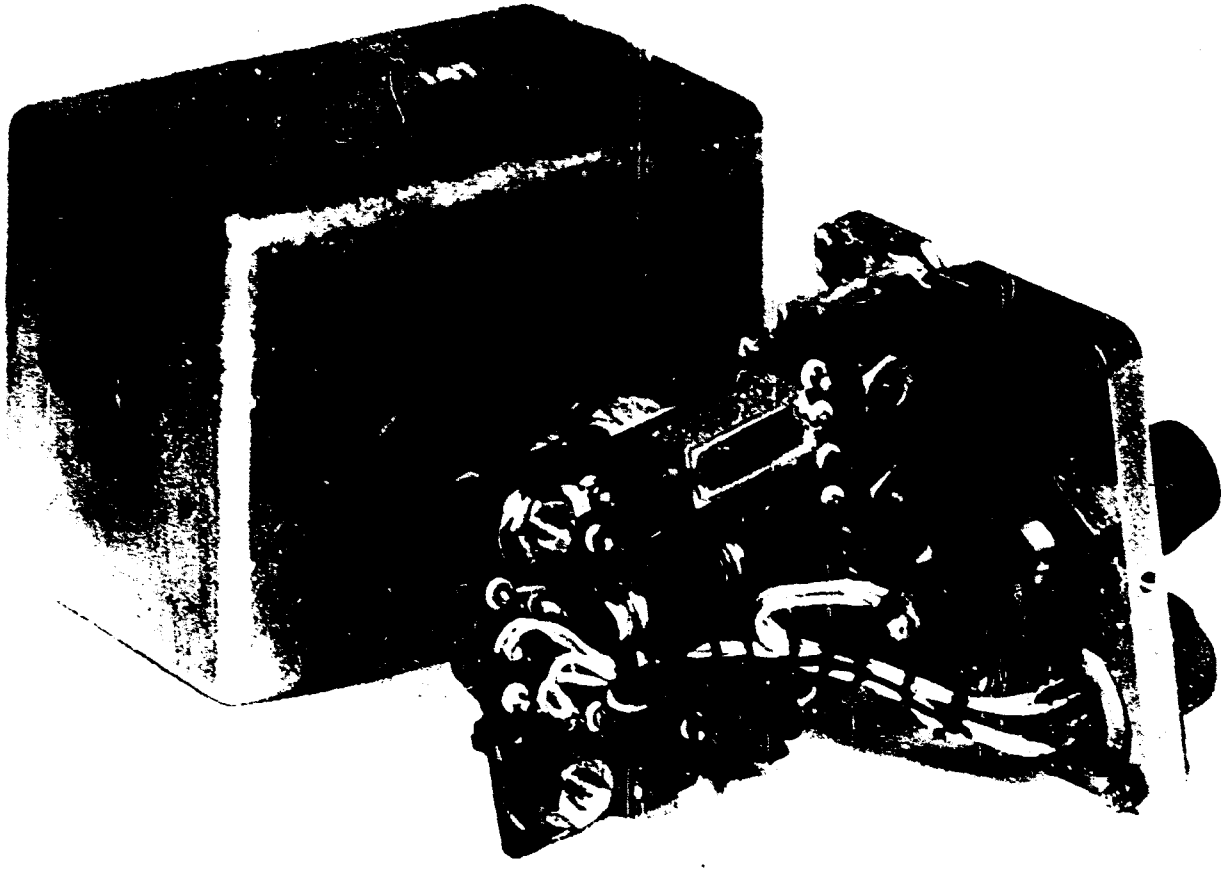

Figure 9.
Motor Power Supply

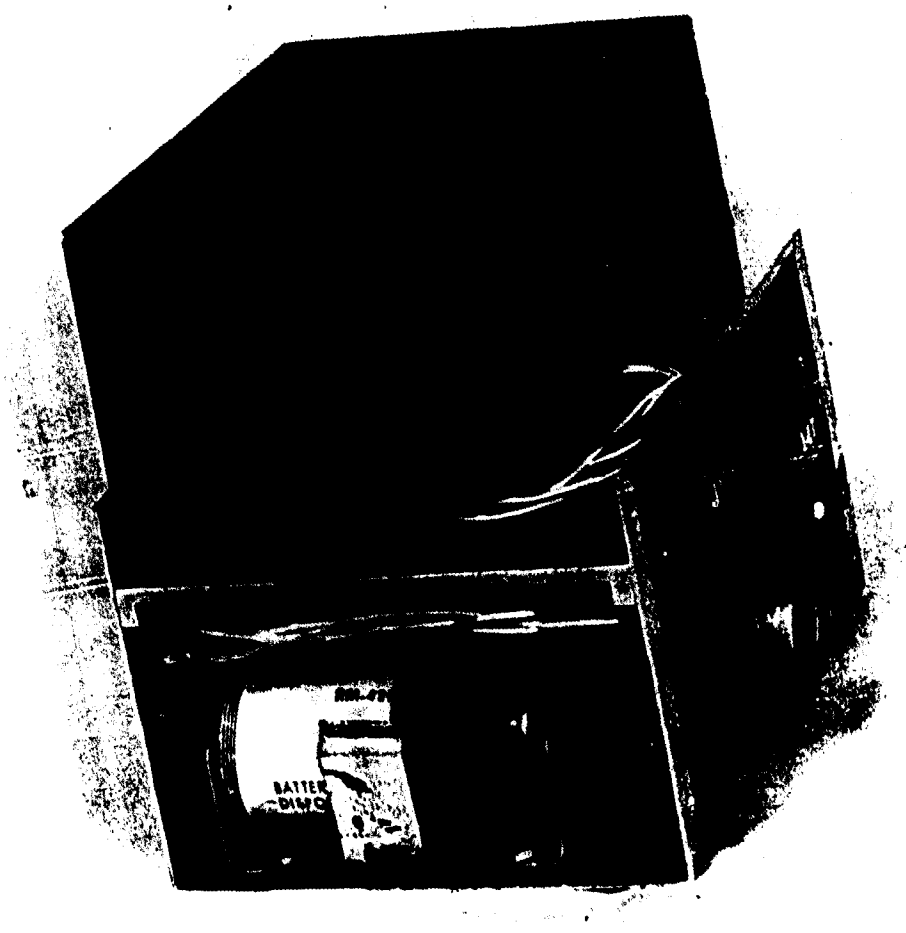

Figure 10.
Commutator.

Flight #1 - I4T	Flight #2 - I4T and I4TC
5. Post amplifier temperature	5. -12 volt regulated power supply voltage
6. Detector temperature	6. Motor Power supply battery voltage
	7. Heater battery voltage
	8. Alternate-view mirror monitor (I4T only)
	9. Detector temperature
	10. Preamplifier temperature
	11. Post amplifier temperature
	12. Gain oscillator temperature
	13. In-flight calibration source temperature
	14. Electronics Chassis temperature
	15. Flight box temperature
	16. Interferometer battery temperature
	17. Motor power supply battery temperature
	18. Heater battery temperature
	19. Motor power supply temperature

Since the telemetry system will not accept signal levels above 5 volts, it was necessary to use divider networks with each of the various voltages except for the two 1.3 volt mercury batteries which were used to calibrate the telemetry channel.

The various temperatures were measured by means of Veco 31W1 thermistor beads. In order to convert their resistance change with temperature change into a voltage change, the +12 volt regulated power supply was used in conjunction with 4.7K ohm load resistors. This resistance value was picked so that the signal levels produced by the expected temperature range would be compatible with the telemetry system. A second consideration was the problem of self heating due to the bias current. Since the nominal resistance of the beads is 1000 ohms at room temperature, then the use of a 4.7K ohm load produces a 2 ma. current through each bead which is small enough to be neglected.

The items which were monitored were based not as much on what any one alone would indicate, but rather on how each item fitted into the overall picture. The two mercury batteries were used not only to calibrate the commutator telemetry channel, but, in addition, any variation with altitude in both of them might indicate a temperature drift in the telemetry system. The interferometer battery voltage, the motor power supply battery voltage and the heater battery voltage were measured to insure that the proper power levels were being supplied to the instruments. Their respective temperatures were monitored so that any decay in current capacity with temperature could be noted. Any change in the plus and minus 12 volt regulated voltage produced by the interferometer itself would affect the gain of the system as well as the temperature readings

and mirror monitor reading since both use +12 as a reference. If, for instance, all the temperature readings and the mirror monitor varied by the same amount, then it could be shown by noting the +12 volt value whether or not a temperature change had actually taken place.

The alternate view mirror monitor consisted simply of a 10K ohms I.R.C. potentiometer coupled to the mirror. The potentiometer was set so that using +12 volts as bias voltage, a reading of 1.6 volts would indicate looking at the nadir while 2.6 volts indicates looking toward the zenith. This information is irreplaceable during the balloon flight data reduction process.

Of the many temperatures measured the most important is the detector temperature since the output signal of the interferometer is a function of the difference in radiance between the detector and source (See Section 6). Measuring the temperature of the gain oscillator, preamplifier and post amplifier helps to indicate any change in the gain of the electronics. The temperature of the in-flight calibration source is monitored in order to validate its use and the temperature of the motor power supply helps to pinpoint the source of trouble if any of the motors fail to operate. The temperatures of the electronic chassis and the flight box in which it was enclosed were measured so that knowledge could be gained as to the heat transfer process, specifically the affect of the sun at high altitudes. The information gained through the use of the commutators is given in the appendix.

3.2.5 Ground Control Station

As a result of the experience gained during flight #1 it was decided to design and construct a so-called ground control station. This system is used on the ground during the pre-launch checkouts to first, provide external power to the gondola, thus maximizing the on-board power capabilities and second, to provide means by which each of the items normally monitored by the commutator can be measured independently. In addition, the interferometer signal and the interferometer sweep signal which are normally telemetered can be examined without telemetry reduction equipment. This system, shown in Figure 11, also is of great value during in-house calibration and environmental testing.

3.2.6 Batteries

Because of their low cost, long shelf life and high cycle rate capabilities, nickel-cadmium batteries with potassium hydroxide electrolyte were used for the on-board power supply on flight #2. The battery power for flight #1 was provided by the other contractor on board the gondola.

Three packs were used for each interferometer system, one for the interferometer itself, one for the motor power supply and one for the heating system. Each pack consisted of 24 cells, each having a nominal voltage of 1.25 volts. The peak voltage after full charge of 1.4 volts decreases to the 1.25 volt value approximately 30 minutes after a load is applied.

3.2.7 Heating System

Since the detector temperature plays an important part in data reduction it was decided to thermostat the optical head so as to maintain the detector temperature constant. A temperature of 35°C was used since the detector tended to run slightly below this

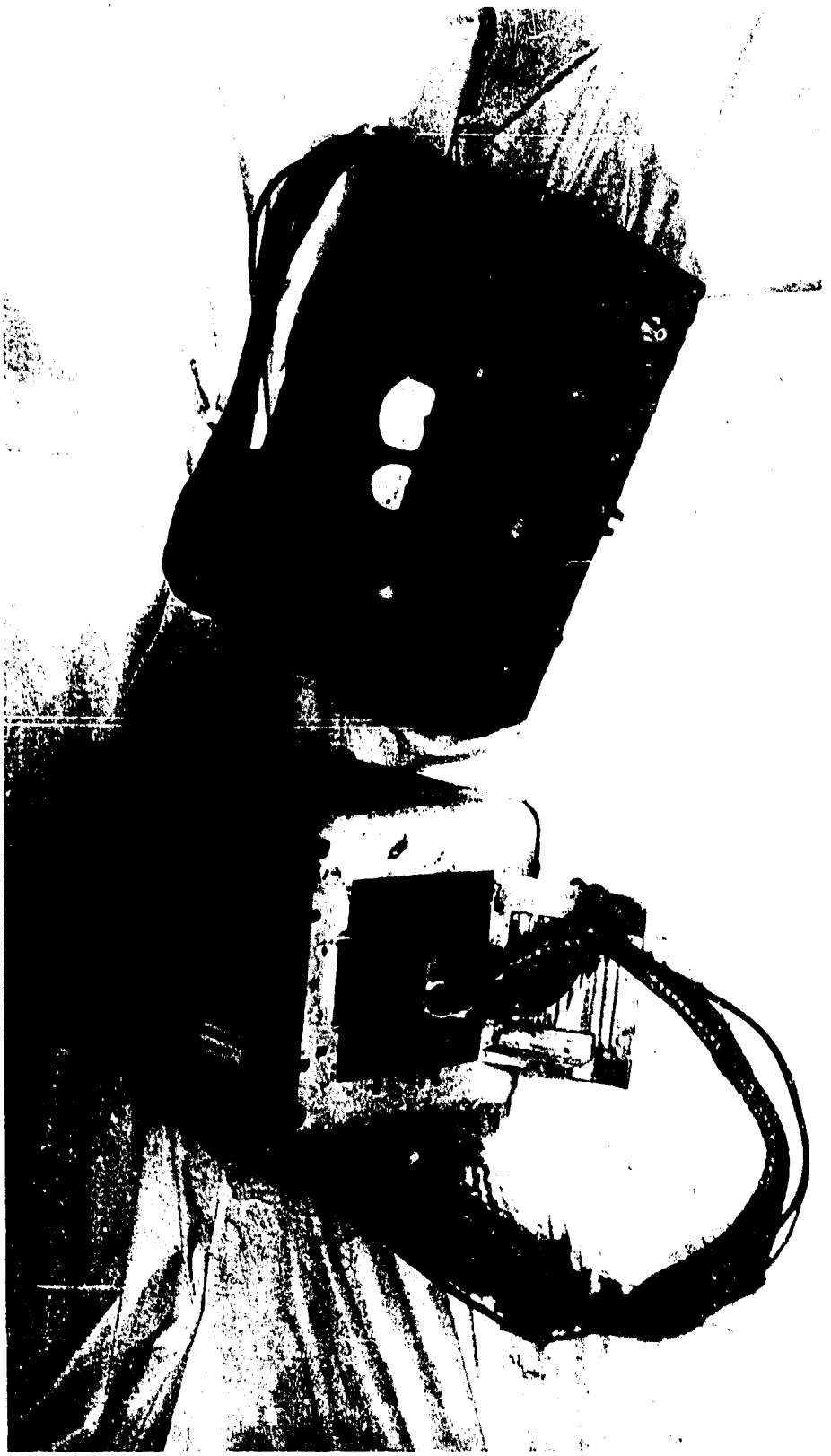

Figure 11.
Ground Control Station With
I-4TC Electronics Chassis.

value at room temperature due to its bias current. For convenience, the entire optical head was heated by wrapping 24 inches of nichrome wire having a resistance of approximately 10 ohms per foot around it in conjunction with a Fenwal thermoswitch having a sensitivity of roughly ± ½°C.

Heating the entire head had a second advantage in that, as a result, the entire optical cube is at the same temperature as the detector and therefore, there was no radiation exchange between the detector and the rest of the instrument.

3.3 Recommendations for Improvements in Future Systems

This section discusses the various improvements which could be made to the interferometer system in the event future balloon flights are contemplated. The most significant one is, unfortunately, also the most expensive; that is, the use of a newly available version of the interferometer known as the I6 model. This version of the interferometer utilizes the identical optical cube as the I4, the sole difference being in the packaging of the electronics. The size of the entire instrument, electronics as well as optics, is 7½"x 7½"x 4" and the weight of an I6 is 8 pounds compared to the 18 pound weight of an I4. In addition, the power consumption is reduced from 25 watts to 4 watts by the use of an I6. Although weight, size and power consumption are not as important considerations for a balloon as for a missile or satellite, they still can play an important role in determining the objectives of a particular flight. For example, the use of an I6 mounted on top of the balloon would make possible atmospheric measurements looking directly at the zenith rather than the 20° or 30° limitation with spectrometers which must be mounted underneath the balloon. It should be pointed out that the I6 itself will offer no large improvement in accuracy or repeatibility but rather is designed to make measurements hereto-

fore impossible with heavier spectrometers, especially from altitudes in the vicinity of 100,000 feet which can only be reached by a combination of large balloons and light payloads.

Other possible improvements would include: thermostating and monitoring alternate-view mirror temperature as well as indexing the mirror so that it is normal to and completely filling the field of view, thus providing an in-flight noise calibration since the detector would be looking at itself and any signal seen is that due to noise either in the instrument or telemetry system; the use of newly available sealed nickel-cadmium batteries which would eliminate the need for replacing electrolyte; and, finally, the monitoring by the commutator of the detector heater in such a manner that the on-off time for the heater could be determined. This information is helpful in designing other balloon instruments.

In addition, the use of a camera with color film during daytime flights would aid greatly in data analysis. The camera could show if the spectrometer were looking at clouds versus snow capped mountains as well as indicating cloud type and size.

Some current developments which may also prove valuable include: the use of the Jamin optical system which is inherently less temperature sensitive than the Michelson system; optical "chirping", a technique similar to "chirp" radar to reduce the dynamic range problem created by the use of FM/FM telemetry (see appendix); increased spectral resolution and accuracy made possible by the use of computers.

It should be noted that since the construction of the instruments used in this program engineering improvements in the transducer have been made such that a resolution of 24 cm^{-1} is now possible.

4.0 Environmental Testing

4.1 Purpose of Tests

The Model I4 interferometers were originally designed for use in scientific laboratories where conditions of temperature and pressure are well known and relatively stable. Balloon-borne experiments experience quite a different environment, however. For example, the ambient pressure at 100,000 feet is 1/100th of what it is at sea level while as far as temperatures are concerned a change from 20°C to -60°C in ambient temperature during a flight is quite common.

To further illustrate the point let's follow a typical hypothetical trajectory. The balloon was launched from Holloman Air Force Base, New Mexico at 3:45 a.m. M.S.T. At that time the air temperature was 10°C and the pressure was 876 millibars. As the balloon slowly ascended the package was cooled both by conduction to the increasingly colder air and to a lesser extent by the forced convection due to movement through the air. At 5:00 a.m. M.S.T. the balloon reached an altitude of 55,000 feet M.S.L. where the temperature was -65°C. At this point two other factors start to play an important part. One is the fact that since the air has a lower pressure and therefore lower density the processes of conduction and convection to the ambient air are hindered. At the same time, moreover, the package temperature comes under the strong influence of heat transfer by radiation to outer space. As the balloon heads towards 80,000 feet the effect of conduction and convection rapidly diminishes while radiative transfer becomes increasingly more significant. On this particular flight the maximum altitude of 83,600 feet M.S.L. was reached at 6:30 a.m. which means that the effect of the sun shining unattenuated on the package must now be considered. The purpose of the environmental

testing, therefore, is to try to insure that the instrumentation will operate properly under these varying conditions.

4.2 Test Procedures

The environmental test program made use of a large temperature-at-altitude chamber at the Acton Laboratories, Inc., Acton, Massachusetts. Altitude was simulated by simply creating the appropriate vacuum while cold temperatures could be produced simultaneously by Freon cooling the walls of the chamber. Since a solar simulator was not available, the effect of the sun could only be accounted for by theoretical calculations in conjunction with the actual flight experience of a group such as the University of Denver. The effect of outer space was noted by cooling the walls of the chamber to - 65°C, the radiation from a source at this temperature being small enough to be assumed zero. For the purpose of these tests a special adapter plate was made and attached to the chamber. This facilitated the electrical monitoring of the instrument's performance while the chamber was under reduced pressure.

4.3 Results

The first item tested was the in-flight radiation source. The purpose in testing was to see if the block remained at a constant temperature independent of ambient temperature and/or pressure. The first test indicated that the temperature of the source tended to follow a change in ambient temperature. In Figure 12, the temperature of the walls of the altitude chamber and the ambient temperature remained constant at 26°C. The system, consisting of source, source housing, yoke, and two plates, reached equilibrium with the surface of the source at 58°C, the source housing at 42°C, the yoke at 38°C, the plate in front of the source at 30°C, and the plate behind the source at 31.5°C. Analysis of this data indicated that the source was losing energy to the source housing, yoke, and plates although the whole system reached a point of equilibrium with the source remaining at a constant temperature when the system was enclosed in a constant ambient temperature of 26°C. Figure 13 is a plot of that constant temperature versus ambient temperature.

Thermocouples placed at one edge of the source and at the center of the source showed no gradient between the center and the edge.

As a result of this test, the two 50 ohm resistors used to heat the source were changed to 25 ohms each, and the resulting improvement is shown in Figure 14.

Next, the I-4T itself was tested. The optical head was mounted in an aluminum box large enough so that approximately two inches of styrofoam could be placed around the head for insulation. The electronics chassis was placed in a second box along with the commutator and motor supply. Again, room was left for two inches of styrofoam insulation. Both boxes were

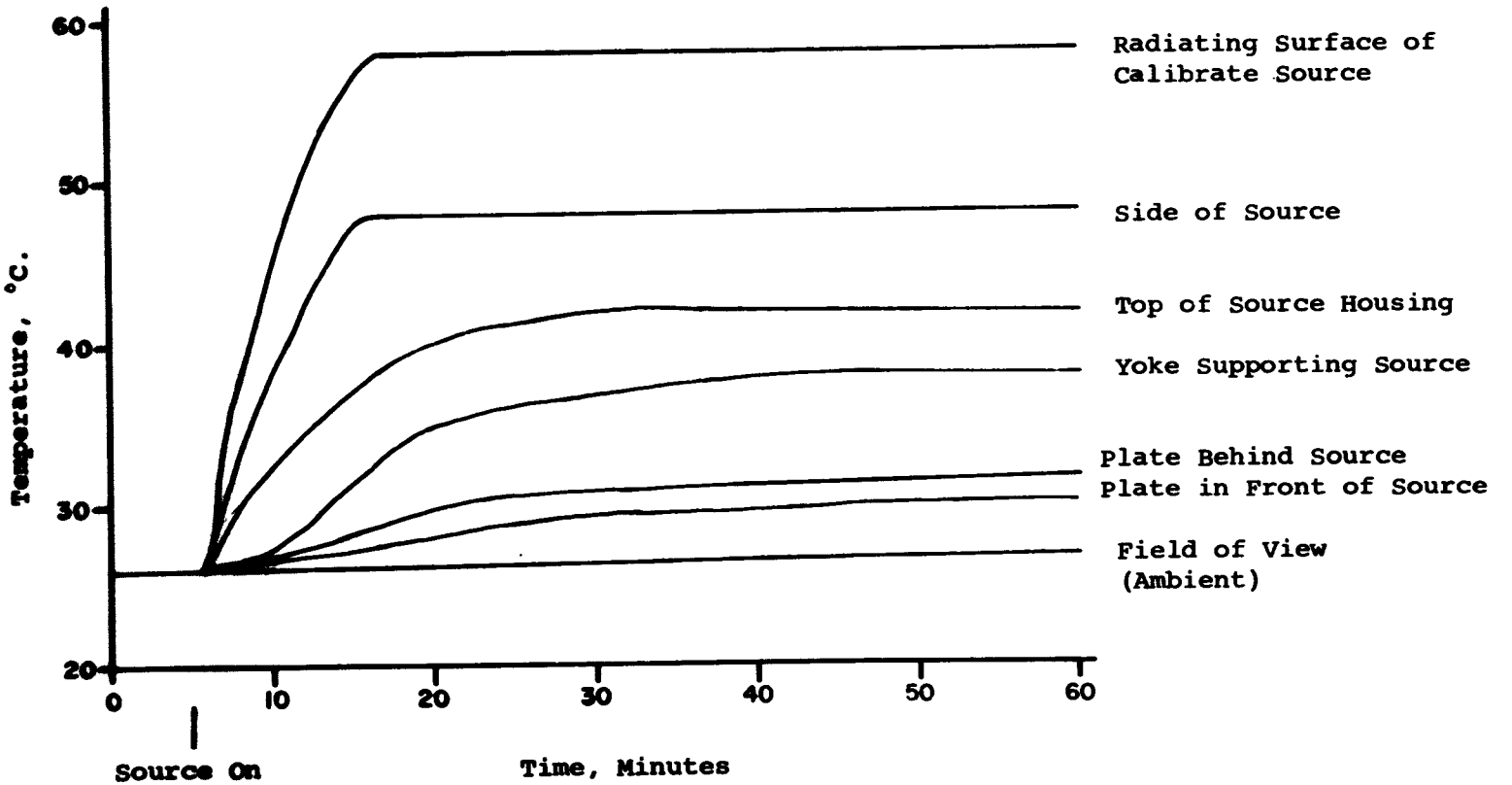

Figure 12.
Altitude Chamber Test on In-Flight Calibration Source Temperature Vs. Time.
Ambient Temperature at 26°C
Atmosphere at 29.92" Hg

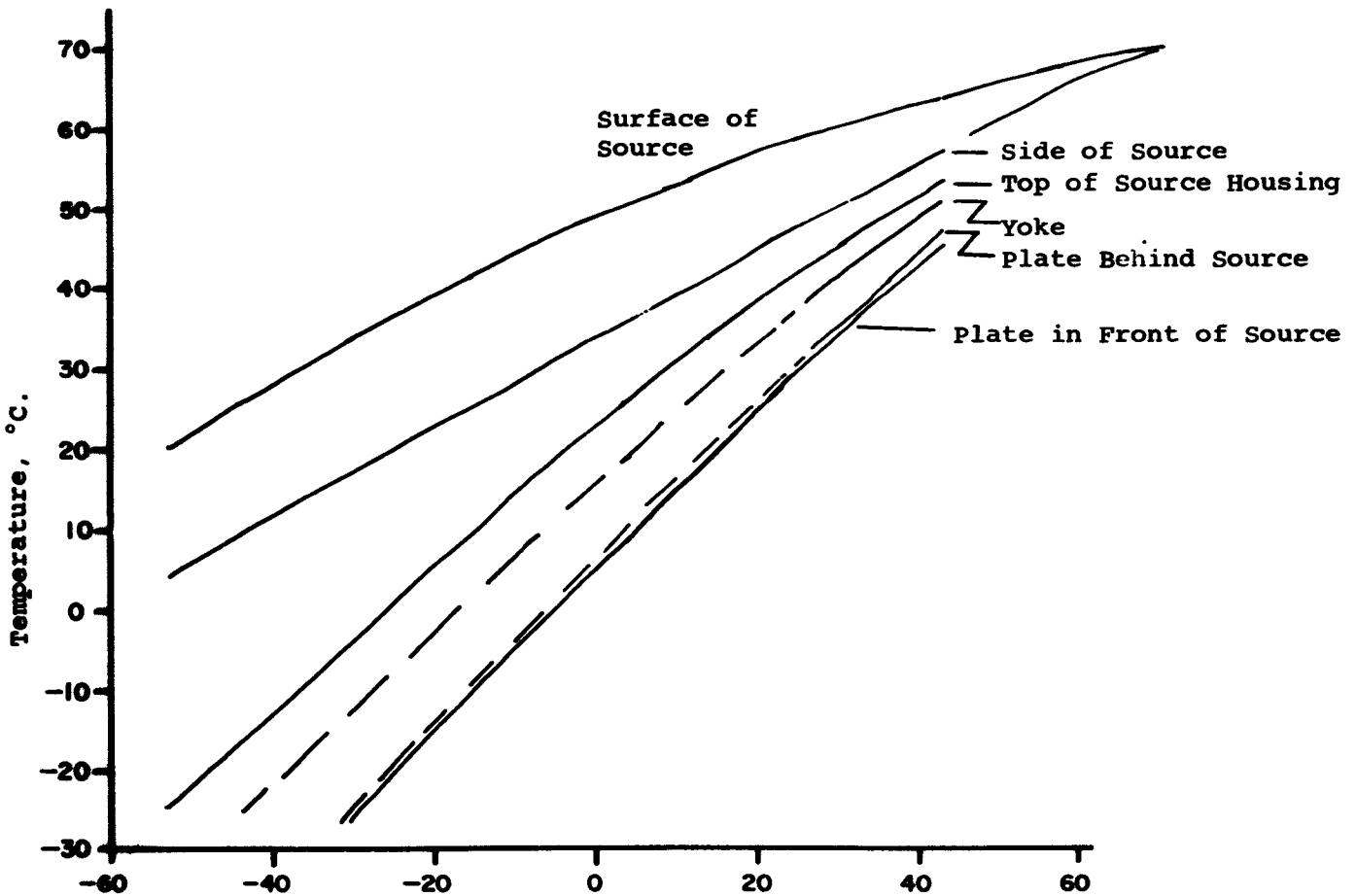

Figure 13.
Calibration Source Temperature
Vs. Ambient Temperature.

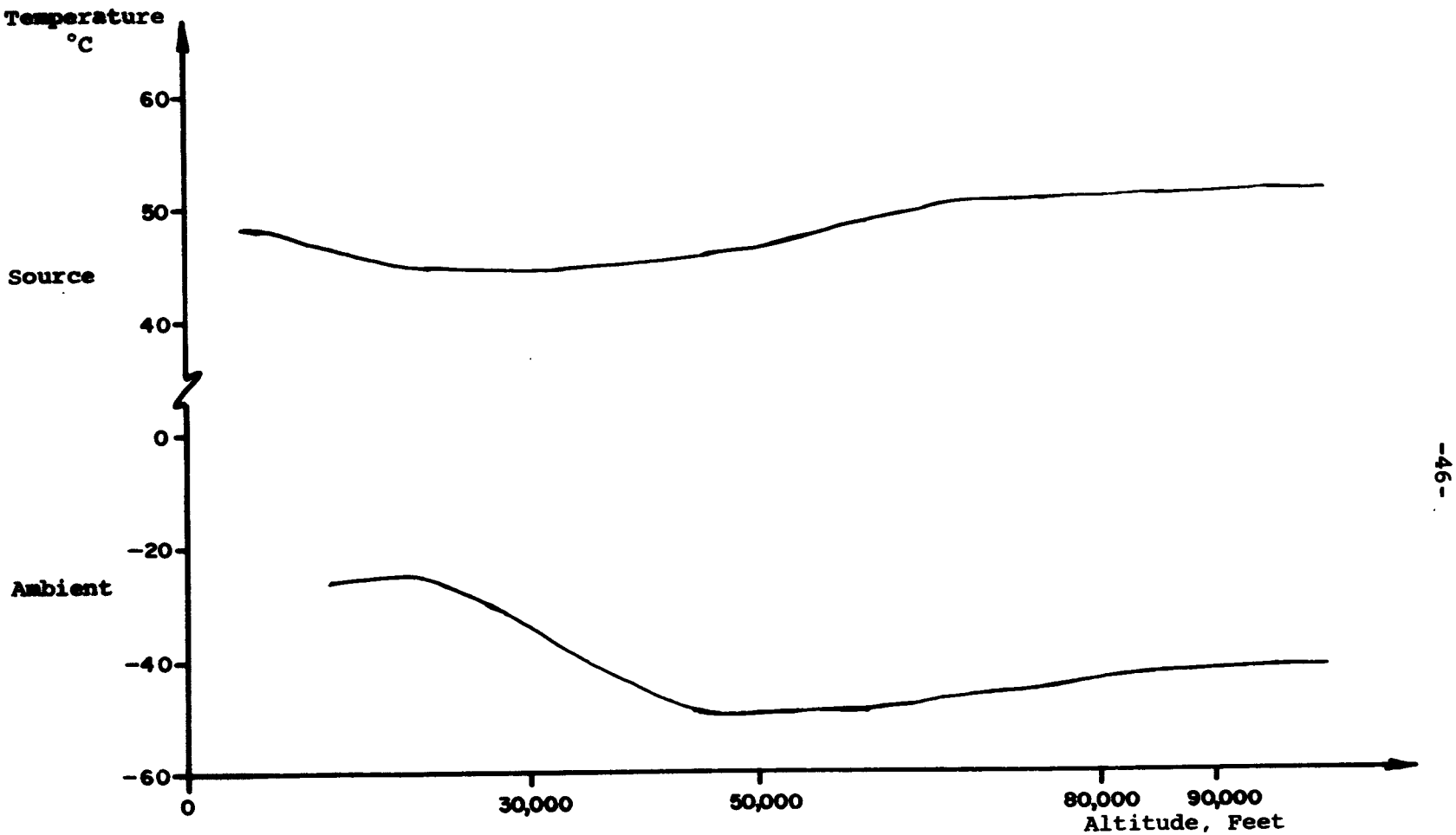

Figure 14
Source Temperature Vs.
Ambient Temperature
and Pressure (Altitude)

spray painted with Krylon white paint. The use of this paint was designed to minimize the overheating due to the sun since its emissivity is 0.15 to 0.3 in the visible and 0.8 to 0.9 in the infrared. The most important conclusion from this test was that the insulation around the optical head was not sufficient to maintain the detector temperature constant. As a result, the nichrome heater system was added and operated satisfactorily during a second environmental test. It is interesting to note in light of the temperature problems which occurred during the first flight (See Section 7) that during both tests the electronics chassis temperature varied from 20°C to 35°C under various temperatures and pressures and operated satisfactorily at all times. The major difficulty appearing during both tests was associated with the Schmidt trigger, the timing device which activated the in-flight calibration source. Large changes in temperature would cause the cycle time to vary, and it was necessary to make several component changes before it would operate satisfactorily.

After the experience of the first flight, a different design approach was used as far as the electronics chassis was concerned. Instead of trying to maintain the temperature relatively constant, it was decided to heat sink the chassis to the outside flight box, thus allowing the electronics to run much cooler than room temperature. Although this would prevent component failure due to possible overheating, there was a possibility that the temperature compensation in the electronic circuitry was not sufficient to prevent gain instability. In preparation for Flight No. 2, another series of environmental tests were conducted; the first of these involved operating both the I-4T and I-4TC over a wide range of temperatures and noting the output of the gain oscillator as well as the output of the amplifier when the instrument was seeing the in-flight calibration source. The results shown in Figures 15 and

16 showed that the gain oscillator in both units would remain constant for all temperatures below 15°C. In addition, the amplitude of the signal while viewing the in-flight calibration source remained constant, these two facts indicating that neither the gain oscillator nor the amplifier would be adversely affected by temperature change.

One other problem presented by this design change was the temperature versus voltage characteristics of the mercury batteries used to calibrate the commutator channel. A test was conducted wherein the temperature was varied from -20°C to +50°C while the voltage was monitored by a voltmeter. The voltage remained constant due to the fact that the current drain was made almost negligibly small by the high input impedance of the voltmeter. Since the telemetry system also has a high input impedance, no problem was anticipated as far as the actual flight was concerned.

During these tests the opportunity was taken to calibrate all ten thermistor beads. A thick aluminum disk was used as a common temperature sink whose temperature was monitored by means of a thermocouple. They were each separately identified by using different color coded wires for the electrical connections. This was done in the event that the spread in calibration points was so large that a common calibration curve could not be used.

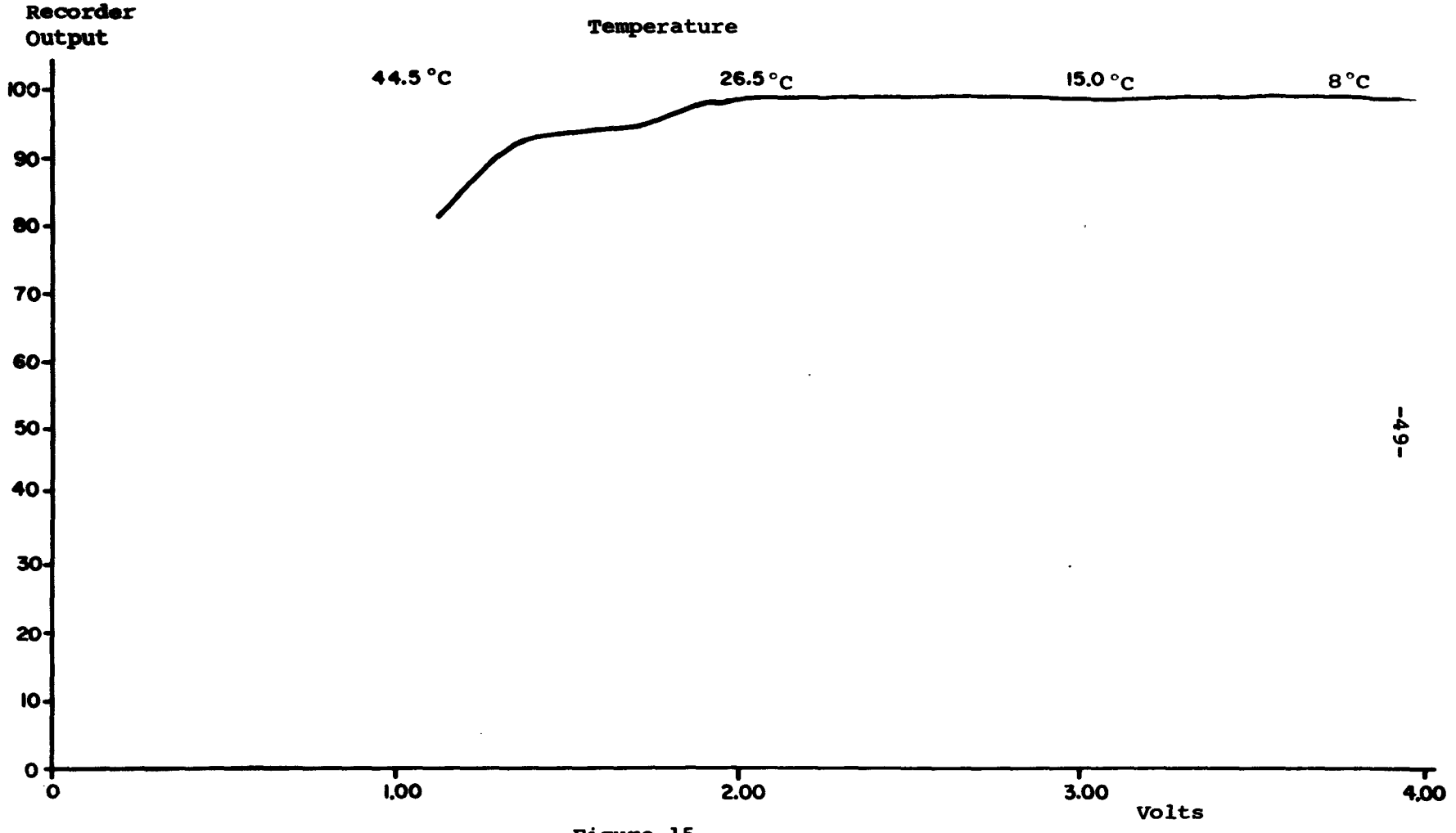

Figure 15.
I-4T Oscillator Output Vs.
Thermistor Bead Voltage

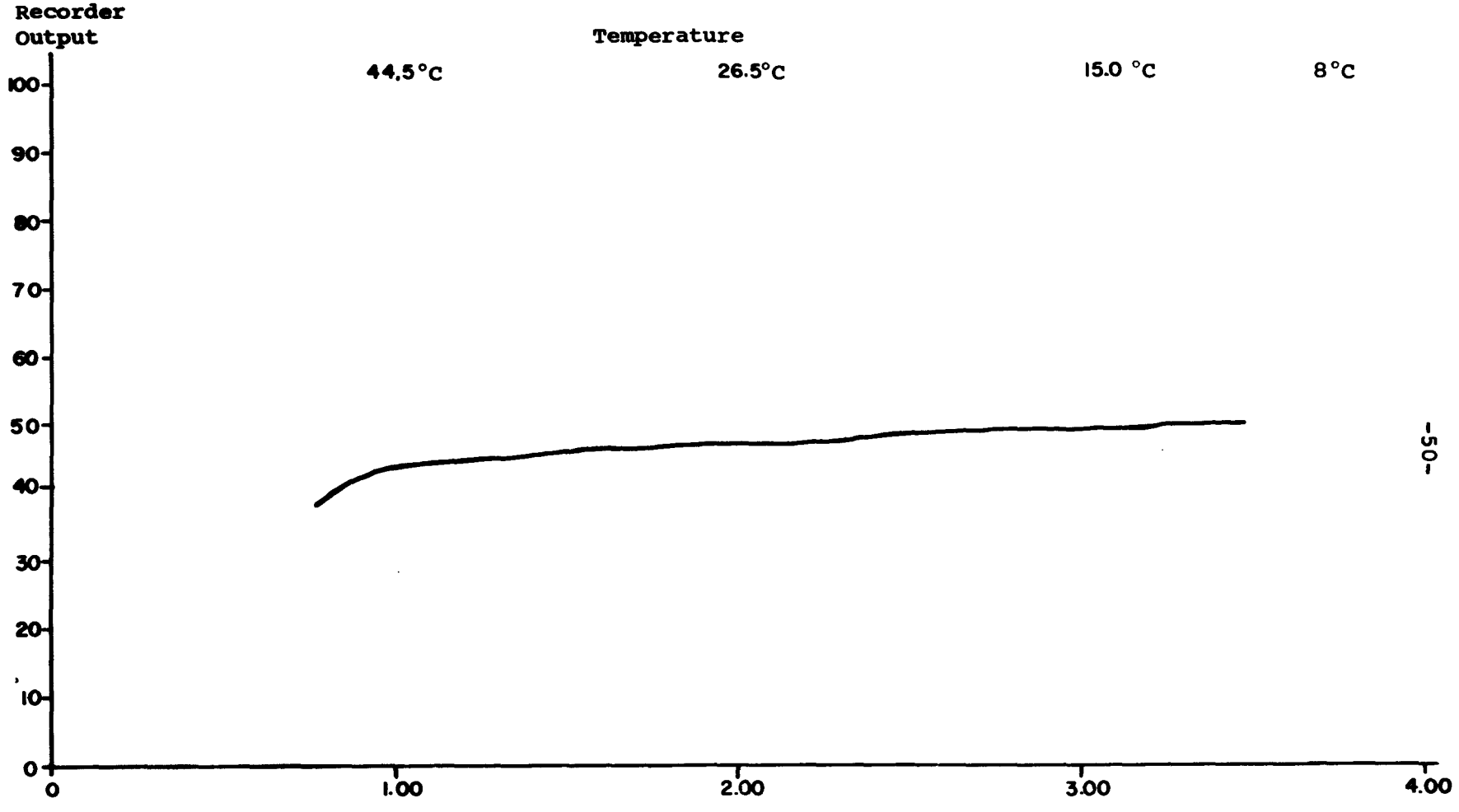

Figure 16
I4TC Oscillator Output Vs.
Thermistor Bead Voltage

5.0 Independent Laboratory Calibration

5.1 Eppley Laboratory, Inc.

The first step in calibrating the spectral response of the I-4T was to make it available to an independent outside laboratory for the purpose of determining the relative spectral response. Due to its vast experience in this type of work, the Eppley Laboratory, Inc., of Newport, Rhode Island, was chosen.

The initial step was to determine the wavelength versus frequency calibration, and this was done by Block Associates personnel using polystyrene absorption as a standard. Then the I-4T was given to Eppley, who performed the actual response calibration.

The method consisted essentially of comparing the relative signals from the I-4T interferometer with those from a detector, which is not wavelength selective (in this case a Golay pneumatic detector), on exposure to monochromatic radiation. The energy source employed was a Perkin-Elmer single-pass monochromator Model 98, with NaCl optics and a Nernst glower as source. The true spectra of output of the source was determined with a Perkin-Elmer Model 99 double-pass monochromator.

Several determinations of the energy density at the entrance to the I-4T instrument were also made using an Eppley working standard thermopile with a gold black-coated receiver. These served to verify the non-selectivity of the pneumatic detector used as reference.

Two complete interferometer scans were made, the first being preliminary in order to assess the entire experimental procedure involved and the second that which provided the data discussed in this report. In this instance, the temperature of the bolometer detector of the interferometer was 300°K.

The experimental set-up is shown, schematically, in Figure 17. Of the two monochromators which were used, the first (P-E 98) served as a source of monochromatic energy for both the Golay detector and the I-4T interferometer. The second (P-E 99) served to analyze the radiation from the first monochromator into its spectral components.

After the apparatus was set up and appropriate spectral bands (free from water vapor and CO_2 absorption and of suitable width for energizing both the Model 99 monochromator and the I-4T interferometer) selected, the output of the Model 98 monochromator was scanned by both the I-4T and the Model 99 instruments. The relative energy was then determined using the laboratory-type thermopile and the Golay detector. The thermopile readings verified the non-selectivity of the Golay detector out to 10μ. Inasmuch as the window material of the Golay detector (CsI) transmits non-selectively to at least 30μ and as a pneumatic detector is inherently non-wavelength-selective, it is considered that the extrapolation to 15μ is valid for all practical purposes.

During the course of the experiment, it was found that the energy at the shorter wavelength positions was saturating the interferometer; and, accordingly, a 30 per cent neutral density filter was used to reduce the energy in these wavelength positions. The neutral filter was also used with the Golay and the Model 99 instruments.

In determining the wavelength distribution of the energy from the Model 98 monochromator, the slit setting of the scanning monochromator was maintained fixed throughout. Table 1 gives the approximate half bandwidth at each of the selected wavelength positions.

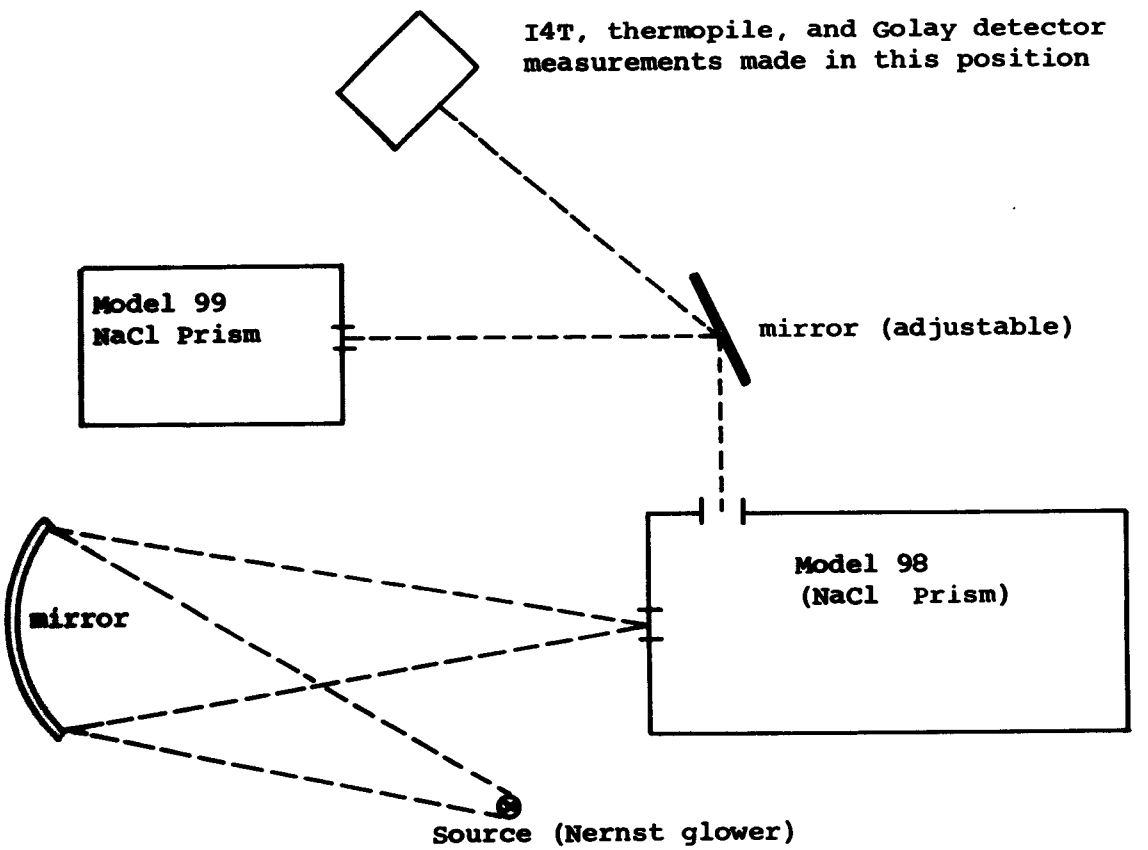

Figure 17. Schematic Diagram of Experimental Set-up.

As the energy curve of the emission by the Model 98 monochromator would be represented by the areas under the chart curves drawn by the analyzing monochromator, it was verified that the peak value of the ordinate was essentially proportional to the area under the curve, irrespective of wavelength. This was effected by planimetering the curves and evaluating the ordinate to area ratio. It was found that this ratio was very nearly a constant over the range 2 - 15μ. This being the case, the Golay indication could be conveniently compared directly with the maximum ordinate of the monochromator trace instead of the area under it. Since this relationship depends only on the exit slit function of the single-pass monochromator, the procedure should be valid for the I-4T instrument as well. The relative spectral response of the interferometer is given in Table II as the ratio of peak ordinate (data supplied by Block Associates) to relative energy.

TABLE I

Wavelength Scale of Monochromator
Versus Wavelength Scale of Interferometer

λ(μ) P-E 99	λ(μ) I-4T	1/2 Bandwidth (μ) P-E 99
2.4	2.4	0.40
3.7	3.4	0.45
5.5	5.4	0.30
7.7	7.7	0.25
9.05	9.0	0.20
10.35	10.4	0.18
11.2	11.6	0.18
12.7	12.5	0.17

TABLE II

Relative Energy Values as Measured
By Golay Detector and Interferometer

(1) $\lambda(\mu)$	(2) relative energy	(3) I-4T (mv)	(3)/(2)	(4) I-4T relative energy	(5) I-4T relative energy (normalize
2.4	100.0	15.5		.155	1.24
3.7	32.6	27.7		.850	6.78
5.5	36.9	88.2		2.39	19.3
7.7	8.89	73.4		8.26	66.6
9.05	3.90	34.6		8.86	71.5
10.35	2.26	24.7		10.9	88.1
11.2	1.63	20.2		12.4	100.0
12.7	0.845	5.4		6.82	51.5

After the data was received from Eppley, (shown as the dotted curve in Figure 18), it was necessary to apply a correction factor due to the fact that the output of the I4T is proportional to energy per wavenumber at a given wavelength, not energy per micron. The correction was made by dividing the amplitude at a given wavelength on the Eppley curve by the square of the particular wavelength, since $\Delta\lambda/\Delta\nu = \lambda^2$. The normalized curve, ("Eppley with bandwidth correction") is also shown in Figure 18.

A third normalized relative response curve, ("Block-Denver") which was determined later at the University of Denver, is also presented. The spread in the latter two curves was quite encouraging, considering the state of development of the calibration procedure at that time.

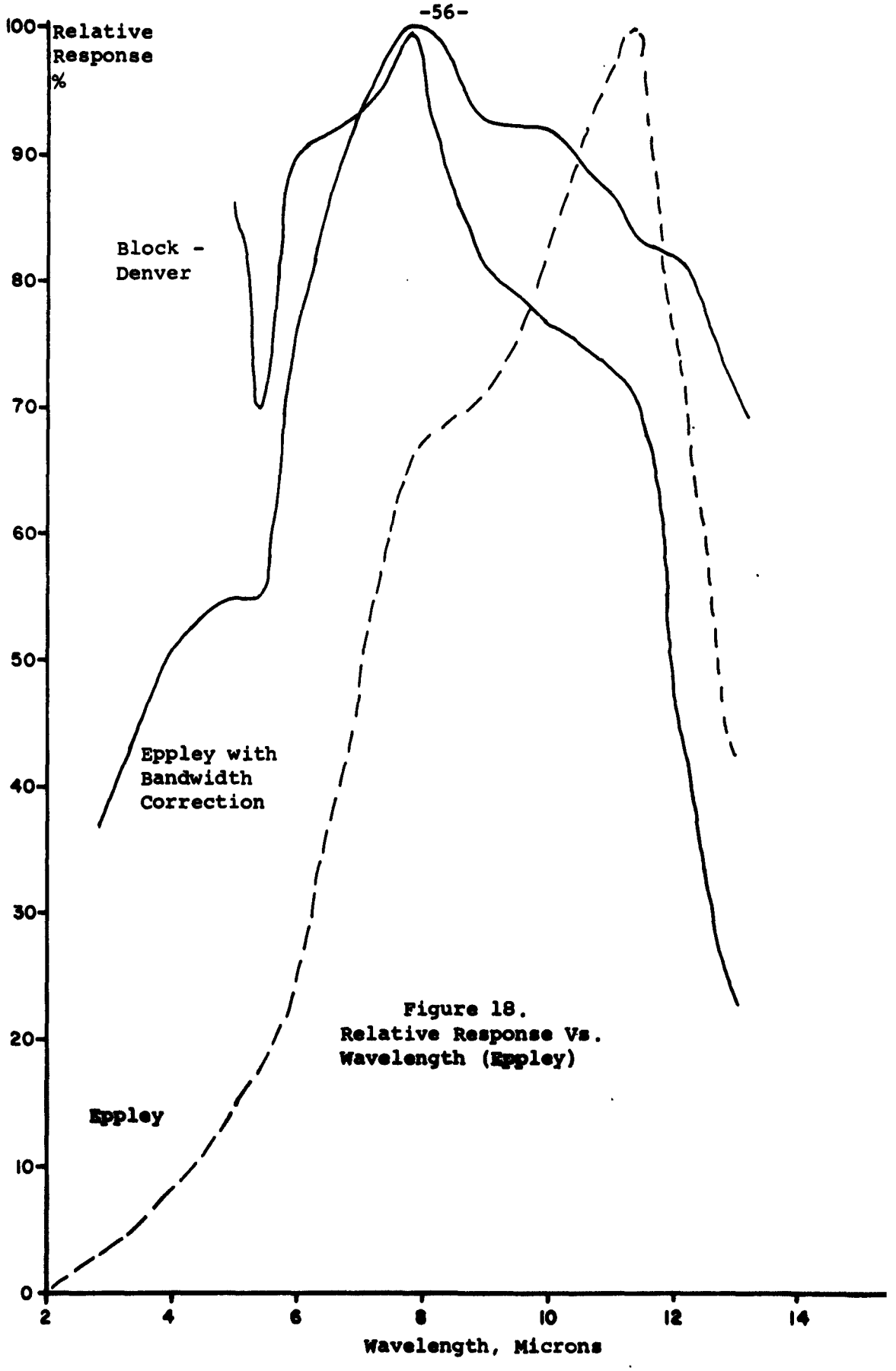

Figure 18.
Relative Response Vs.
Wavelength (Eppley)

5.2 University of Denver

In preparation for the first balloon flight, the I4T and its supporting equipment were transferred to the University of Denver, Denver, Colorado. The purpose of this trip was to take ground-based spectra of the sky under varying cloud conditions, times, and zenith angles and to compare the results with those obtained by the spectrometer employed by the University of Denver. The latter instrument was a prism spectrometer, incorporating a Reeder thermocouple detector and had been previously used for making this type of measurement.

The essential differences between the two instruments are threefold. The Denver spectrometer requires about 180 seconds for a spectral scan, whereas a 12-second scan (equivalent to 12 interferograms) was used by the I4T; the resolution of the two instruments varies inversely, i.e., the I4T has its best resolution, in microns, at short wavelengths while the University of Denver spectrometer has its best resolution at long wavelengths; and finally, the field of view is a 15° cone for the I4T as compared with about 7° for the other instrument.

In the comparison runs, the I4T took two 12-second scans toward the start and finish of each Denver University scan. Taking two runs instead of one was necessitated by the presence of a rapidly moving temperature inversion, or chinook, which appeared during the runs taken of a cloudless sky. The angles chosen were zenith, 30° from zenith, and 60° from zenith. Spectra were also taken of a cloudy sky. The same angles were used as on the cloudless sky runs.

The results obtained from both instruments are presented in Figures 19 and 20.

The comparison of data from the two units indicated that the results from the I4T were consistently lower in absolute value. It became evident that the difference in the radiance values would be reduced by improving our calibration techniques. The calibration method finally decided on is discussed in Section 6.

The spectral response calibration applied to these ground measurements was determined by the graphical method later employed for the balloon flight data. The black-body calibration sources used were room temperature, ice, liquid nitrogen, (see Figure 21) and three temperatures between 25°C and 50°C produced by a large black-body "cannon-shaped" source. The major sources of error involved in this determination were inaccuracies in measuring the temperature of the calibration sources and the temperature of the detector as well as the presence of carbon dioxide and water vapor in the path between the sources and the I4T.

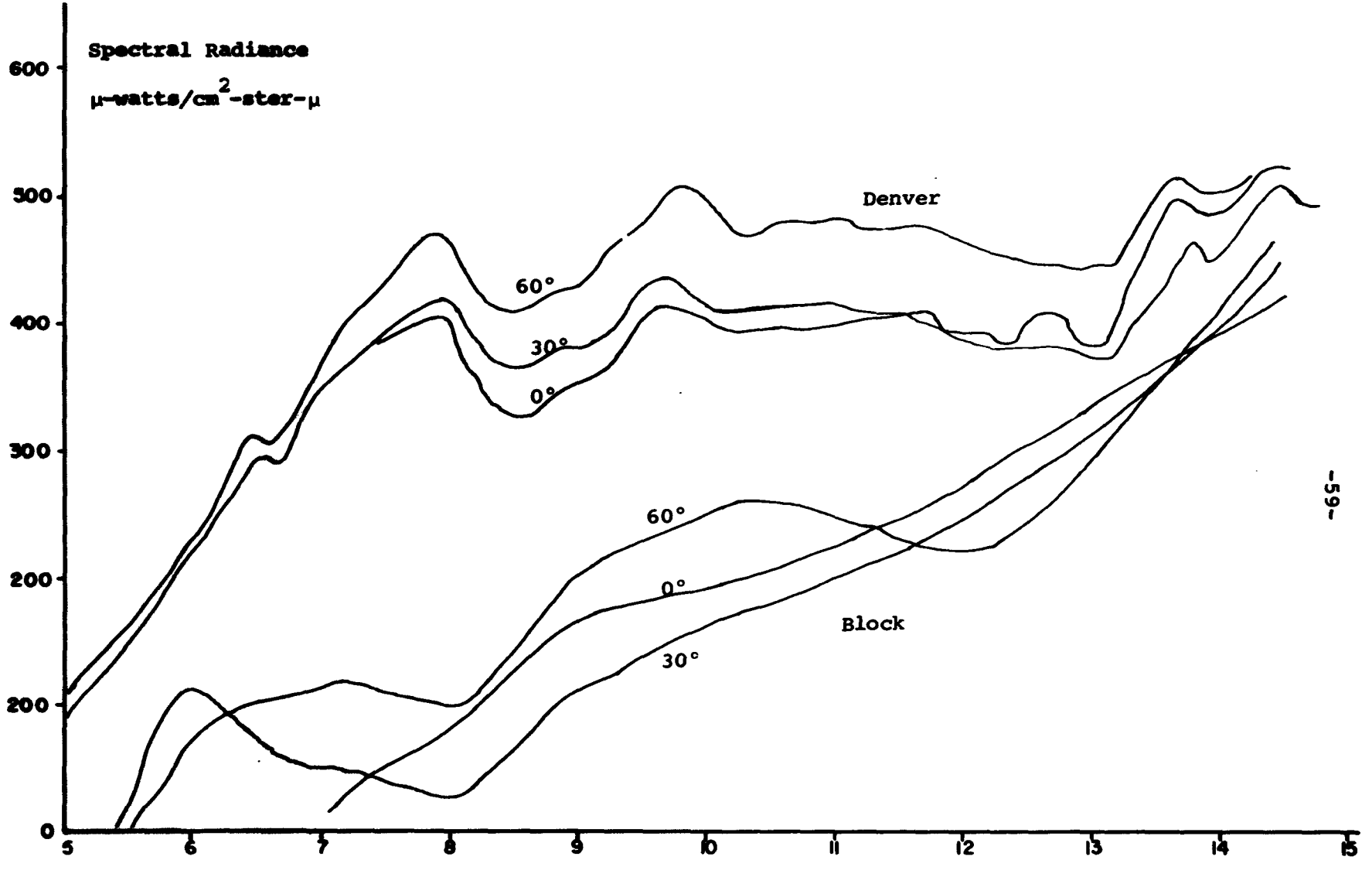

Figure 19
Cloudy Sky at Various
Zenith Angles

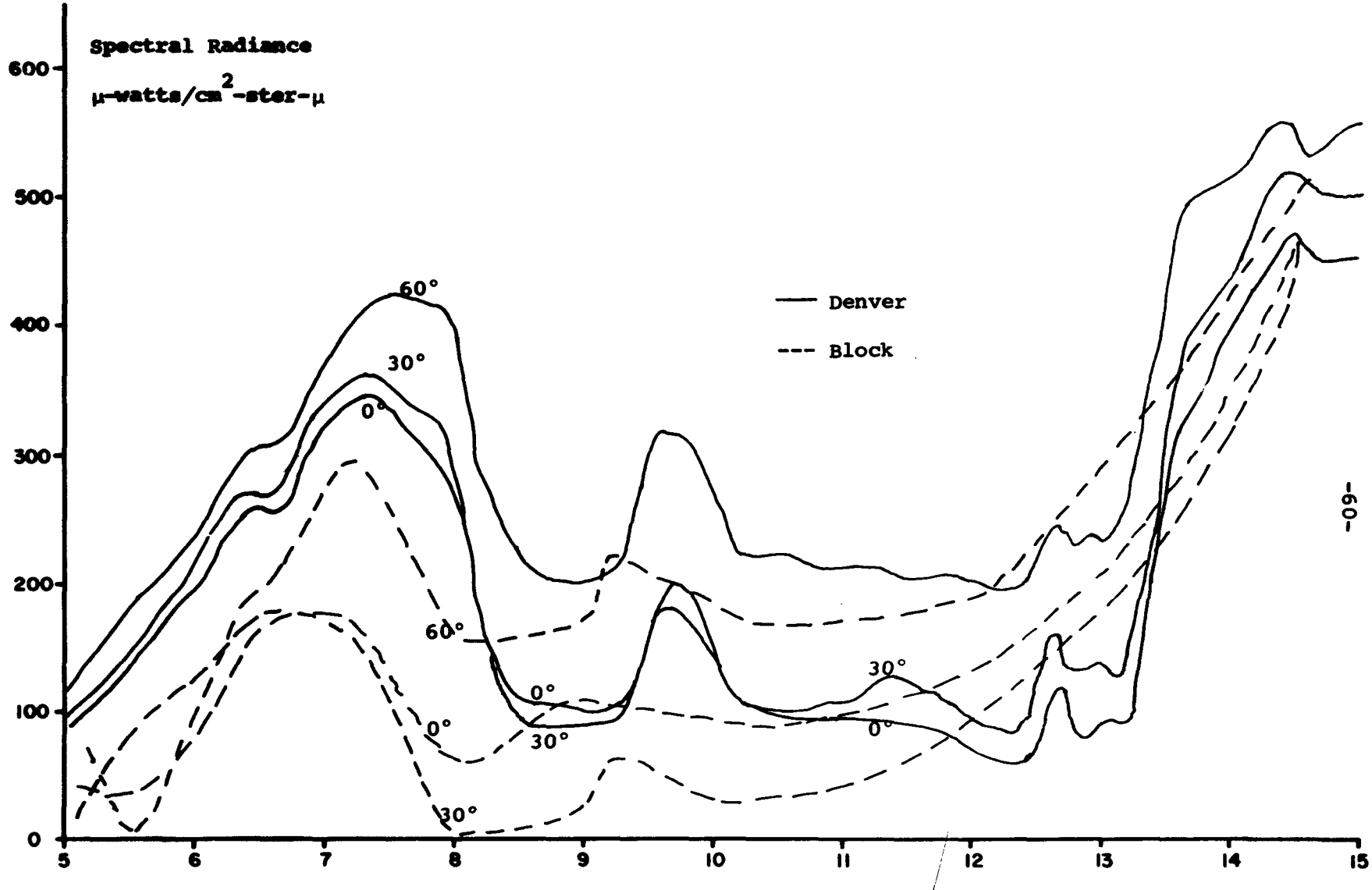

Figure 20
Clear Sky at Various
Zenith Angles

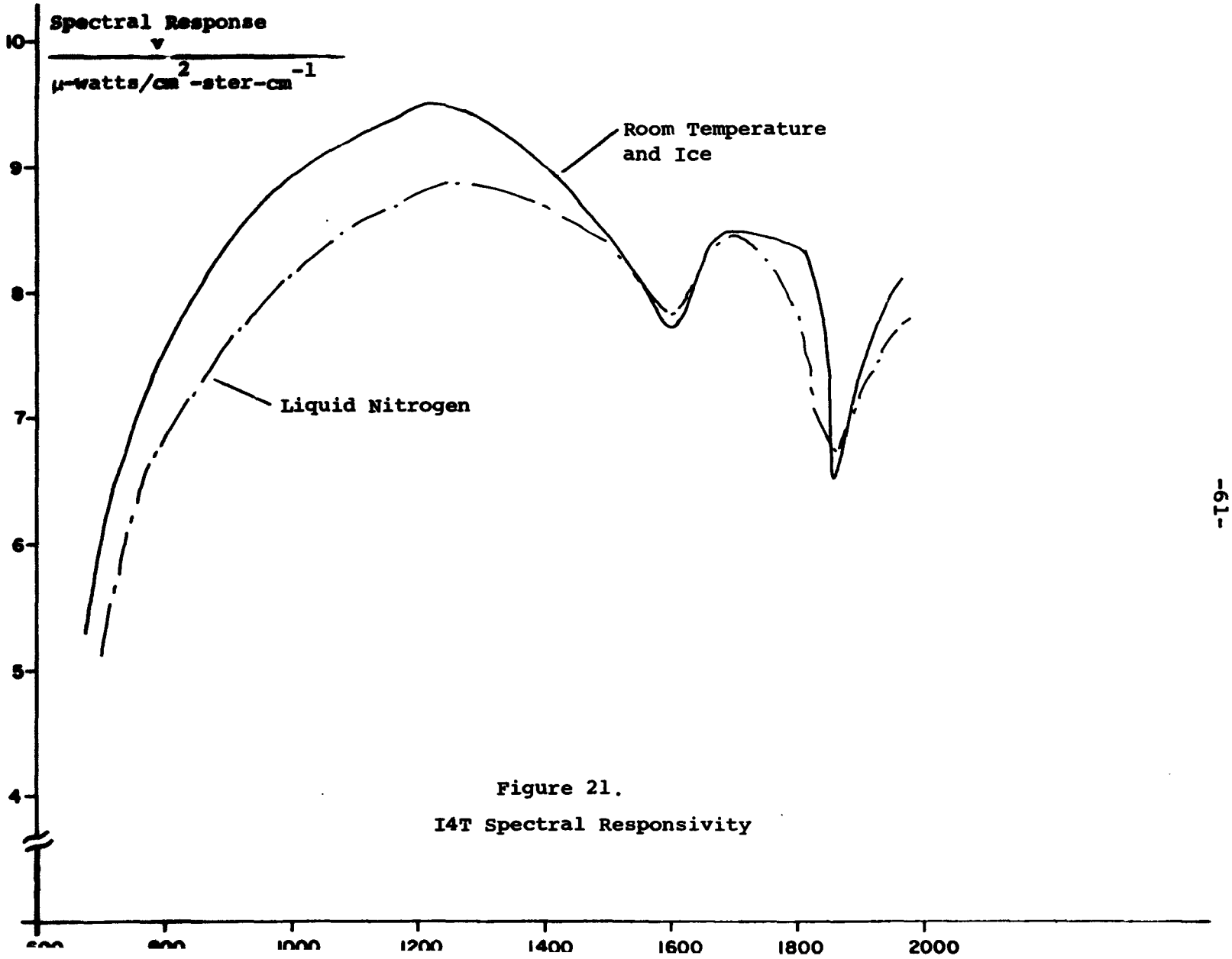

Figure 21.

I4T Spectral Responsivity

6.0 In-House Calibration

As a result of the experience gained at Eppley and Denver the following calibration procedure was adopted.

6.1 Wavelength

6.1.1 Sources

Since the instrument produces an output that is linear in wavenumber (or frequency), the treatment of wavelength calibration is relatively simple. A convenient method for laboratory and field work is to use a soldering iron as source and place a polystyrene film of known absorption lines in front of the I4T window. Figure 22 shows the output on the graphic recorder. The soldering iron allows good coverage of the region 3 to 15 microns without any problem of saturating the instrument since it does not fill the field of view. Information on the resolution of the instrument can also be obtained from some of the closely spaced absorption lines of the polystyrene.

The emission and absorption lines of gases can also be used as well as interference filters in front of hot sources. However, one is generally limited to shorter wavelengths in the infrared by these methods.

6.1.2 Frequency Conversion

What we are trying to relate in the wavelength calibration is the audio frequencies of the interferogram as read on the wave analyzer to the wavenumbers of incident radiation. This relationship is given in the equation

$$f = 10^{-4} \cdot \frac{B}{T} \nu \qquad (1)$$

where f is the audio frequency, B is the light path retardation

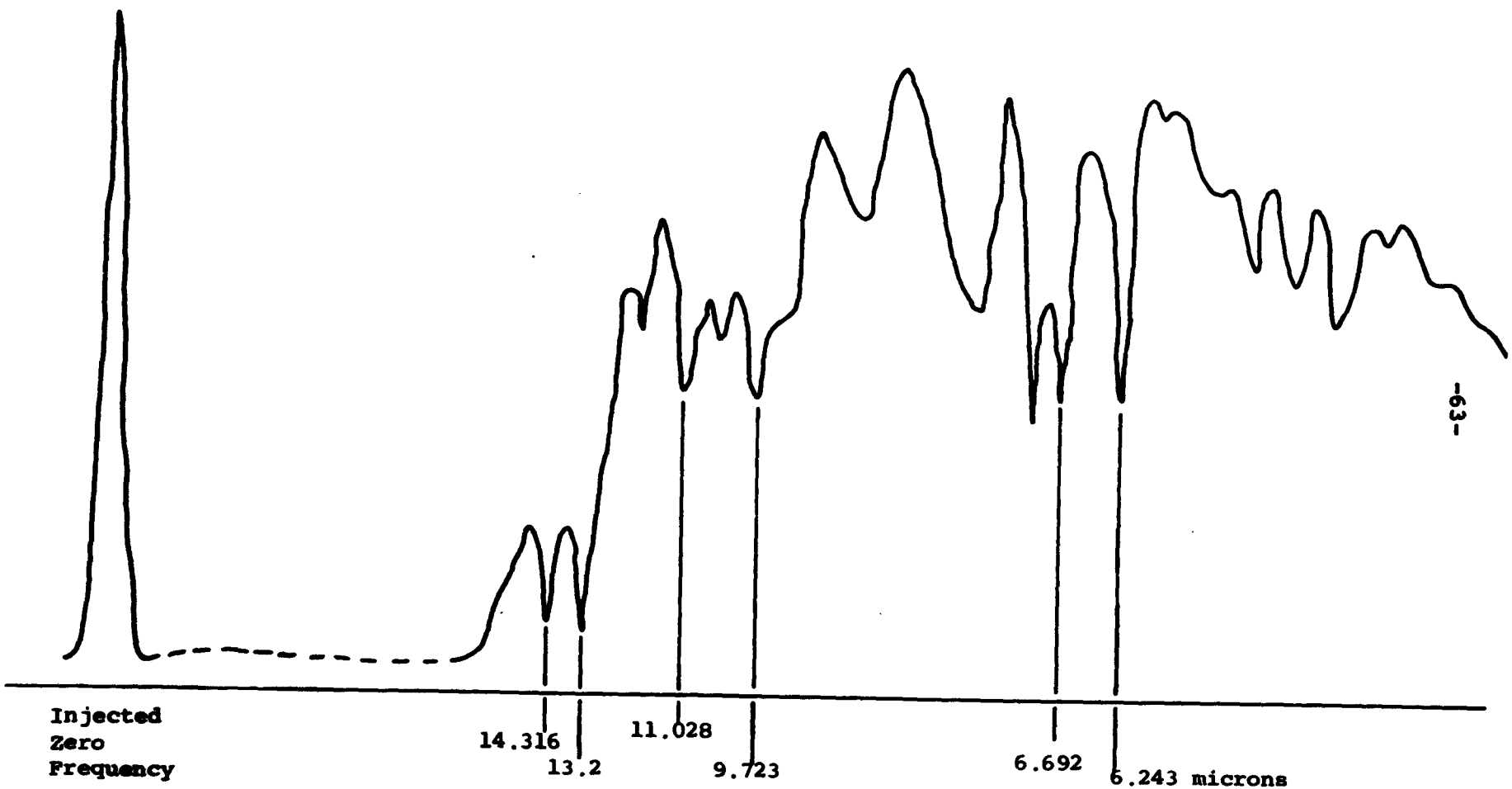

Figure 22.
Typical Polystyrene Spectrum

(twice mirror travel in microns), T is the time of the ramp on the sawtooth generator in seconds and ν is the wavenumber of the radiation.

For example, if 75 cps on the wave analyzer corresponds to the 6.692 micron absorption dip (1494 cm^{-1}), B/T equals 500. The audio frequency would read 300, rather than 75, since there is a factor of 4 on tape playback. Therefore Eq. (1) should be modified to

$$\frac{f}{p} = 10^{-4} \frac{B}{T} \nu \qquad (2)$$

where p is the playback to record ratio.

T can easily be measured separately if desired by examining the output of the sweep generator. Taken in conjunction with B/T, the retardation B can also be obtained.

Given the ratio B/T, p and the zero frequency injected by the wave analyzer, it is then possible to construct an overlay of vertical lines giving the frequency to wavenumber (or wavelength) conversion to apply to subsequent chart recordings.

It was found advisable to perform this wavelength calibration from time to time, depending on the use and shocks the instrument is subjected to as the magnet of the transducer may tend to lose gauss and lower the value of B. It should be noted that before each flight the instrument was realigned optically to insure maximum resolution. Care was also taken to correct for frequency drift in the wave analyzer, as this was found to be a source of some of the inaccuracies in the Denver measurements.

6.1.3 Accuracy and Precision of Wavelength Calibration

The accuracy and precision of the wavelength calibration was determined by taking two polystyrene absorption spectra using

a soldering iron as source. (A typical polystyrene spectra as seen on the Varian is shown in Figure 22.) The wavelength calibration data for the second balloon flight of the I4T is presented in Table I.

Table I

Wavelength Calibration Data

λ, microns	ν, cm^{-1}	f, cps	Run #1 $\frac{f}{\nu}$ $\frac{cps}{cm^{-1}}$	f, cps	Run #2 $\frac{f}{\nu}$ $\frac{cps}{cm^{-1}}$	Ave.(
14.32	698	145	2080	147	2113	2097
13.15	760	159	2088	161	2115	2102
11.03	905	194	2143	194	2114	2129
9.72	1030	220	2128	218	2118	2123
8.56	1169	250	2140	248	2124	2132
7.22	1388	291	2100	291	2100	2100
6.90	1450	314	2162	310	2138	2150
6.69	1497	324	2165	320	2140	2153
6.24	1604	337	2100	337	2100	2100
5.55	1801	383	2122	383	2122	2122

The average of all the f/ν for Run #1 is the value which was used as the wavelength calibration. The accuracy of this wavelength calibration is found by comparing f/ν at a specific wavelength with the average. The average for Run #1 is 2123 cps per cm^{-1}. The maximum deviation from the average was 43 cps per cm^{-1} and occurre at both 14.32μ and 6.69μ. This deviation indicates that the accuracy in wavelength calibration at any wavelength is equal to or better than $\pm 2\%$. The average error over the entire spectral region was $\pm \frac{1}{2}\%$.

To determine the precision of the wavelength calibration the second measurement, Run #2, was made some 20 days after Run #1.

The wavelength calibration determined from this run was 2128 cps per cm^{-1}, which differs from the Run No. 1 calibration by 1/4%.

6.2 Field of View

The field of view was determined by mounting the optical head on a small indexing table. A small soldering iron was used and was positioned so as to be a point source. It can be seen from Figure 23 that the acceptance angle is greater for shorter wavelengths. This is attributable to the dispersion in the KRS-5 lenses which causes long wavelengths at extreme acceptance angles to focus outside the thermistor bolometer flake. With extended sources, this difference is accounted for in the spectral response curve of the instrument.

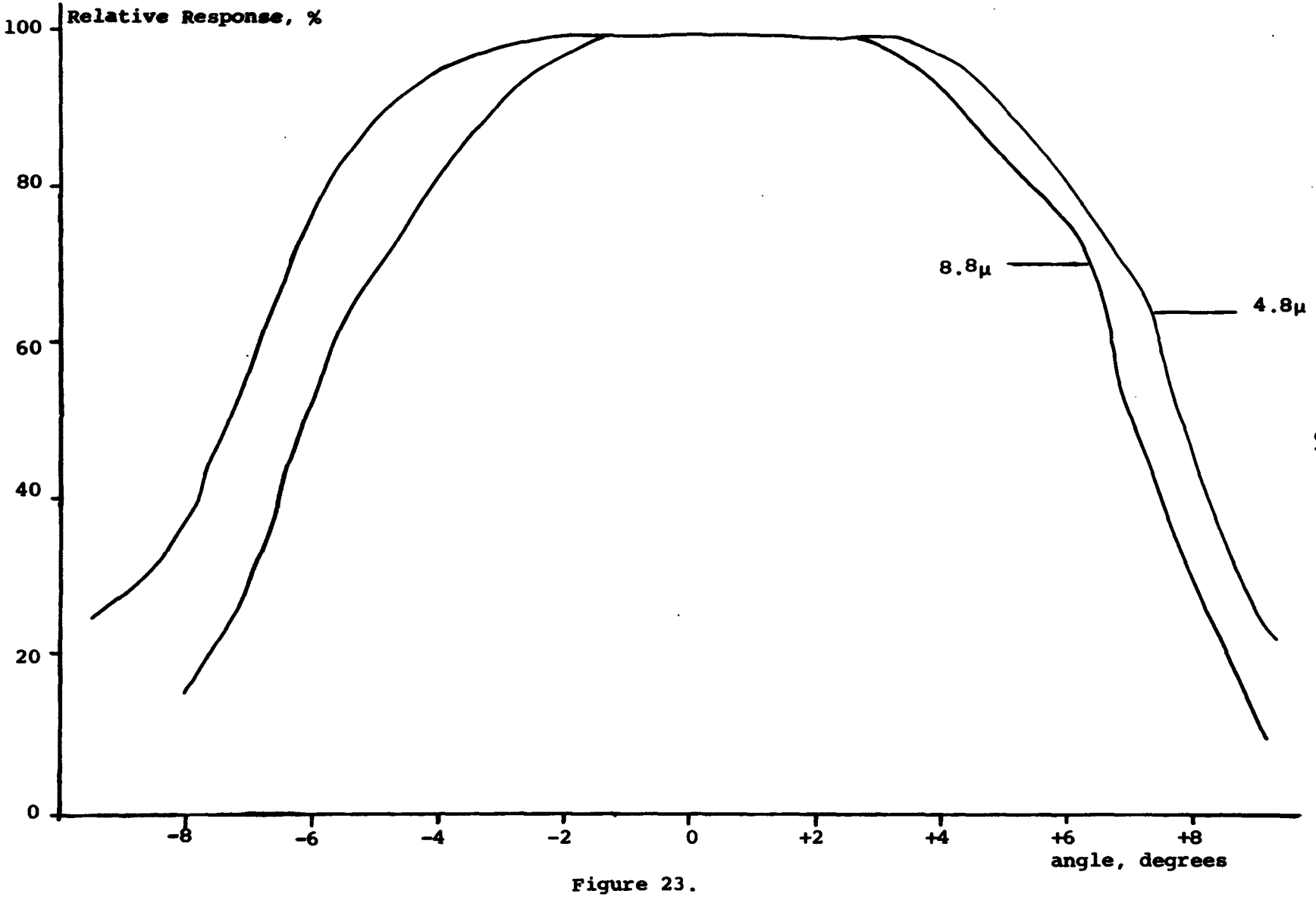

Figure 23.
I4T Field of View

6.3 Spectral Responsivity

6.3.1 Procedure

In order to obtain absolute radiance values while looking at an unknown source it is necessary to first determine the spectral radiant responsivity of the spectrometer. This is because the output signal from the spectrometer is proportional to the differential radiance between the source and some known reference such as the detector itself. We will define the proportionality constant as the spectral radiant responsivity. Thus, for a given wavelength (wavenumber) we have,

$$R = \frac{V_{1\nu}}{\Delta N_\nu} = \frac{V_{1\nu}}{N_{\nu B} - N_{\nu S}} \tag{1}$$

where $V_{1\nu}$ is the output voltage, R_ν is the spectral radiant responsivity, $N_{\nu B}$ is the spectral radiance of the detector and $N_{\nu S}$ is the spectral radiance of the source.

R_ν is determined experimentally by noting the signal out at each of several different known black-body source temperatures which, therefore, represent $N_{\nu S}$. The signal out is first interpreted as divisions on the Varian chart. The divisions are then converted to volts by means of the gain oscillator. The noise in the system is accounted for by the equation,

$$V_1^2 = V_s^2 - V_N^2 \tag{2}$$

where V_1 represents the actual signal and is the value which is used, V_s is proportional to the reading on the Varian and V_N is the noise signal. One means for determining the noise level is to take a spectrum while the instrument is looking directly at a mirror which, in effect, means that it is looking at a source whose temperature exactly equals its own.

Figure 24 shows a set of typical plots of signal out versus black-body radiance each at a specific wavenumber. The slope of each line is R_ν for that wavenumber. The points where the R_ν line crosses the abscissa give the values of $N_{\nu B}$.

It should be noted that since the responsivity of the detector (a thermistor bolometer) is somewhat a function of its temperature each set of response curves is valid for only one detector temperature.

In order to determine the magnitude of this effect several responsivity measurements were made at different bolometer temperatures using the I4T. The first step was to calibrate the detector thermistor bead output versus temperature. Since there is a temperature gradient between this bead and the detector flake, the curve was then modified by using the $N_{\nu B}$ points for bolometer temperature. The final plot of bolometer temperature versus thermistor bead output is shown in Figures 25 and 26. Next, the spectrometer and the radiation source, an aluminum cone, were placed in an evacuated chamber (see Figures 27 and 28). The inside of the cone was painted with Parsons Black, and nine thermocouples were imbedded on its outside surface. The combination of paint and conical geometry provided an emissivity better than 0.99. The entrance of the cone was placed so as to fill the field of view of the instrument.

The temperature of the cone was controlled by the temperature of the chamber itself, and the bolometer was held at the points of interest by a heater surrounding the optical head. Spectra were recorded when the thermistor bead indicated the desired temperature and while all the thermocouples were within ½°C of the average thermocouple reading. Using an evacuated chamber facilitated measurements in the absorption regions of water vapor and carbon

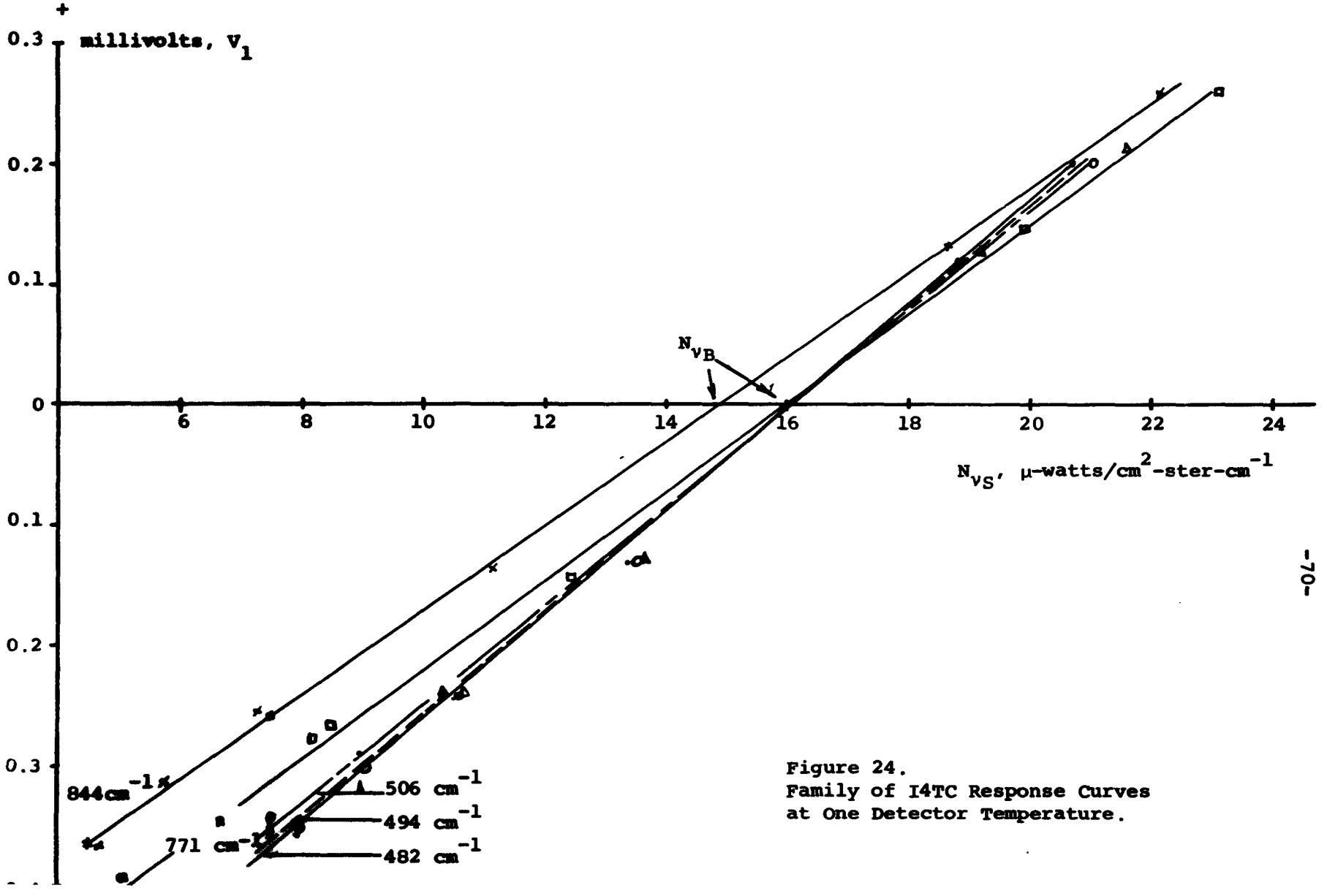

Figure 24.
Family of I4TC Response Curves
at One Detector Temperature.

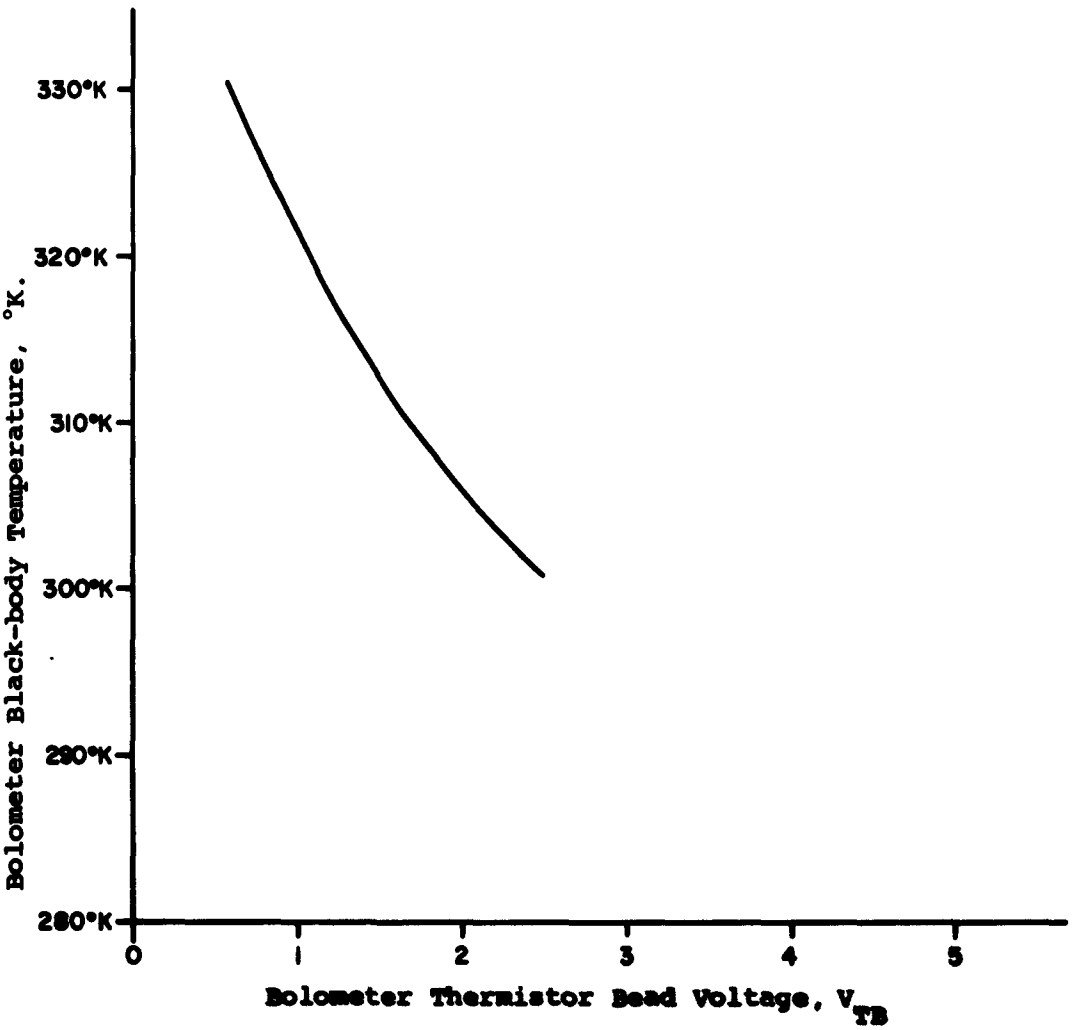

Figure 25.

I4T Bolometer Black-body Temperature Vs. Thermistor Bead Voltage

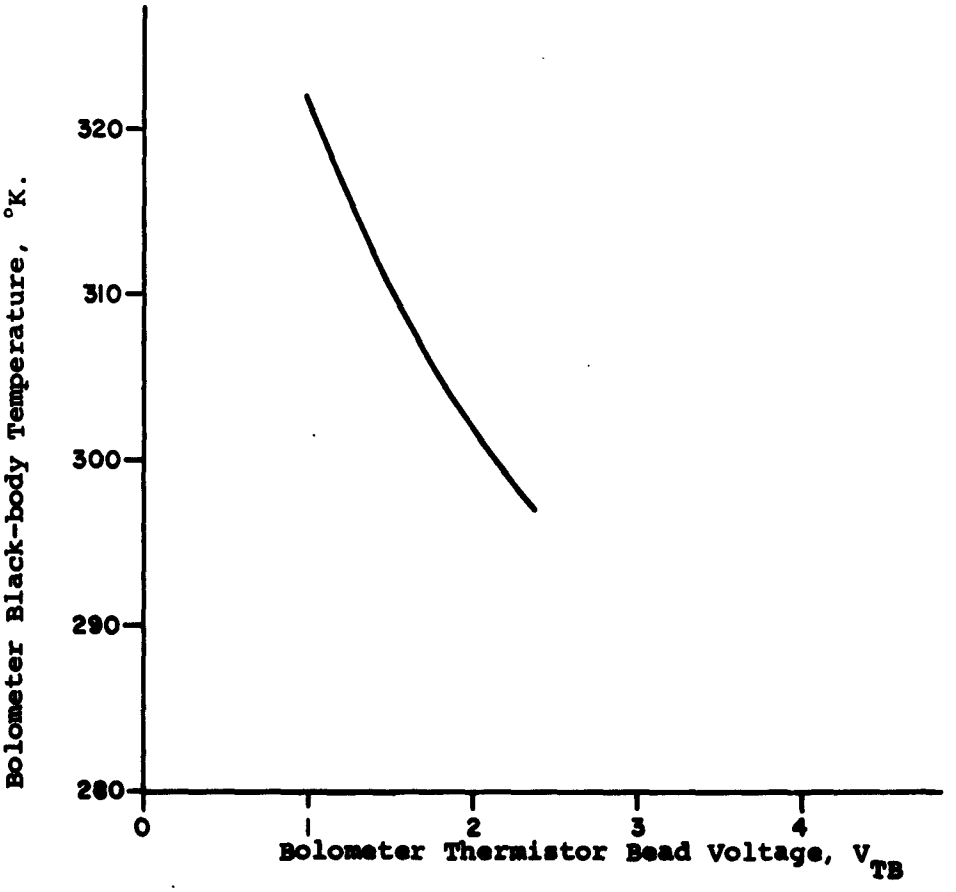

Figure 26.

I4TC Bolometer Black-body Temperature Vs. Thermistor Bead Voltage

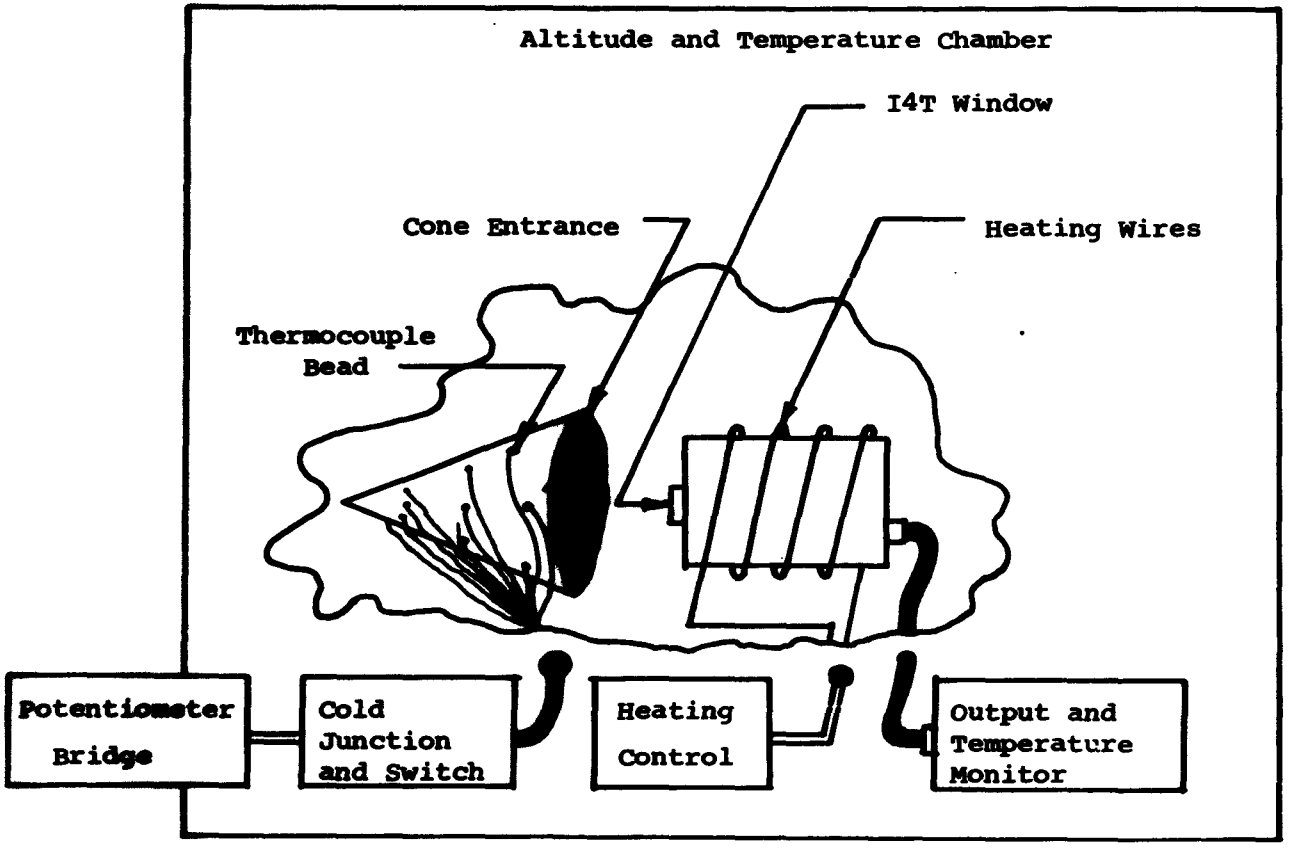

Figure 27.
Set Up For Response Measurements

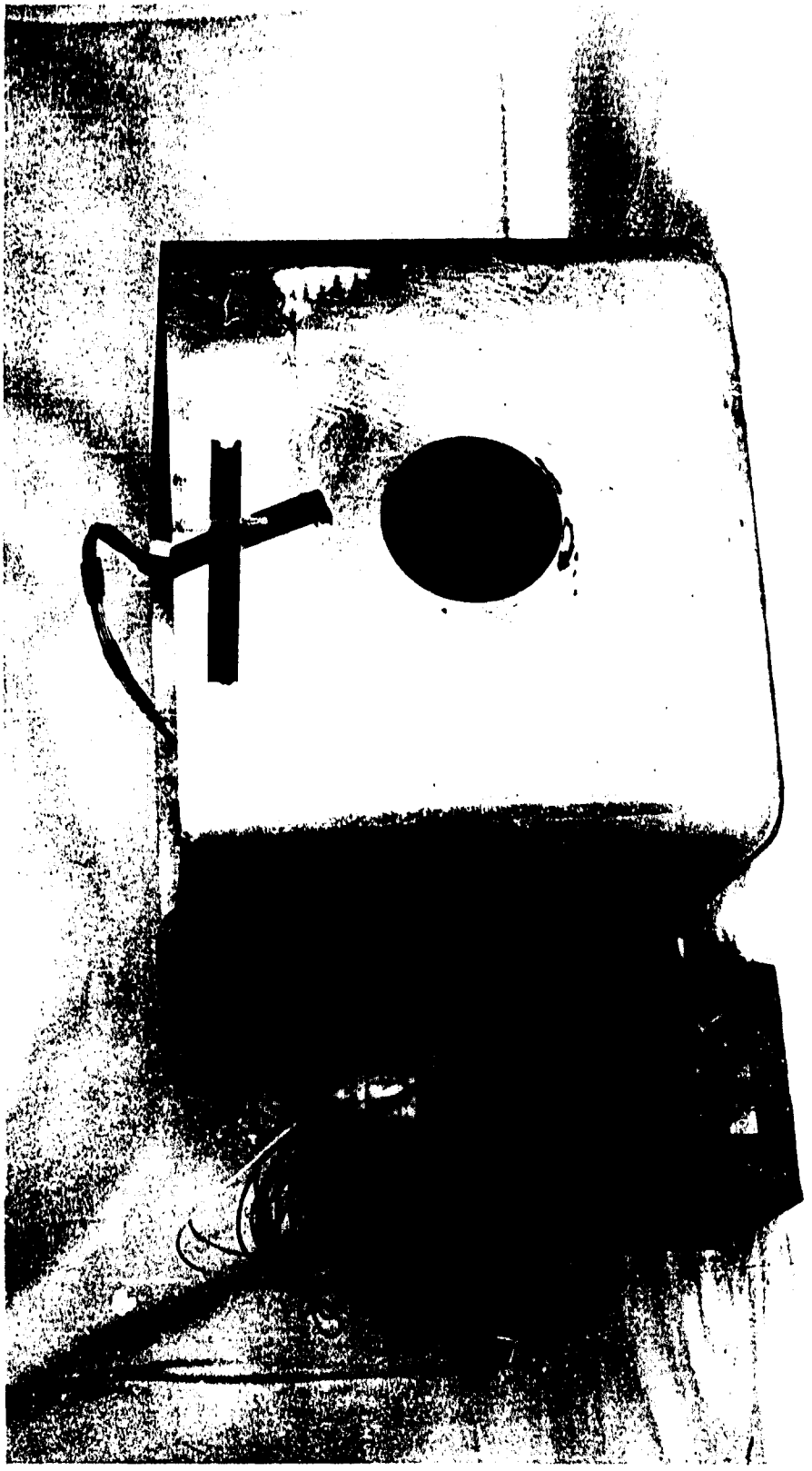

Figure 28.
Calibration Source.

dioxide. Figures 29 through 32 show the various spectral response curves determined by this method.

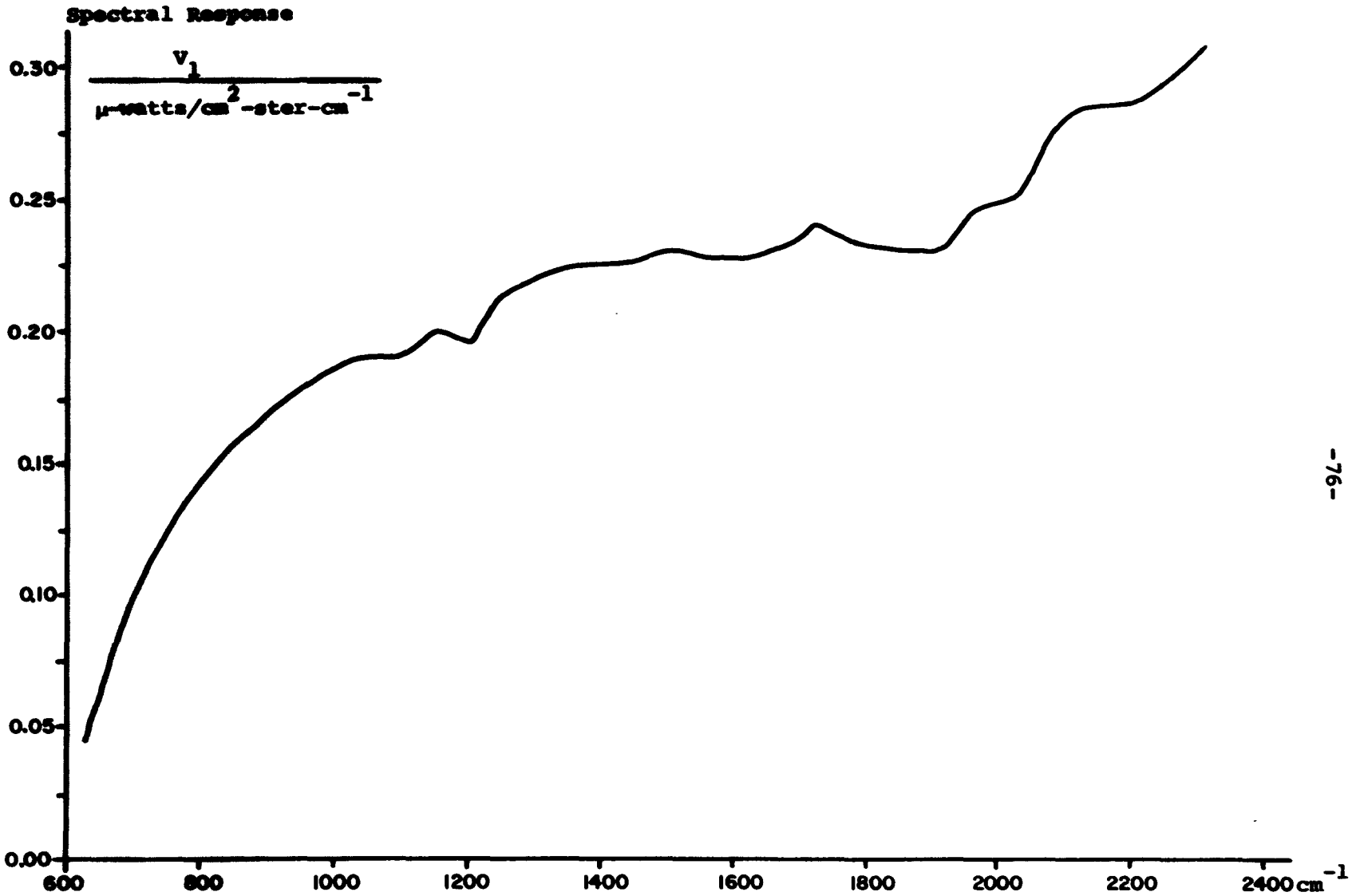

Figure 29.
I4T Spectral Response - Flight No. 1

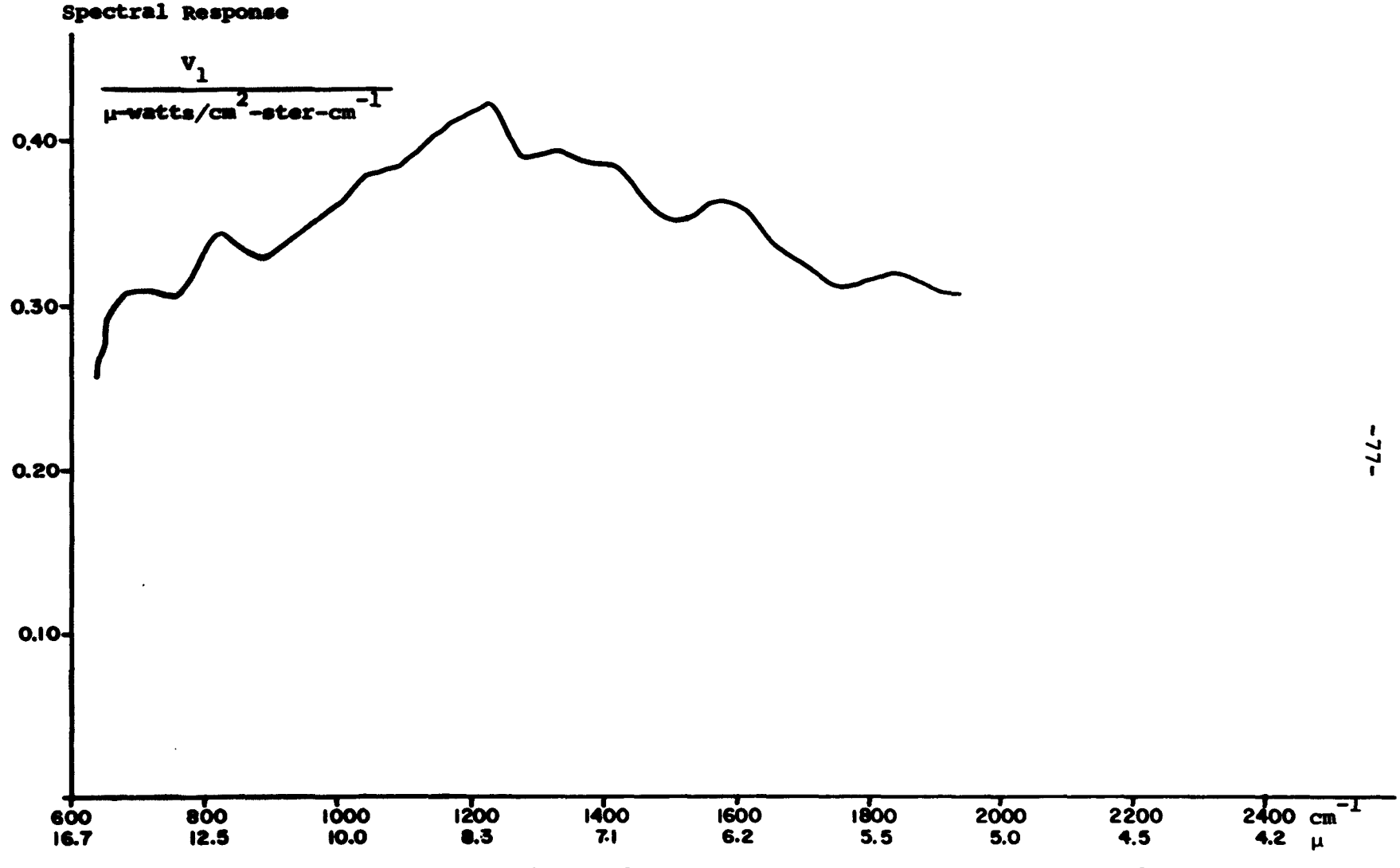

Figure 30.
I4T Spectral Response - Flight No. 2
V = 1.50 volts

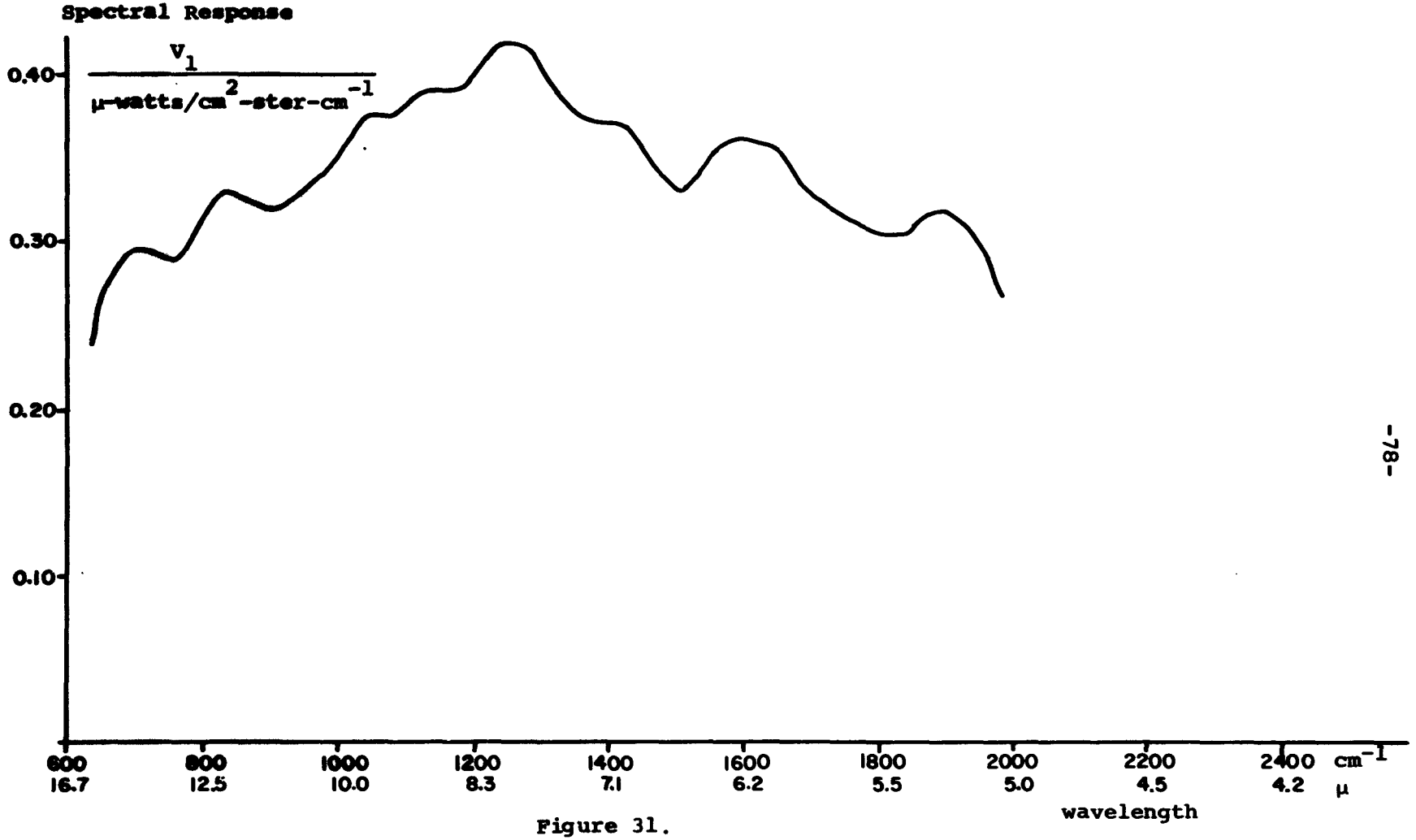

Figure 31.
I4T Spectral Response - Flight No. 2
V_{TB} = 1.75 volts

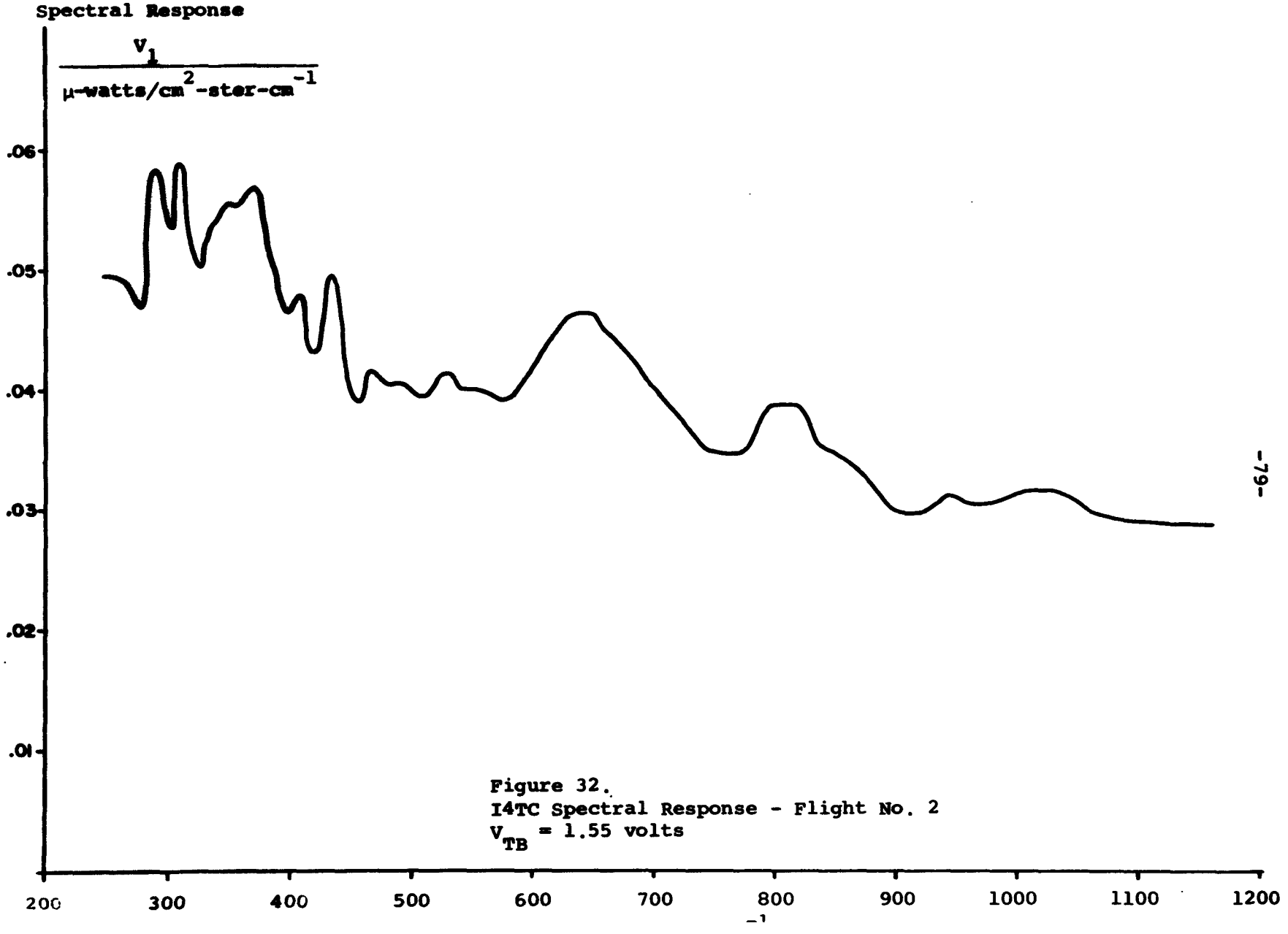

Figure 32.
I4TC Spectral Response - Flight No. 2
V_{TB} = 1.55 volts

6.3.2 Discussion of Results

Comparison of Figures 30 and 31 shows that the responsivity would increase 5% for a 3°C decrease in temperature. The shape of the curve remains the same, however.

The difference in the shapes of Figures 29 and 30 (I4T - Flight #1 and I4T - Flight #2) was caused by a better noise estimate used for the Flight #2 responsivity data. Since the temperatures of interest are relatively low the amount of energy both from the source and the detector is low at the short wavelengths and, thus, the noise estimate becomes increasingly more important for wavelengths in the vicinity of 6μ.

The general shape of the curves as well as the dips and peaks shown are a result of several factors including the emissivity of the detector, emissivity of the optical elements in the cube, the reflective properties of the dielectric coating on the beamsplitter as well as the frequency response of the signal amplifiers. In addition, the low frequency characteristics of the tape recorder used for recording data can effect the response at the longer wavelengths (15μ for the I4T and 40μ for the I4TC).

The amplitude of the response curves is dependent not only on the electronic gain of the signal amplifiers but also on the amplitude of the gain oscillator which is used as a signal reference for both calibration data and flight data.

6.3.3 Accuracy and Precision

In order to estimate the amplitude precision of the interferometer system three separate spectra were taken by the I4T while the instrument and radiation source temperatures were maintained constant. Each spectrum was recorded on tape and the data was reduced in the normal manner. The data, presented in Table I, indicates that the average precision over the entire spectral region was $\pm 2\%$.

In order to estimate the contribution of the data reduction system to the overall precision the spectrum recorded on one tape loop was processed three times to determine the precision of the data reduction system alone. This data is presented in Table II and indicates an average precision of $\pm 1\%$.

As a check on interferometer system accuracy, the voltage outputs at each calibration source temperature were compared to what would be expected using the slope of the response curve which they generated. Over the 6μ to 15μ spectral range, the average deviation was $\pm$ 6%.

It should be noted that while both the precision and accuracy measurements were made using the I4T, we would expect the results to hold true for the I4TC as well.

Table I

I4T Precision Measurement

Source Temperature = 239°K

Detector Temperature = 310°K

V, cm^{-1}	V Run#1	V Run#2	V Run#3	% Error	V, cm^{-1}	V Run#1	V Run#2	V Run#3	% Error
660	3.24	3.20	3.26	±1	1085	3.06	3.04	3.04	≈ 0
684	3.28	3.32	3.39	±1½	1132	2.98	2.98	2.96	≈ 0
708	3.28	3.32	3.32	±½	1179	2.82	2.80	2.82	≈ 0
731	3.24	3.28	3.37	±2	1226	2.72	2.72	2.72	≈ 0
755	3.24	3.28	3.35	±1½	1274	2.34	2.28	2.33	±1½
778	3.41	3.44	3.48	±1	1321	2.12	2.04	2.13	±2
802	3.62	3.60	3.61	±½	1368	1.83	1.76	1.85	±2
825	3.62	3.60	3.70	±1½	1415	1.66	1.60	1.66	±2
849	3.53	3.48	3.61	±2	1462	1.40	1.24	1.37	±8
896	3.28	3.32	3.37	±1½	1509	1.19	1.12	1.22	±4½
943	3.37	3.32	3.37	±1	1557	1.11	1.00	1.17	±8
991	3.37	3.32	3.37	±1	1604	0.98	0.88	1.04	±8
1038	3.24	3.24	3.30	±1	1651	0.81	0.72	0.87	±9

Table II

Data Reduction System Precision

V,cm^{-1}	V Run a	V Run b	V Run c	% Error	V,cm^{-1}	V Run a	V Run b	V Run c	% Error
660	3.47	3.44	3.47	$\pm\frac{1}{2}$	825	3.39	3.88	3.96	±1
684	3.58	3.50	3.53	±1	849	3.87	3.79	3.83	±1
708	3.53	3.50	3.53	≈0	896	3.58	3.56	3.58	≈0
731	3.53	3.50	3.53	≈0	943	3.62	3.62	3.64	≈0
755	3.53	3.56	3.58	±1	991	3.58	3.59	3.62	$\pm\frac{1}{2}$
778	3.76	3.74	3.76	≈0	1038	3.53	3.54	3.53	≈0
802	3.93	3.91	3.93	≈0	1085	3.30	3.34	3.41	$\pm1\frac{1}{2}$
1132	3.36	3.22	3.18	$\pm2\frac{1}{2}$	1415	1.79	1.72	1.74	$\pm1\frac{1}{2}$
1179	3.01	2.99	2.95	±1	1462	1.45	1.38	1.39	$\pm2\frac{1}{2}$
1226	2.89	2.88	2.89	≈0	1509	1.27	1.27	1.27	0
1274	2.49	2.48	2.49	≈0	1557	1.21	1.20	1.16	±2
1321	2.20	2.18	2.20	$\pm\frac{1}{2}$	1604	1.10	1.09	1.10	$\pm1\frac{1}{2}$
1368	1.91	1.90	1.91	≈0	1651	0.87	0.89	0.87	±1

7.0 Balloon Flights

7.1 Flight #1

7.1.1 Description of Flight

The purpose of flight #1 was to obtain data on the upward atmospheric radiance utilizing both the I4T and the University of Denver's prism spectrometer. In addition four experimental frost-point hygrometers built by Minneapolis-Honeywell were being flight tested. The gondola, battery power supply and telemetry system were furnished by the University of Denver who also were in over-all charge of the flight.

The telemetry channels used are as follows:

1.	I4T Interferogram	40 KC	±7½%
2.	I4T Commutator	1.3 KC	±7½%
3.	University of Denver Spectrometer	2.3 KC	±7½%
4.	University of Denver Spectrometer	3.9 KC	±7½%
5.	Minneapolis Honeywell	7.35KC	±7½%
6.	Minneapolis Honeywell	14.5 KC	±7½%

The launching had been originally scheduled for 0300 hours, 5 April 1962, from a runway at Holloman Air Force Base, New Mexico. However, at 0250 hours the Holloman command package developed battery trouble and was removed, postponing the launch. The launch was at 0348 hours. The trajectory as supplied by Holloman and the temperature profile supplied by Rawinsonde probes are shown in the Appendix.

When the balloon had reached an altitude of approximately 20,000 feet M.S.L., it was observed in the telemetry recording van that the interferograms appeared to cease at a time coincident with a series of voltage spikes picked up by both the Denver and Minneapoli

Honeywell equipment aboard the gondola, which could not be accounted for. In addition, the input voltage to the I4T from the battery supply had dropped from 28 volts down to 24 volts which is the absolute minimum acceptable voltage. As a result, the operation of the electronics became very erratic, and the interferometer ceased to function.

An examination of the thermistor bead voltage from the commutator showed the I4T electronics to be above its normal operating temperature. When the package was recovered and examined, it was found that a resistor in the power input circuit had become open circuited. Although the reasons for this failure are not well known it may have been caused by either higher than expected temperatures surrounding the electronics and/or low frequency supply voltage surges. Although the Block instrumentation had undergone extensive simulated environmental tests, the complete gondola package including the other experimental instruments, telemetry transmitter, command package, and styrofoam insulation, had not been subjected to any environmental tests, due to the difficulty in obtaining a test chamber large enough to accomodate the bulky gondola. Such tests might have indicated the reason for the high temperature of the electronics. It should be noted that since the telemetry checkout van had left the launch site an hour before the actual launch, the increase in temperature could not be discovered until after the balloon had left the ground.

7.1.2 Discussion of Flight Results

The data obtained by the I4T is presented in Figures 33 through 38. In addition, the applicable Denver data, plotted in ½ micron increments, is presented on Figure 34 and Figure 38.

The significant differences between the two instruments are twofold. First, the scan rate is approximately three minutes for the Denver instrument and is, effectively, 12 seconds for the I4T and thus it is not possible to present data from both instruments at exactly the same altitude. And second, the resolution in microns varies inversely; that is, the resolution of the Denver instrument improves towards longer wavelengths while the resolution of the I4T improves towards shorter wavelengths. As a result each instrument might see absorption bands which the other could not (a graph of $\Delta\lambda$ vs. λ for $\Delta\nu = 40\ cm^{-1}$ is presented in the Appendix).

The data indicates reasonable agreement between the two instruments in both the 6.3μ water vapor region and in the 10μ window region although the I4T tends to be 5 to 10% higher. In addition the data is consistent with the Rawinsonde data which indicates a ground temperature of 10°C.

The largest difference in data occurs at the 15 micron CO_2 band. Using a method described in Section 7.2 the Rawinsonde data was used to determine theoretical values of radiance for this region as seen by an "observer" at 12,600 feet. As is seen in Figure 38 both instruments deviated an equal amount from this theoretical.

Assuming a balloon ascent rate of 600 feet per minute we can hypothesize that perhaps the Denver data at 15μ corresponds to either 14,100 feet or 10,500 feet rather than 12,300 feet.

We find, however, that the magnitude of this effect would be less than 10% and, therefore, the difference in scan rate is most probably not contributing to the discrepancy. Since the data is presented in terms of radiance, the difference in resolution is not a factor. The only other possibility is the difference in field of view where the I-4T's is slightly larger. However, since the optical path is relatively short at 15μ, it is unlikely that the atmosphere is nonhomogeneous to the extent that the two instruments were viewing CO_2 layers at different temperatures, at least not to the extreme which the data indicates. It is evident that there is no systematic error on the part of either instrument since the data agrees at the other wavelength regions. As of the writing of this report, therefore, there is no explanation as to the difference in radiance values obtained by the two instruments in the 15μ CO_2 region.

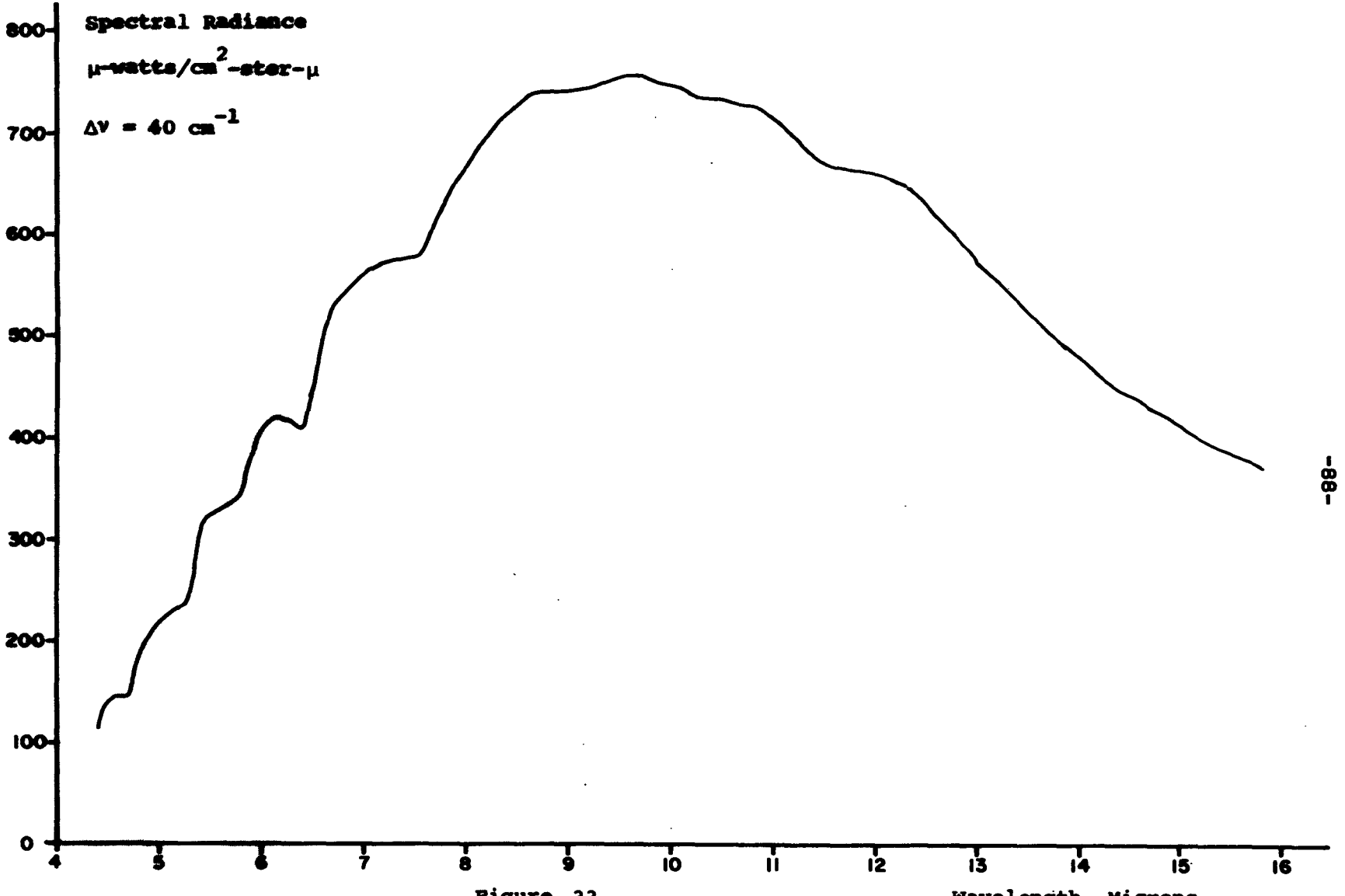

Figure 33
Upward Radiance at
4,100 feet M.S.L

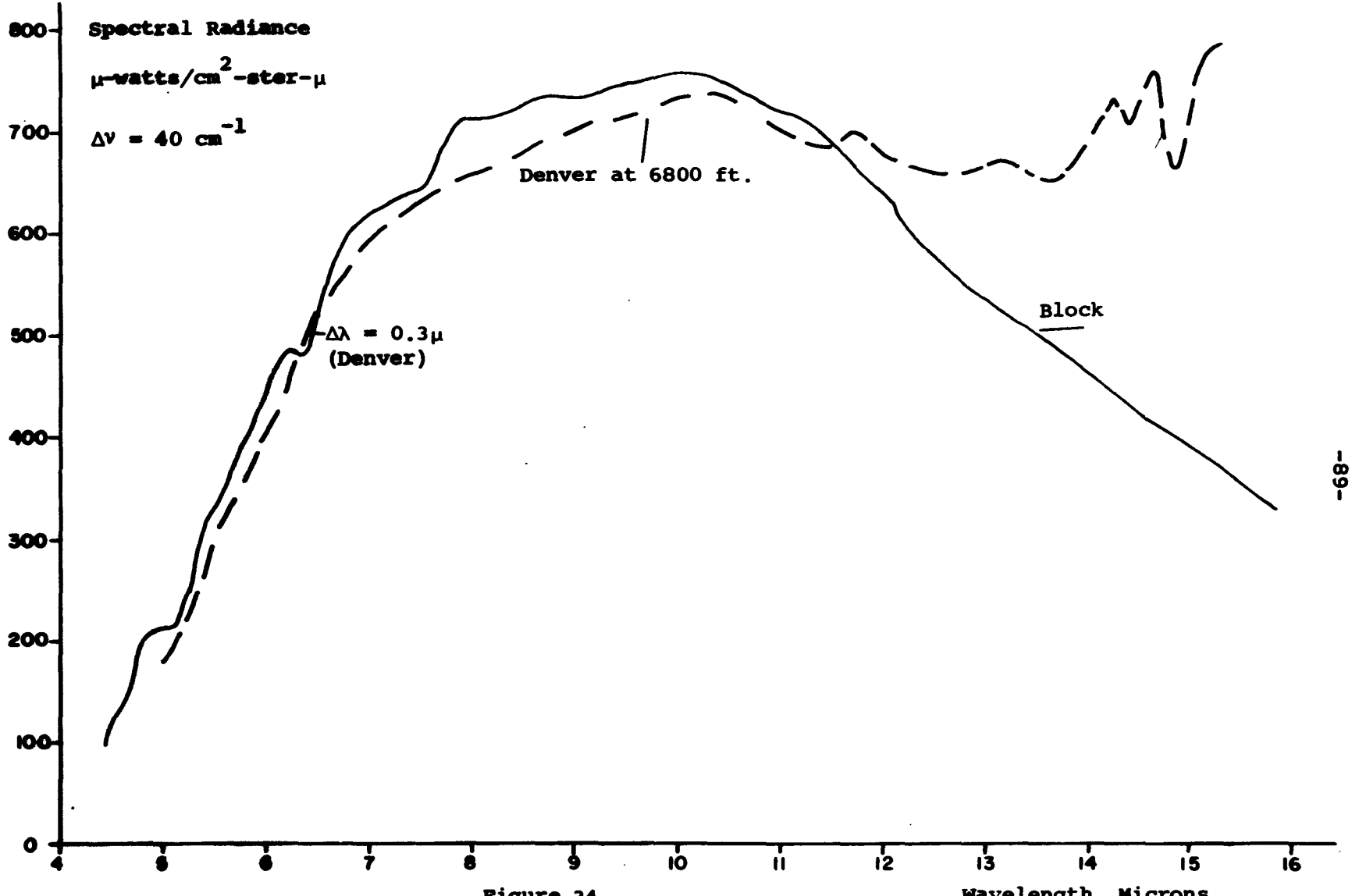

Figure 34
Upward Radiance
at 5,900 feet M.S.L.
5 April 1962

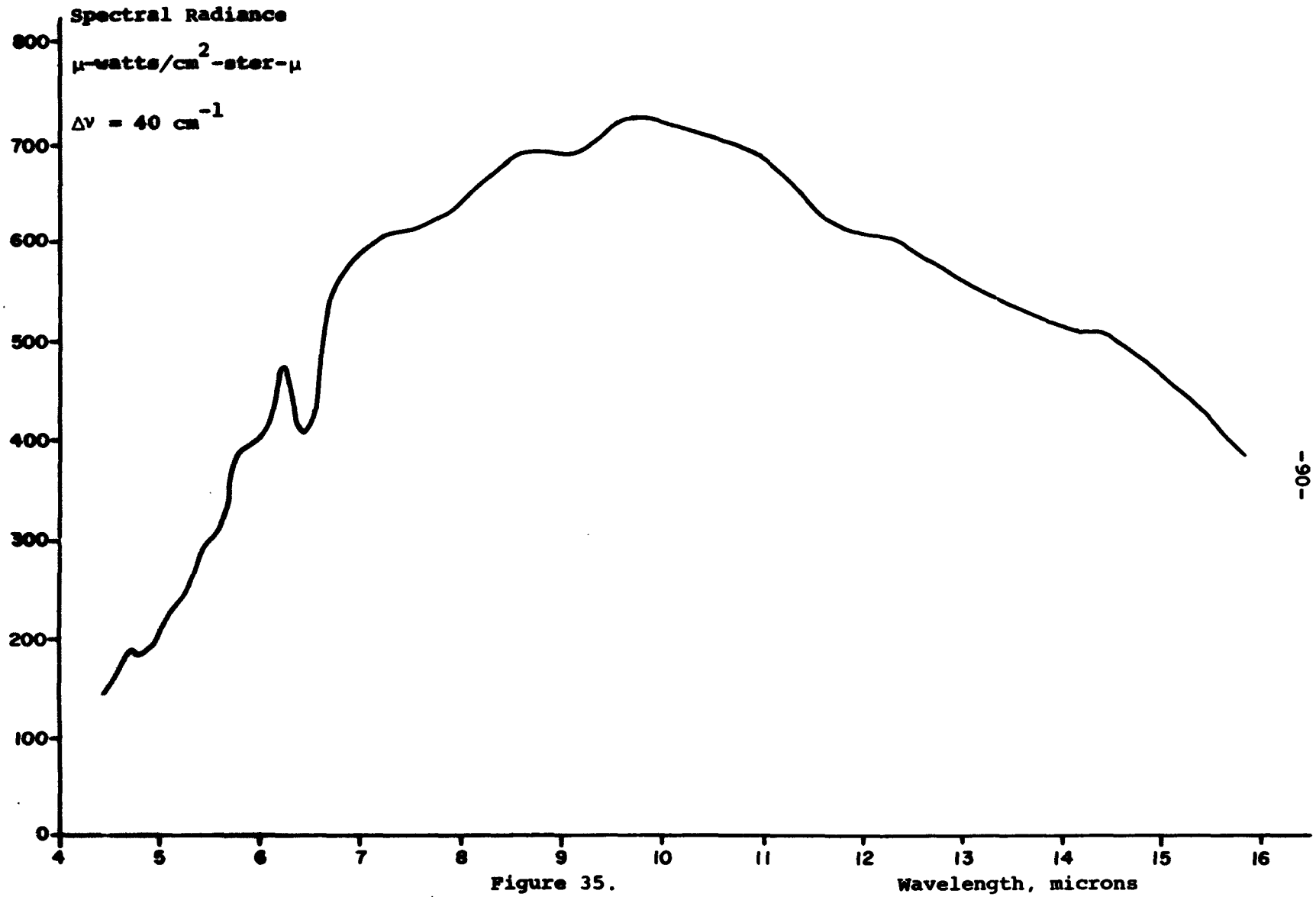

Figure 35.
Upward Radiance at
10,000 feet M.S.L.
5 April 1962

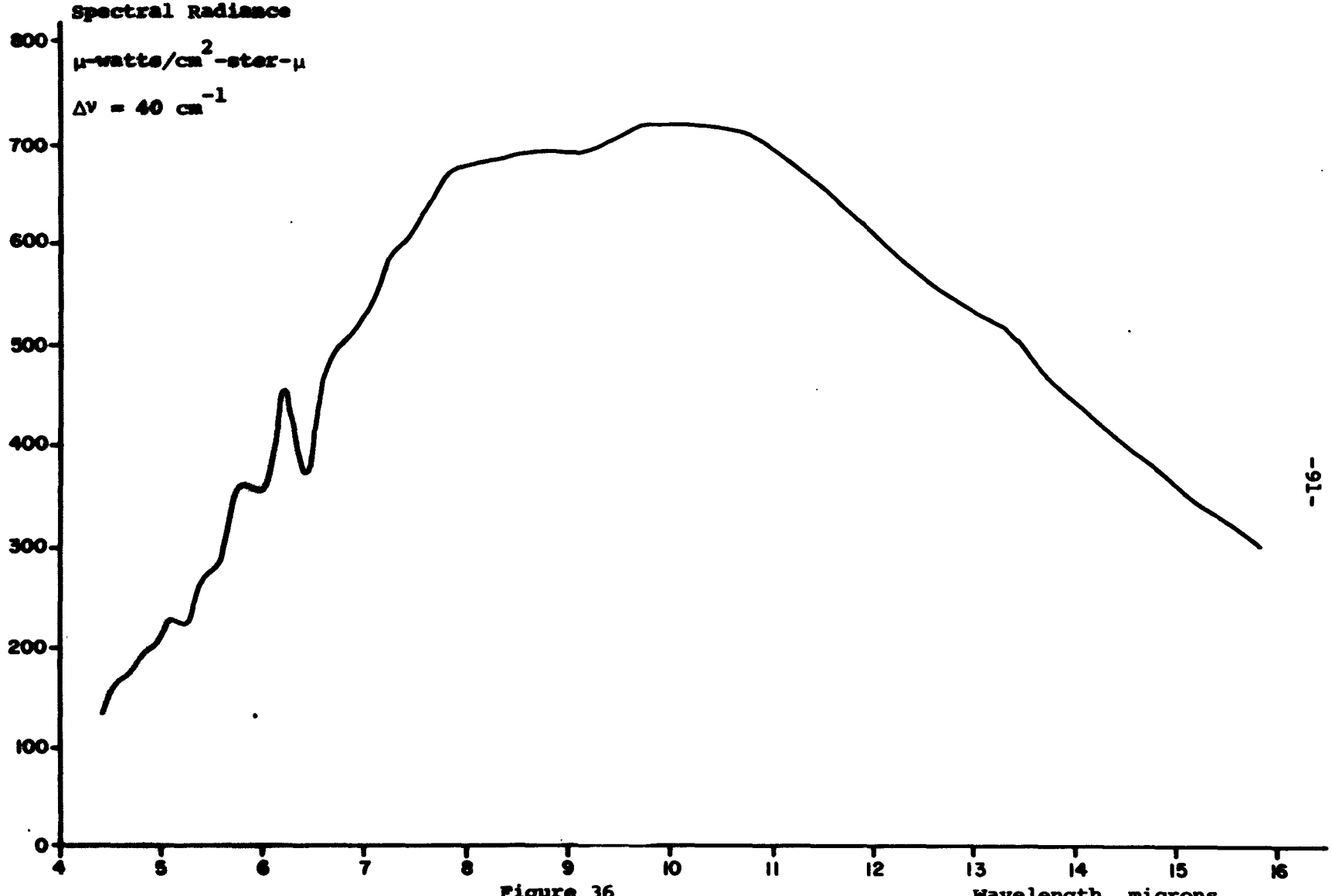

Figure 36.
Upward Radiance at
10,000 feet M.S.L.

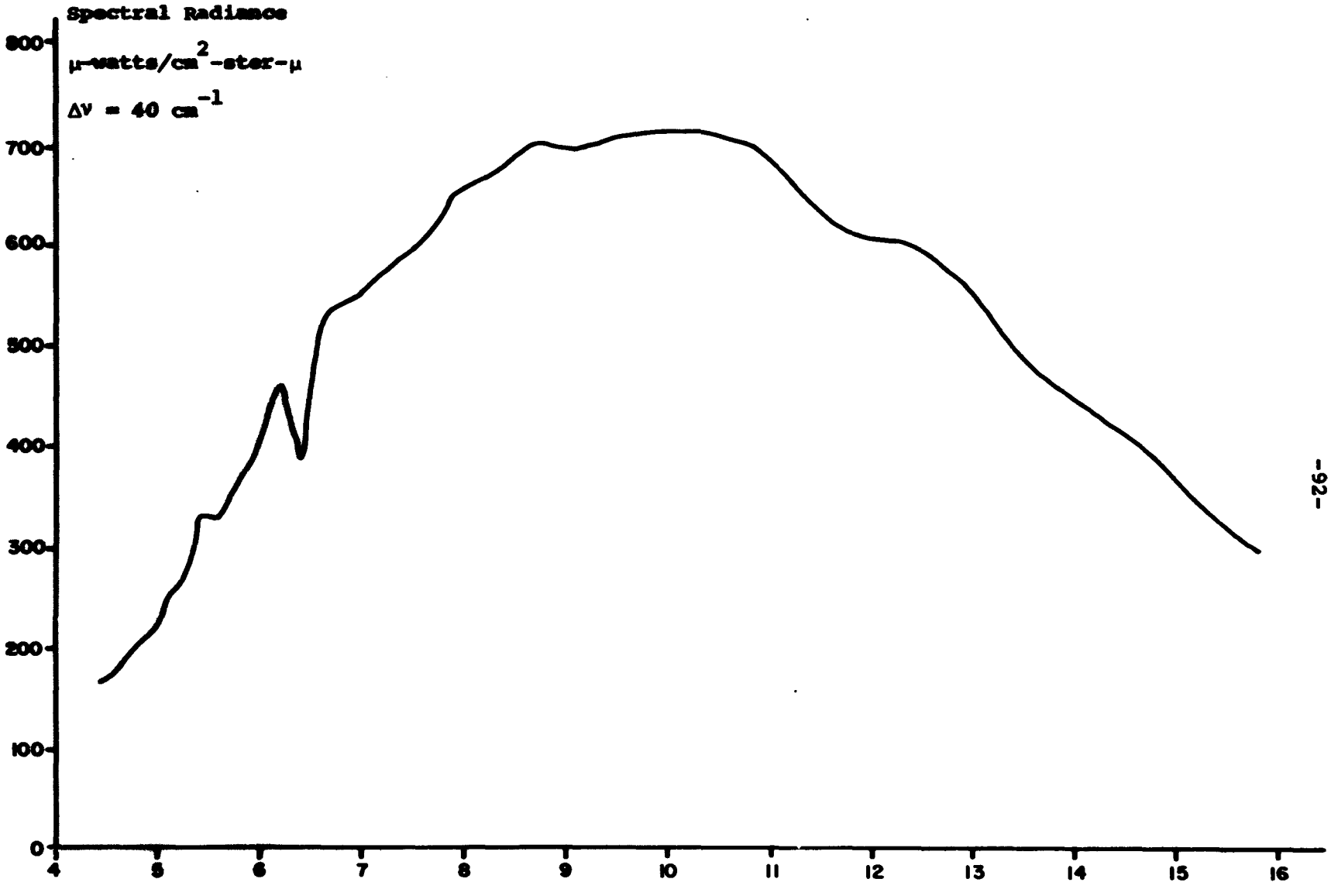

Figure 37.
Upward Radiance at
11,300 feet M.S.L.

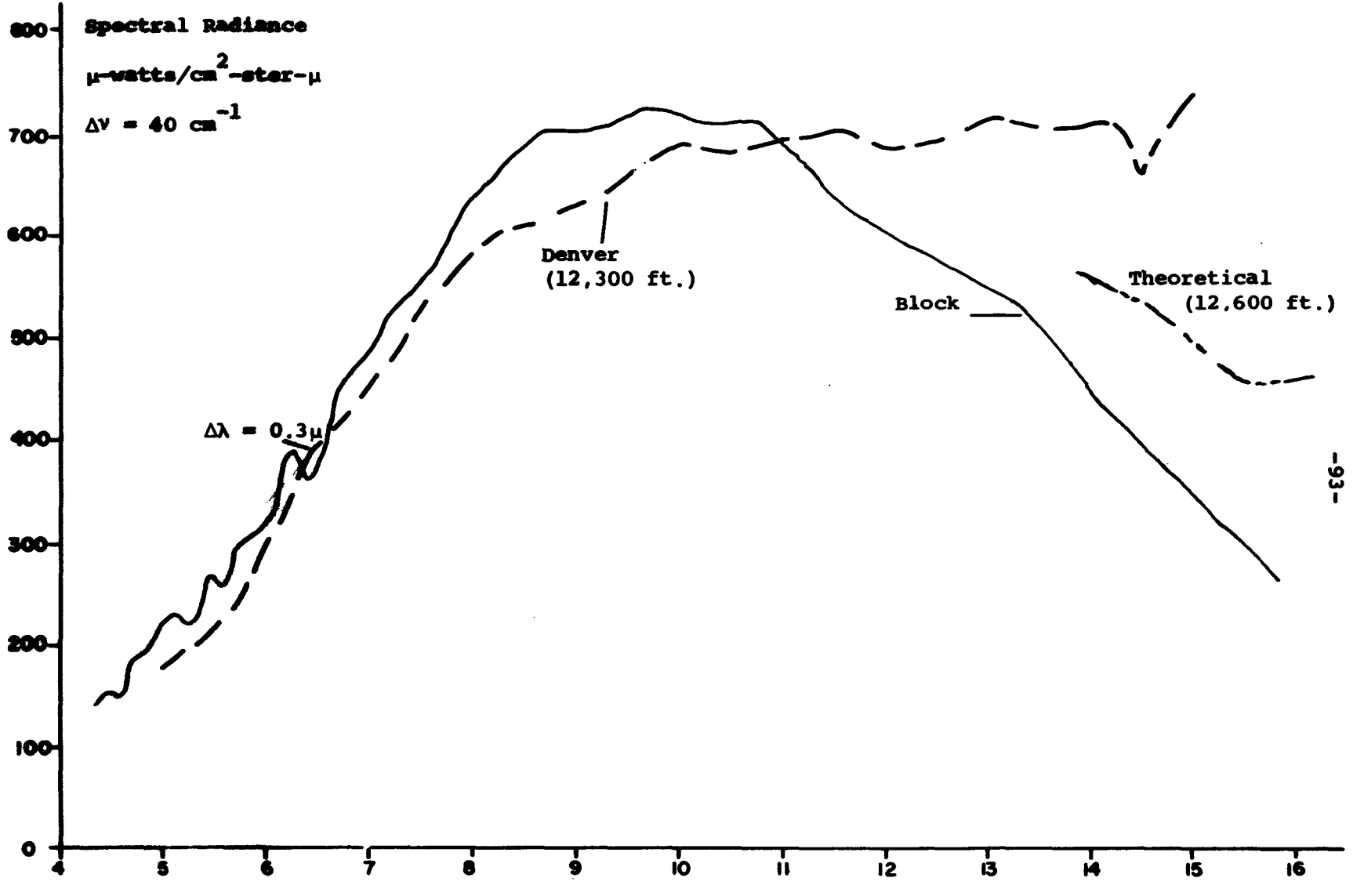

Figure 38.
Upward Radiance
at 12,600 feet M.S.L.

7.2 Flight #2

7.2.1 Description of Flight

The purpose of flight #2 was to gather data regarding both the upward and downward radiative energy flux in the atmosphere. For this purpose two interferometer spectrometers were used, one, the I4T, looking alternately at the nadir and at an angle of 30° to the zenith, provided data in the 5μ to 15μ spectral region, while a second instrument, an I4TC, looking only at the nadir, obtained data in the 9μ to 40μ spectral region. Also on board were four experimental frost point hygrometers supplied and serviced by Minneapolis-Honeywell. The telemetry system used for data transmission during the flight was supplied by Northeastern University, who also fabricated the gondola. For this flight ten telemetry channels were used as listed below.

1.	I4T Interferogram	70	KC	±7½%
2.	I4TC Interferogram	52.5	KC	±7½%
3.	I4T Sweep Drive	40	KC	±7½%
4.	I4TC Sweep Drive	30	KC	±7½%
5.	I4T Commutator	22	KC	±7½%
6.	I4TC Commutator	14.5	KC	±7½%
7.	Frostpoint Hygrometer #1	10.5	KC	±7½%
8.	Frostpoint Hygrometer #2	7.35	KC	±7½%
9.	Frostpoint Hygrometer #3	5.4	KC	±7½%
10.	Frostpoint Hygrometer #4	3.9	KC	±7½%

The balloon was launched at 1:27:30 a.m. Mountain Standard Time, on 2 August 1962 from Holloman Air Force Base, New Mexico. The flight proceeded normally until the balloon reached an altitude of 54,000 feet, M.S.L., at which point it burst; the exact cause is

uncertain, but the probable cause was an extremely cold tropopause. At this point, the mission was terminated, and the payload was parachuted back to earth.

Both spectrometers operated successfully and, although the flight was terminated before the balloon reached float altitude, all the data obtained up to that point was valid due to the high spectral sampling rate.

The flight profile, temperature versus geometric altitude, and pressure versus altitude is presented in the appendix in addition to the engineering information provided by the commutators.

The spectral data is presented in Figures 39 through 58. Figures 39 and 40 indicate the variation in radiance with altitude for several wavelengths and in Figures 42, 44, 45, 48, 50, 51, and 52 the data from both instruments at common altitudes is presented for comparison.

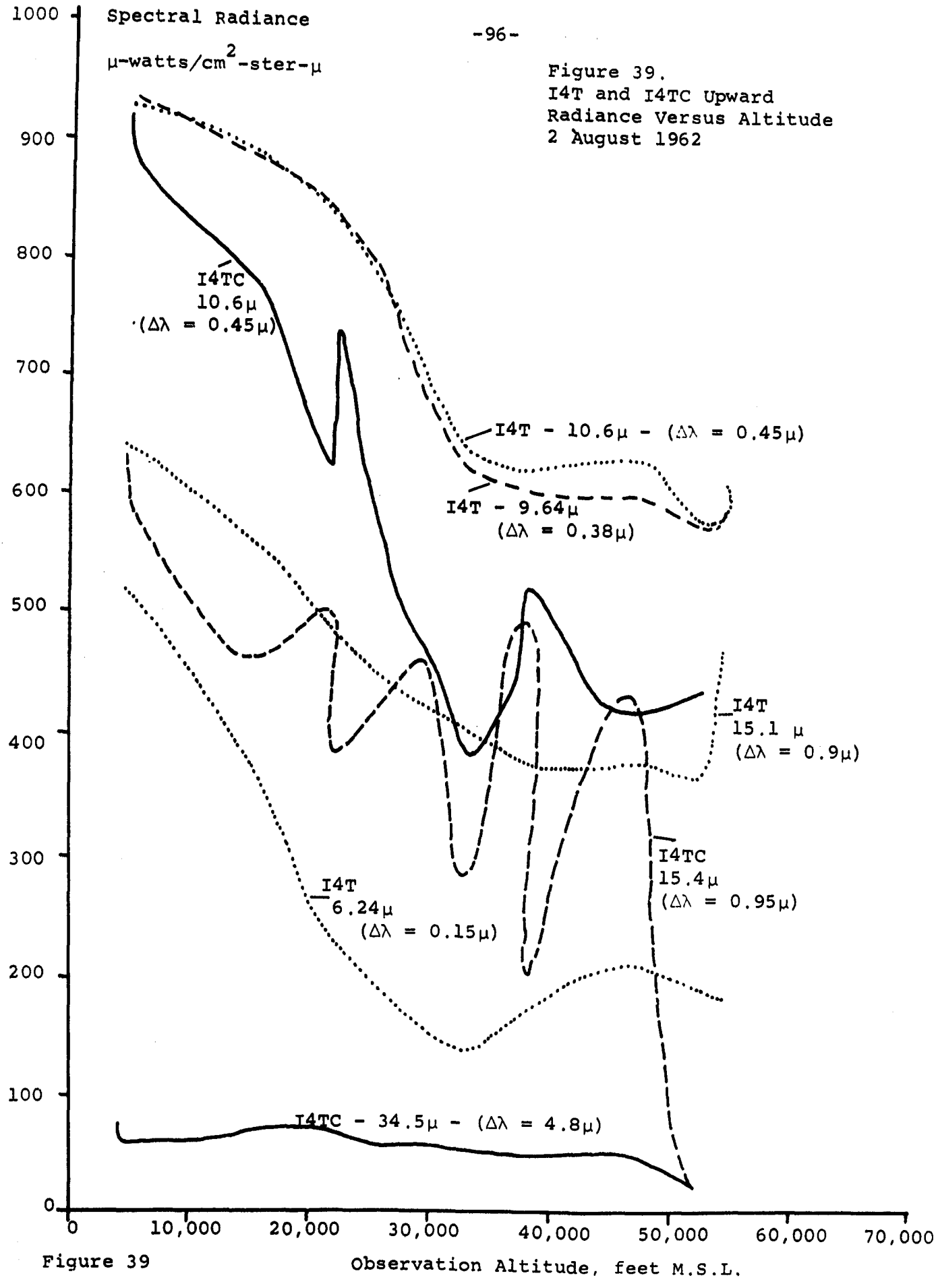

Figure 39.
I4T and I4TC Upward
Radiance Versus Altitude
2 August 1962

Figure 39

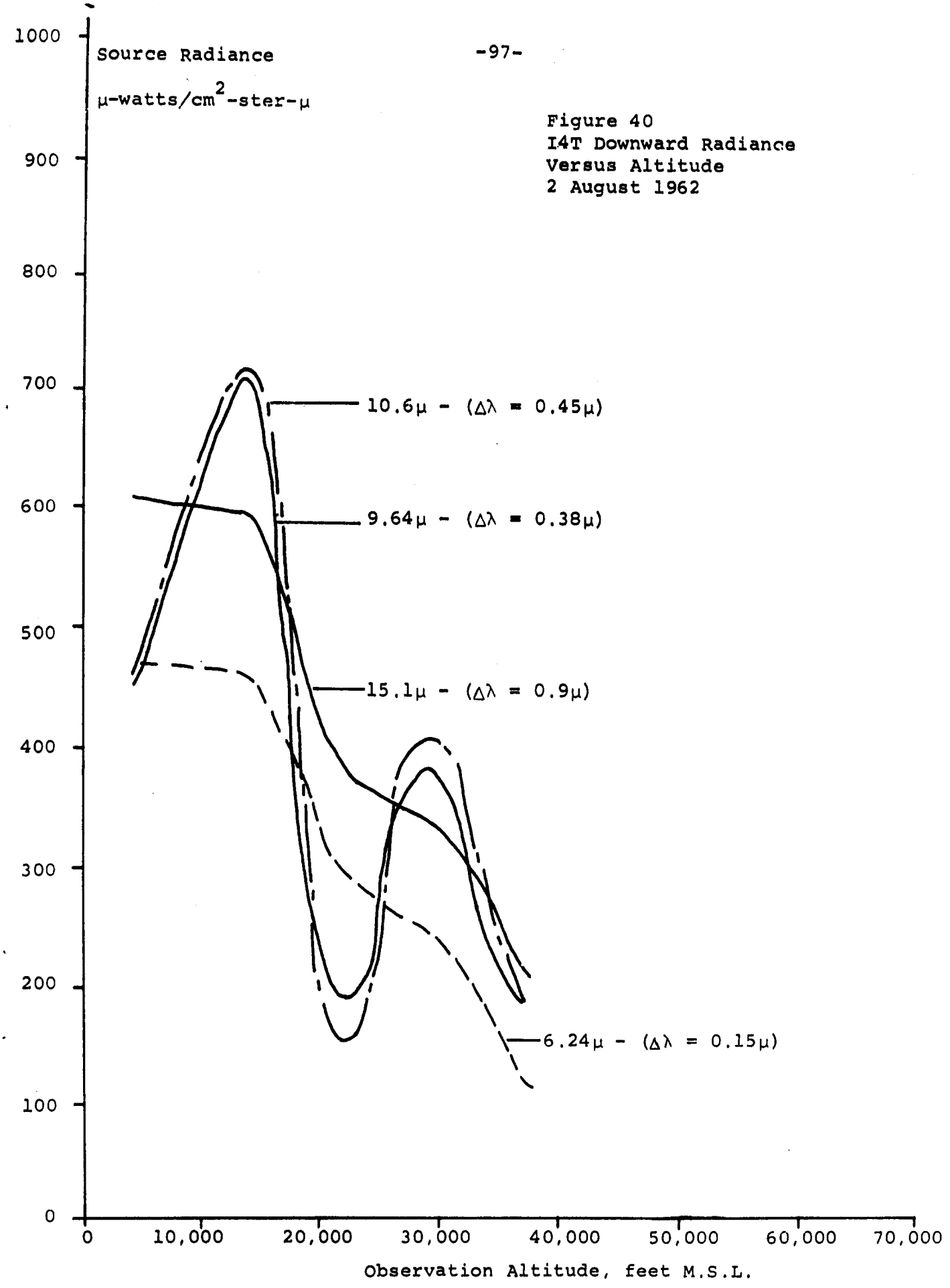

Figure 40
I4T Downward Radiance
Versus Altitude
2 August 1962

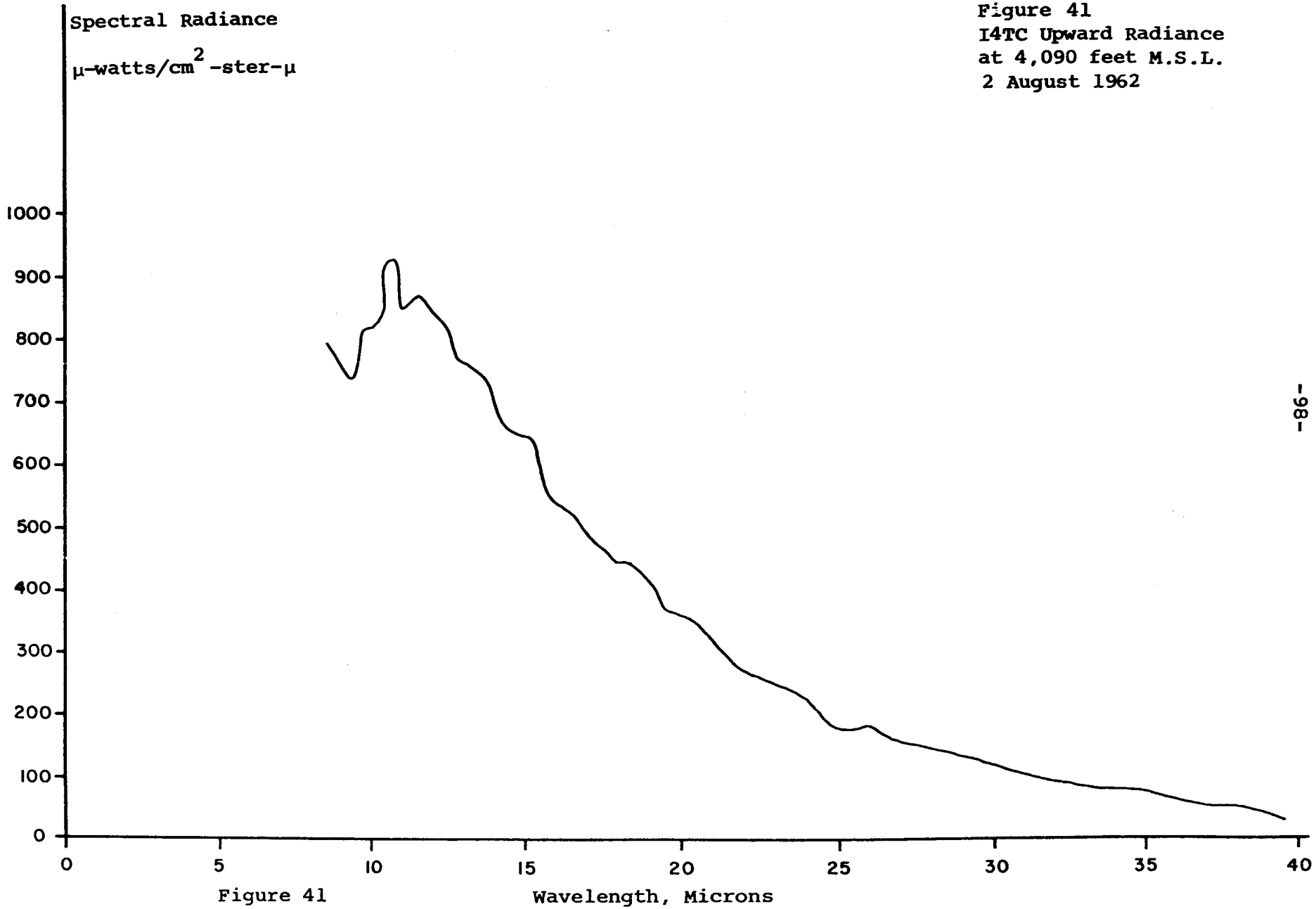

Figure 41
I4TC Upward Radiance
at 4,090 feet M.S.L.
2 August 1962

Figure 41

Figure 42.
I4T and
I4TC Upward Radiance
at 4,340 feet M.S.L.
2 August 1962

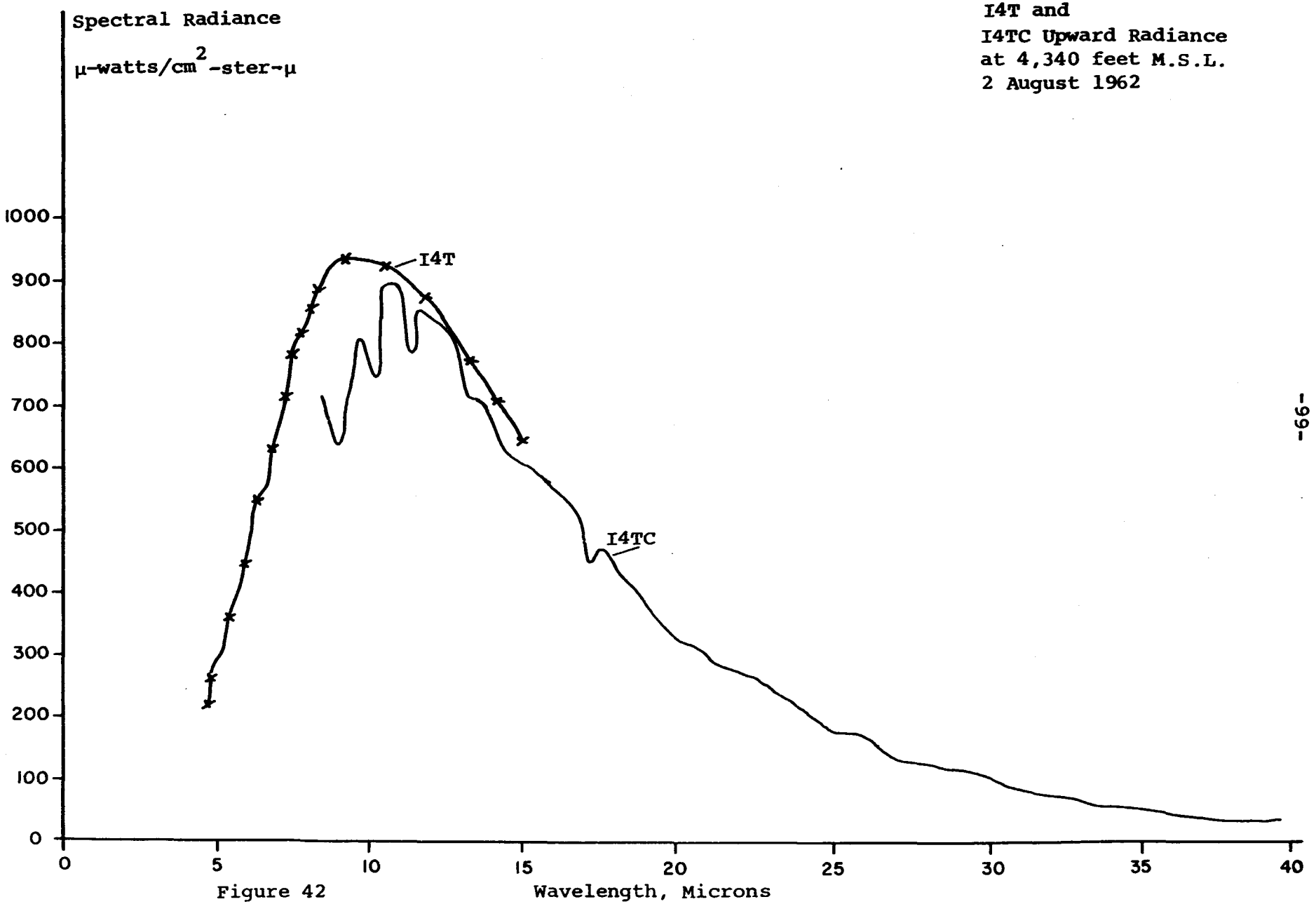

Figure 42

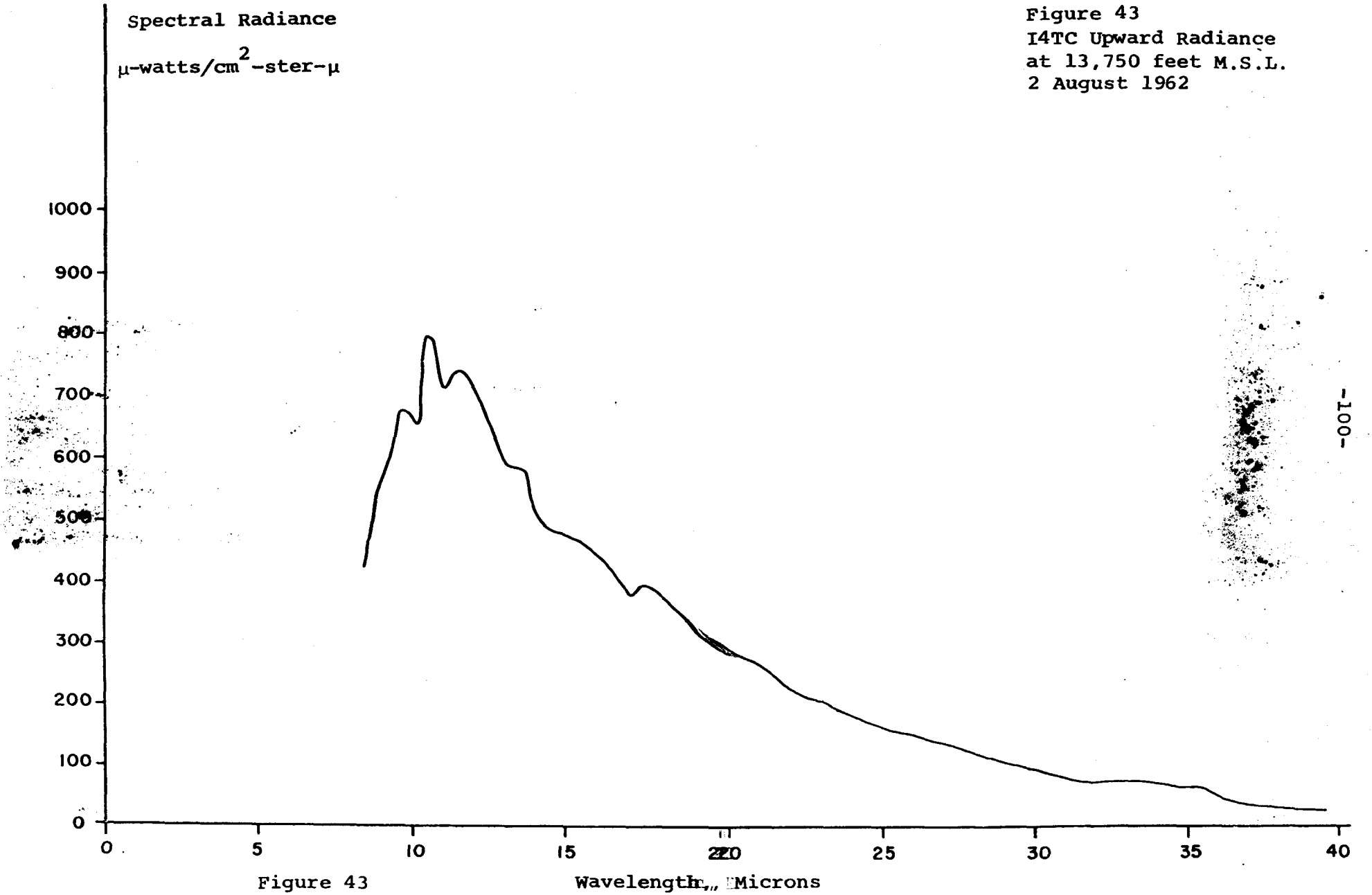

Figure 43
I4TC Upward Radiance
at 13,750 feet M.S.L.
2 August 1962

Figure 43

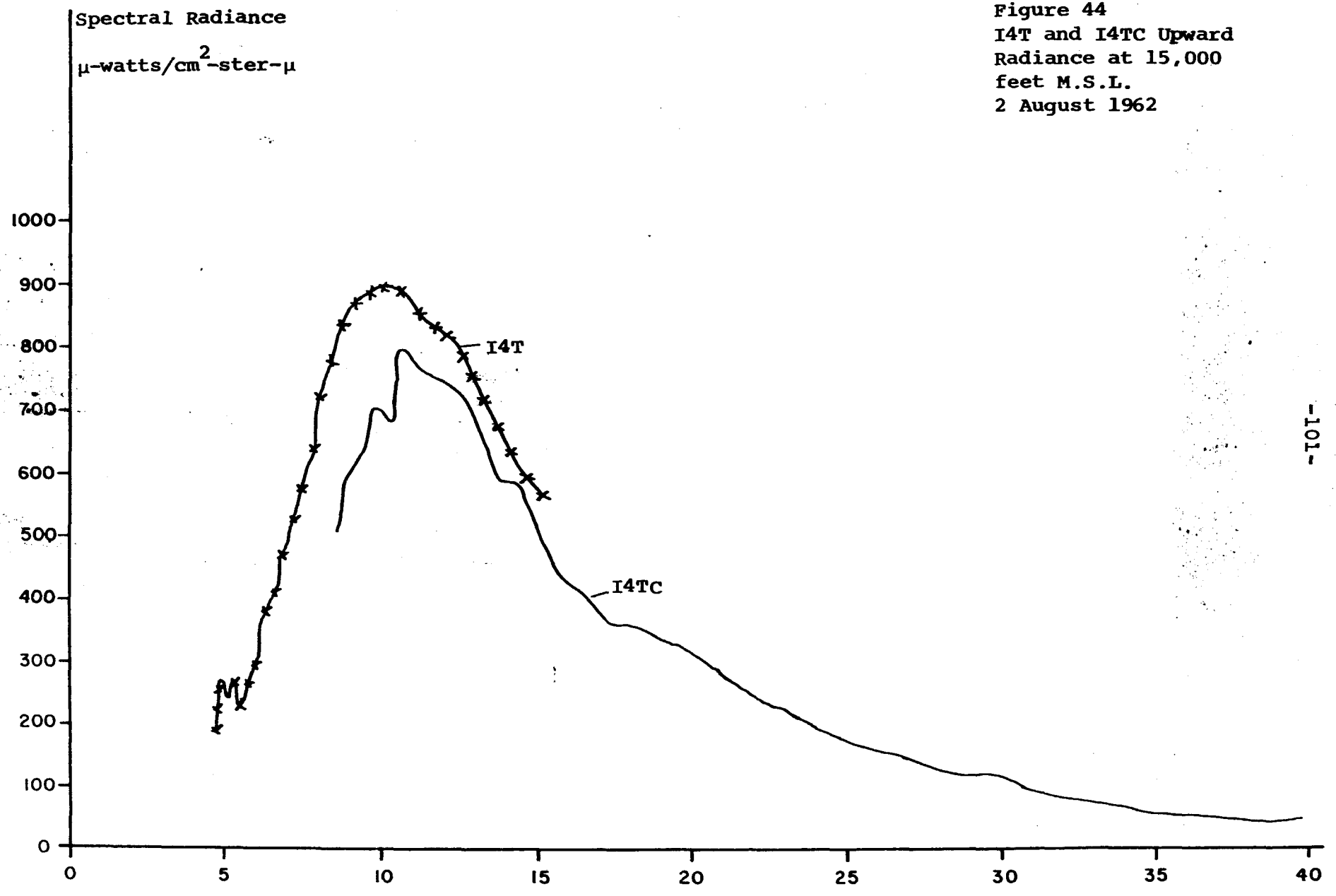

Figure 44
I4T and I4TC Upward Radiance at 15,000 feet M.S.L.
2 August 1962

Figure 44

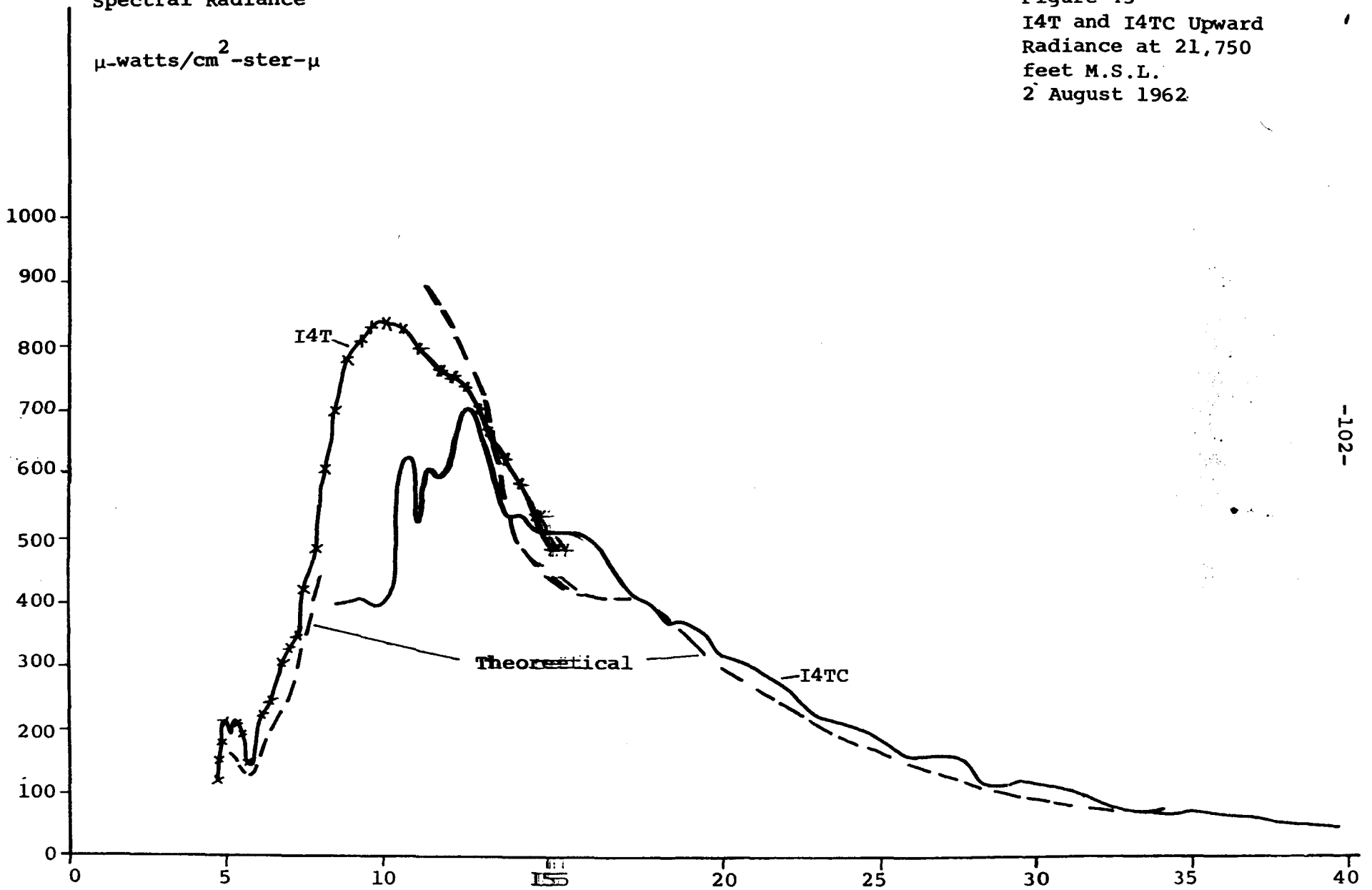

Figure 45
I4T and I4TC Upward Radiance at 21,750 feet M.S.L.
2 August 1962

Figure 45

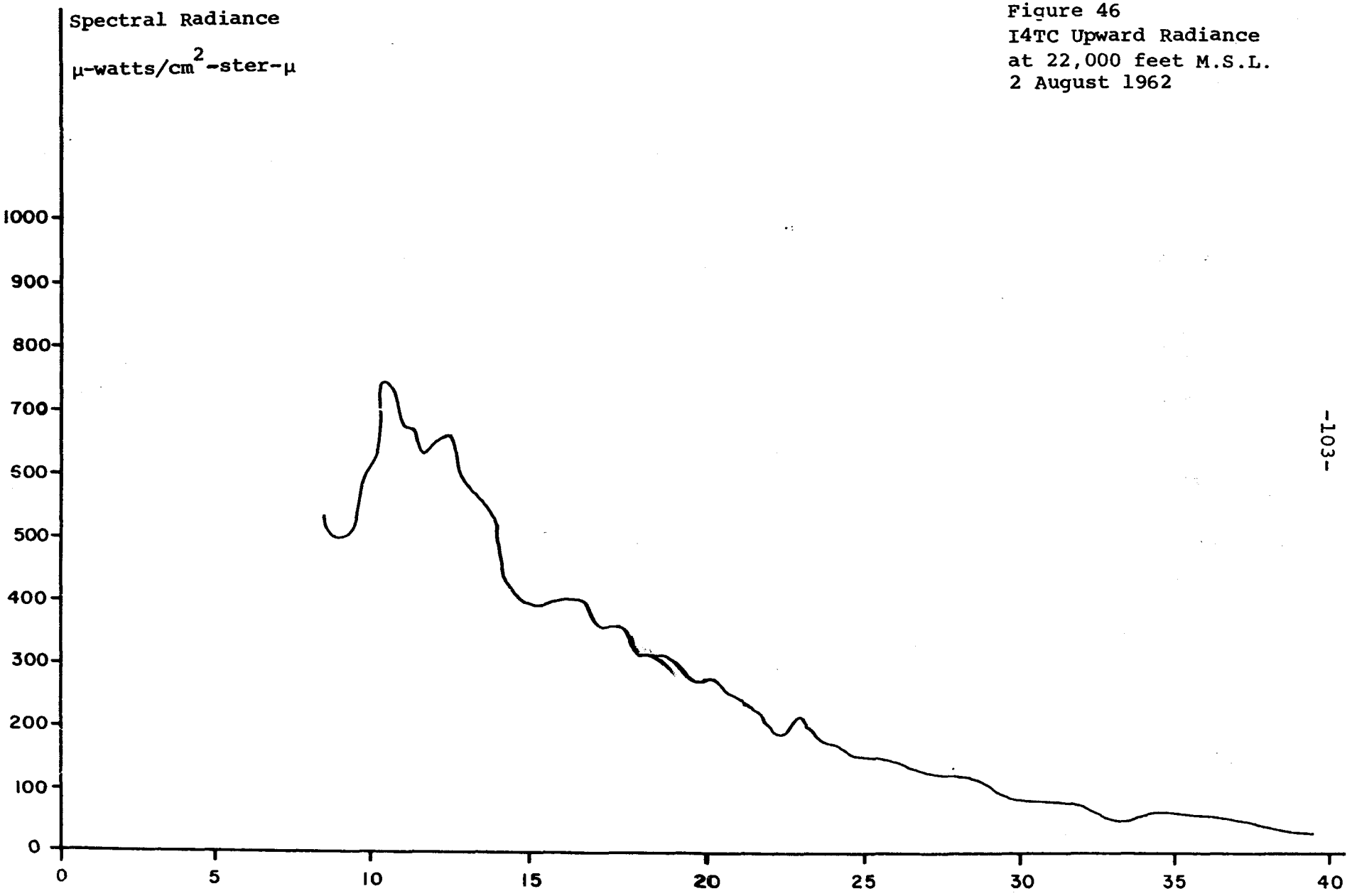

Figure 46
I4TC Upward Radiance
at 22,000 feet M.S.L.
2 August 1962

Figure 46

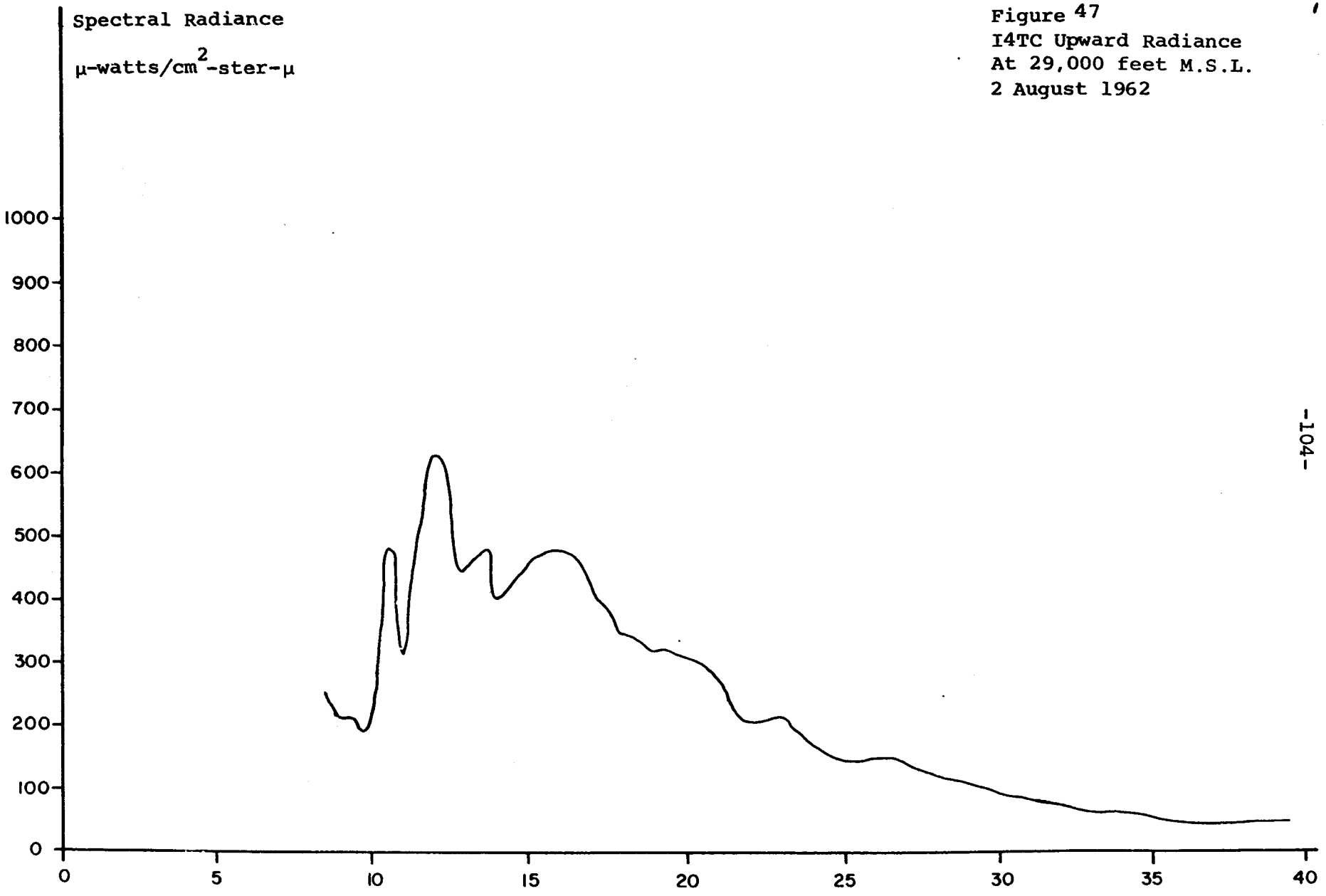

Figure 47
I4TC Upward Radiance
At 29,000 feet M.S.L.
2 August 1962

Figure 47.

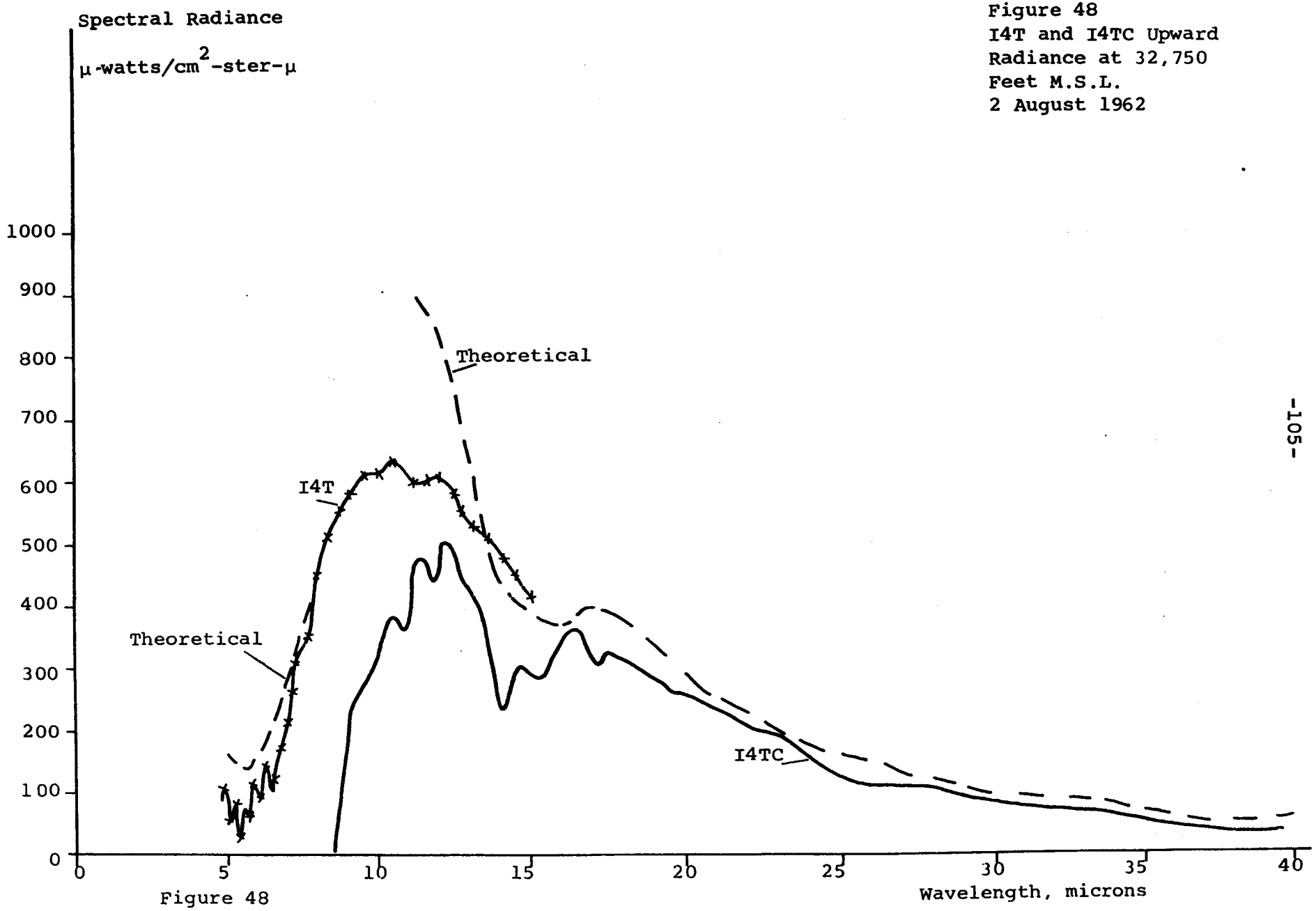

Figure 48
I4T and I4TC Upward
Radiance at 32,750
Feet M.S.L.
2 August 1962

Figure 48

Figure 49
I4TC Upward Radiance
at. 37,500 feet M.S.L.
2 August 1962

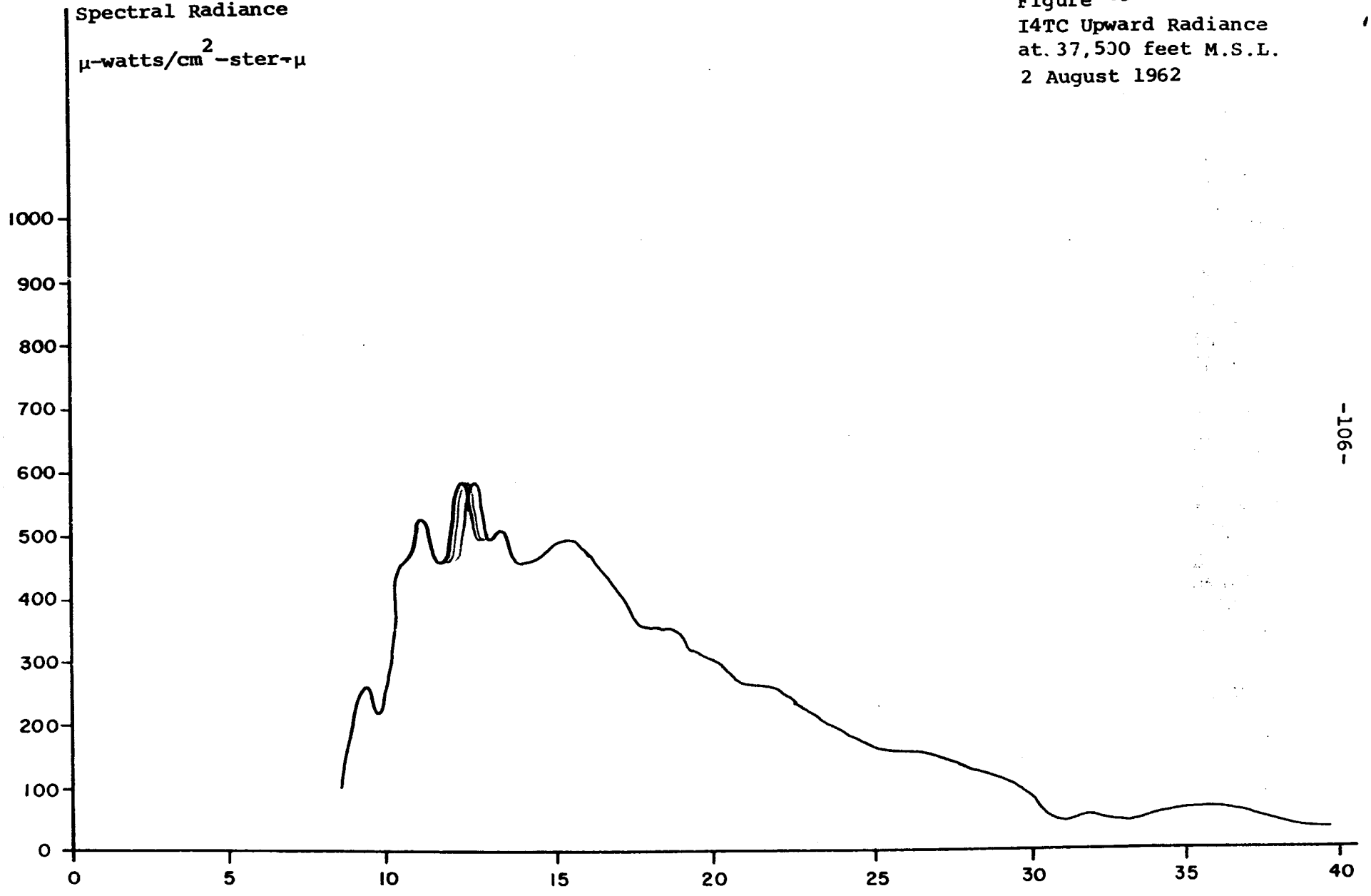

Figure 49

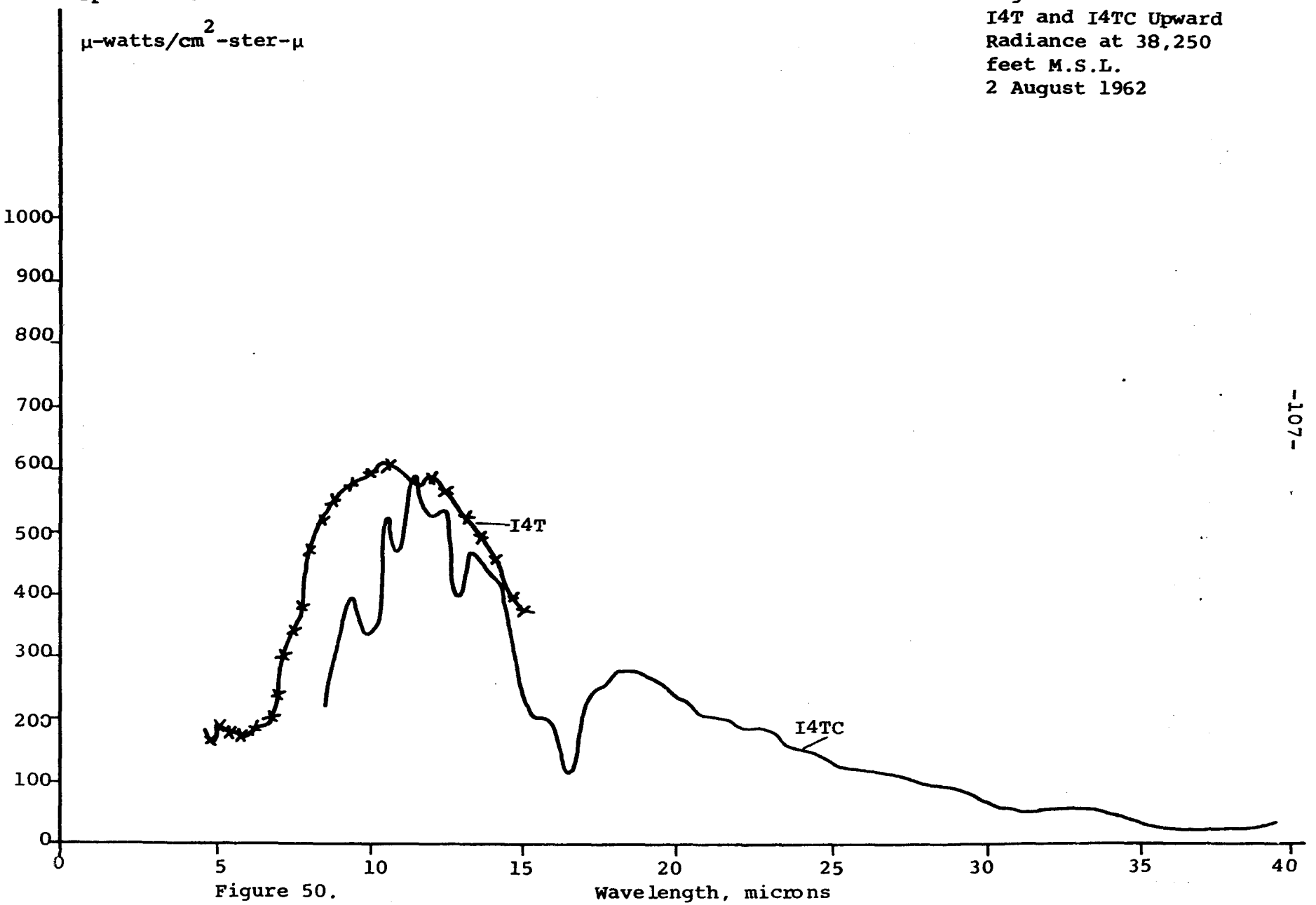

Figure 50
I4T and I4TC Upward Radiance at 38,250 feet M.S.L.
2 August 1962

Figure 50.

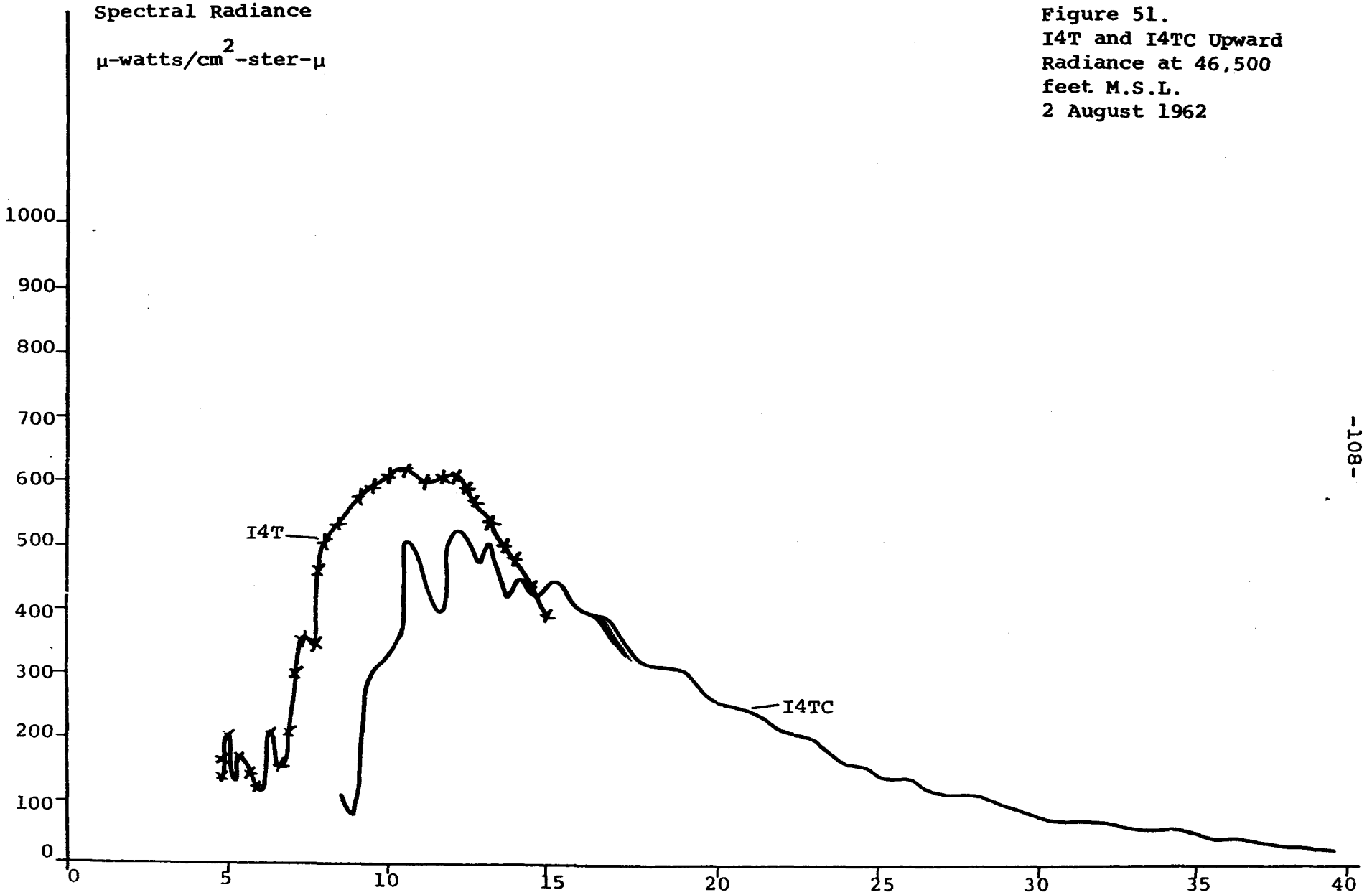

Figure 51.
I4T and I4TC Upward Radiance at 46,500 feet M.S.L.
2 August 1962

Figure 51.

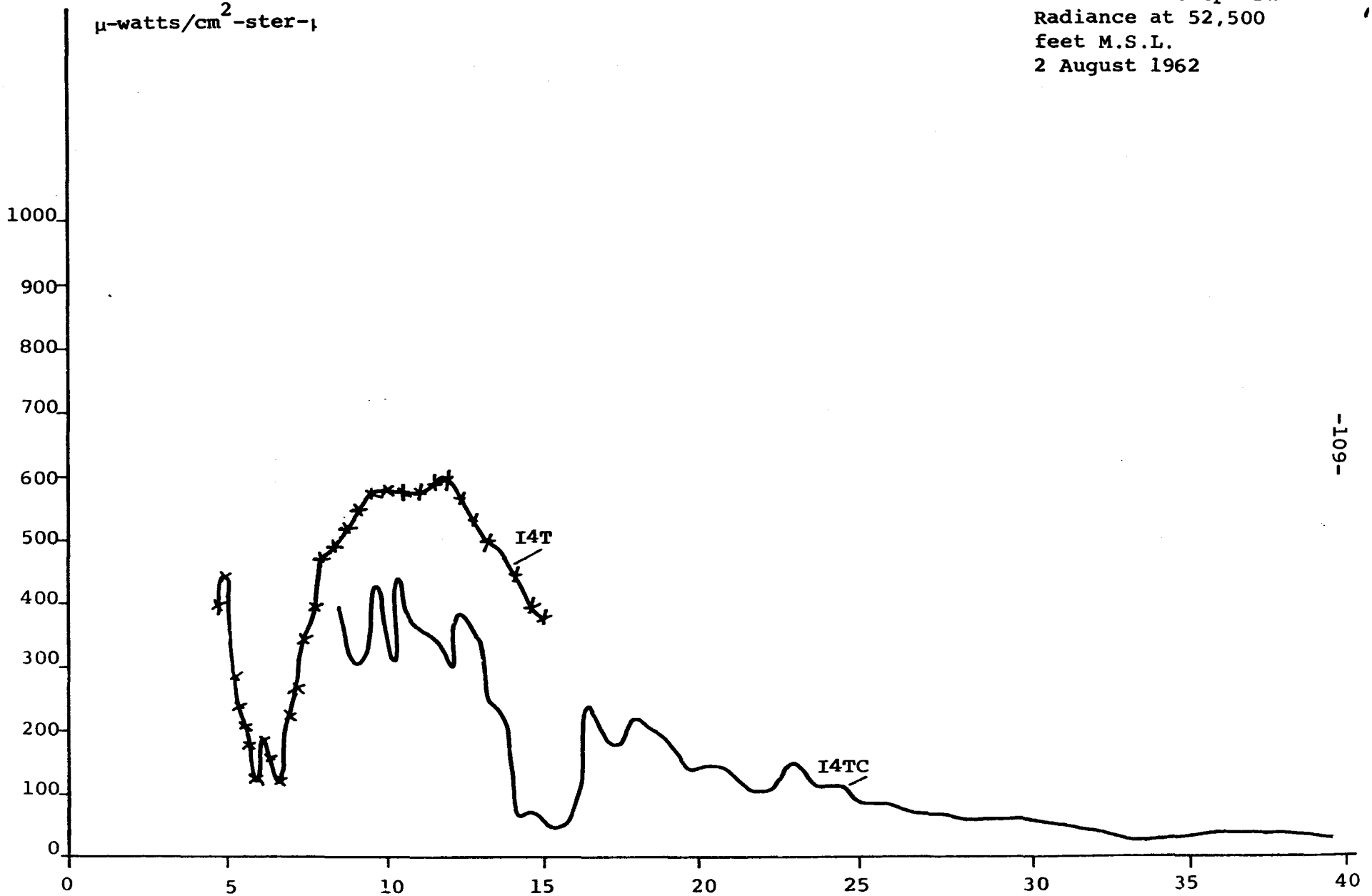

Figure 52
I4T and I4TC Upward
Radiance at 52,500
feet M.S.L.
2 August 1962

Figure 52.

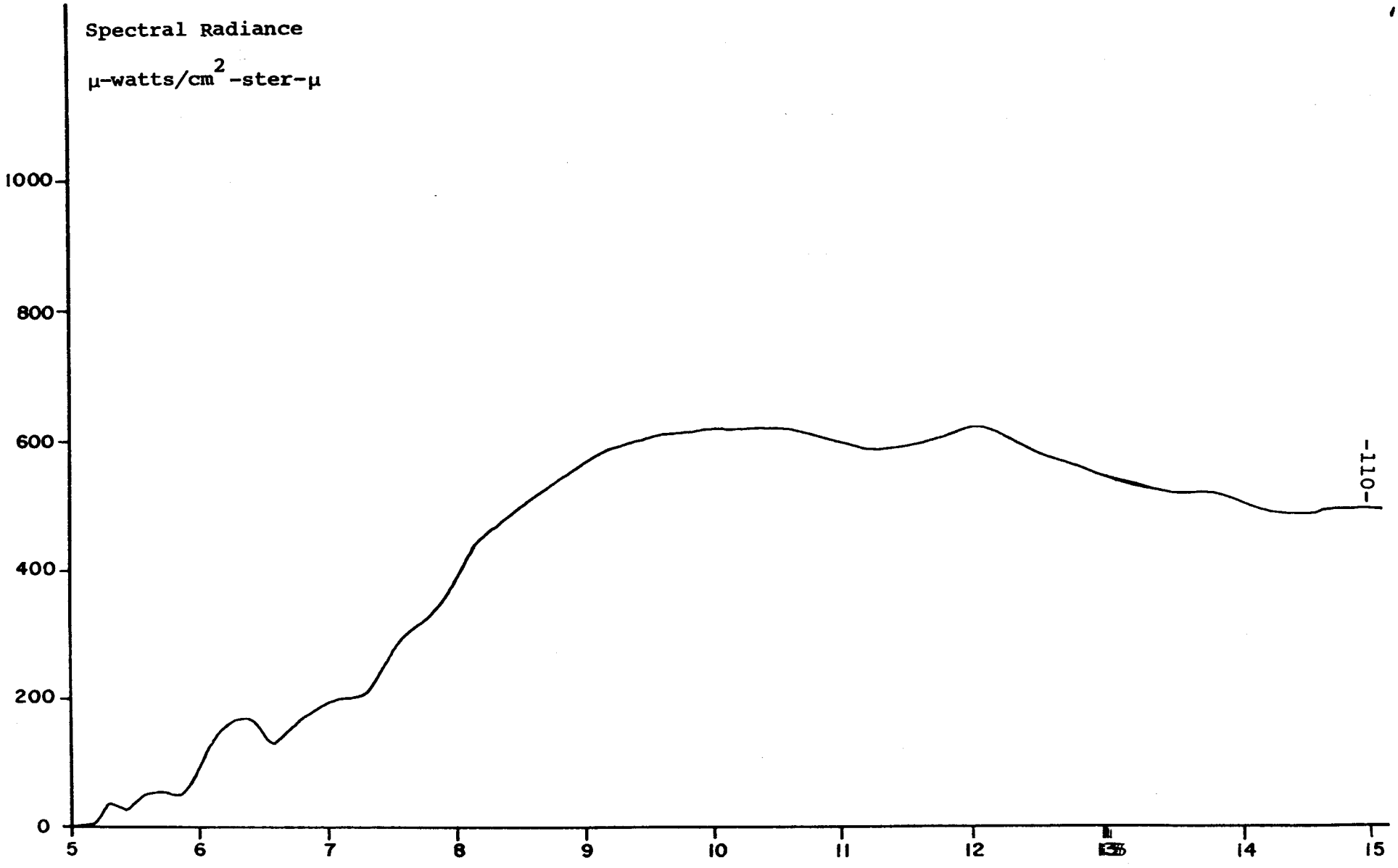

Figure 53
I4T Upward Radiance at
54,250 feet M.S.L.
2 August 1962

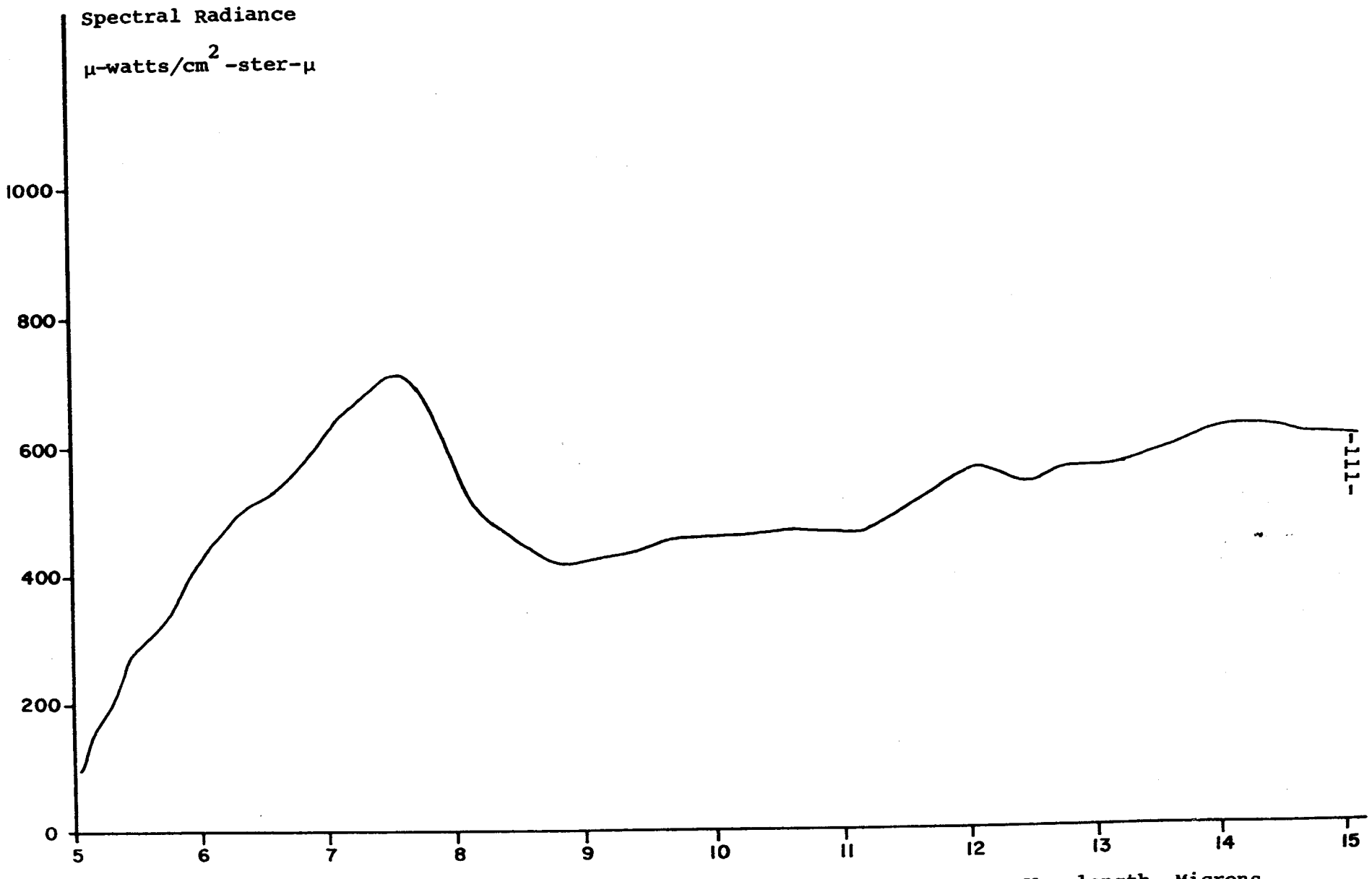

Figure 54
I4T Downward Radiance
at 4090 feet M.S.L.
2 August 1962

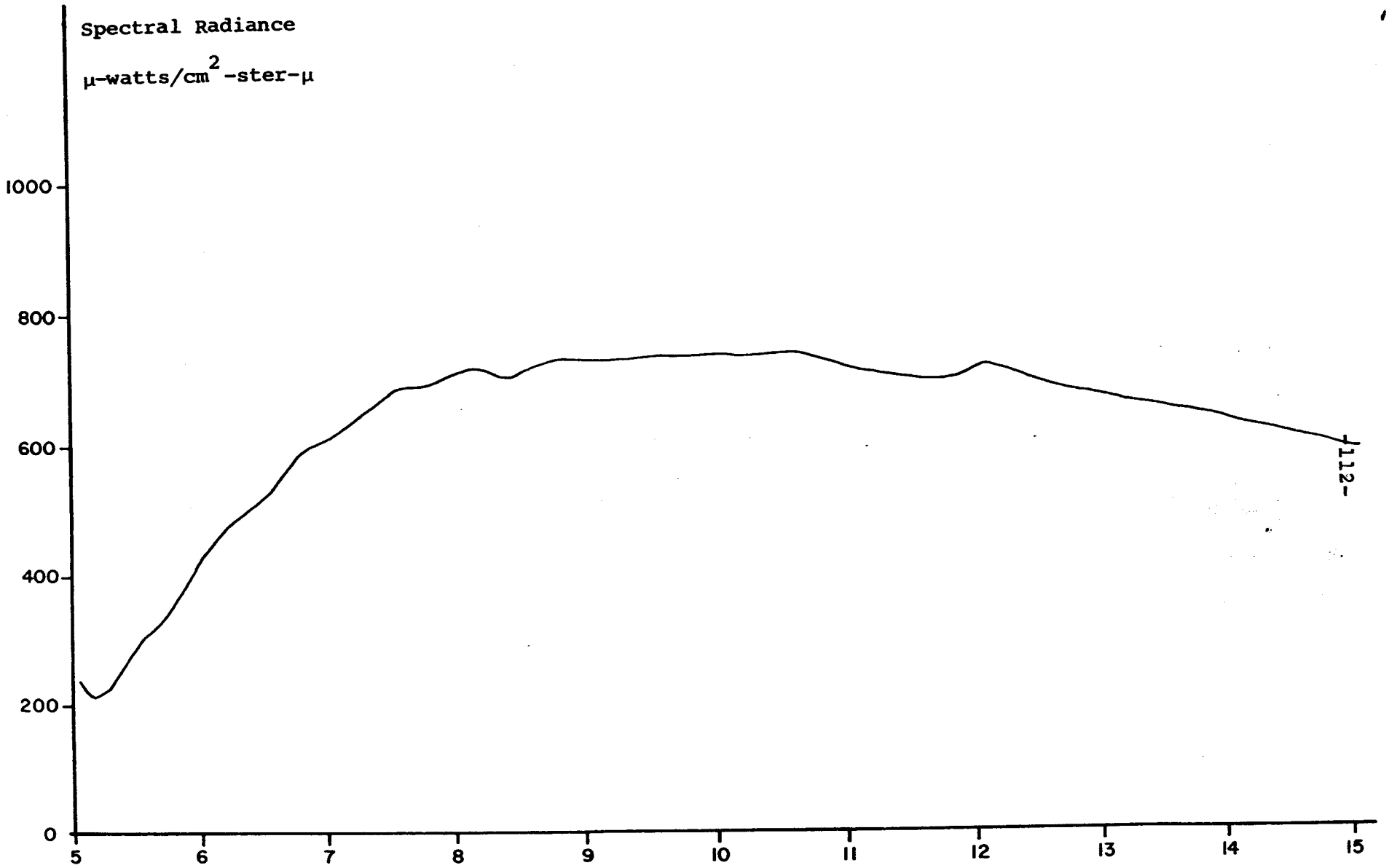

Figure 55
I4T Downward Radiance
at 13,750 feet M.S.L.
2 August 1963

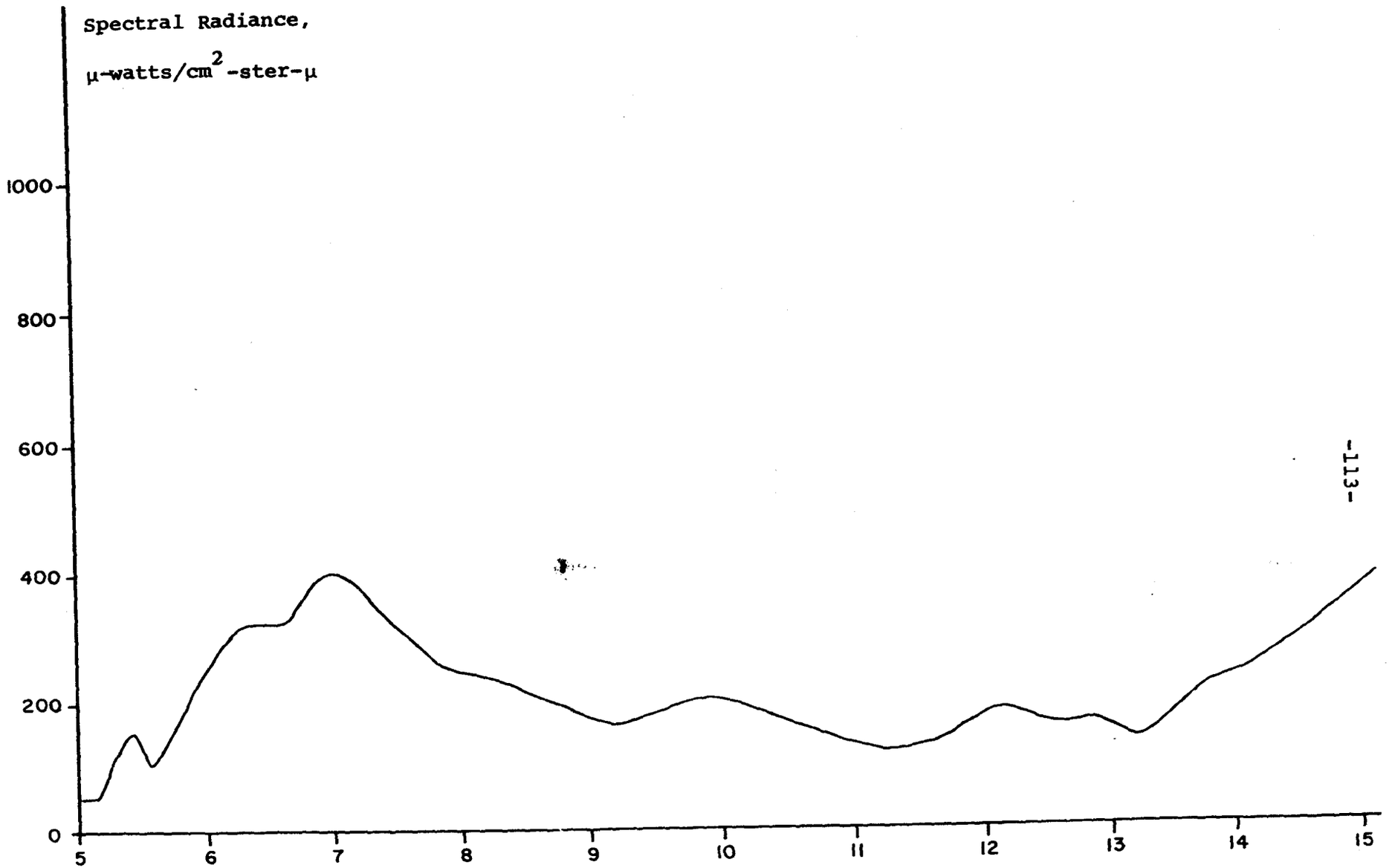

Figure 56
I4T Downward Radiance
at 22,000 feet M.S.L.
2 August 1962

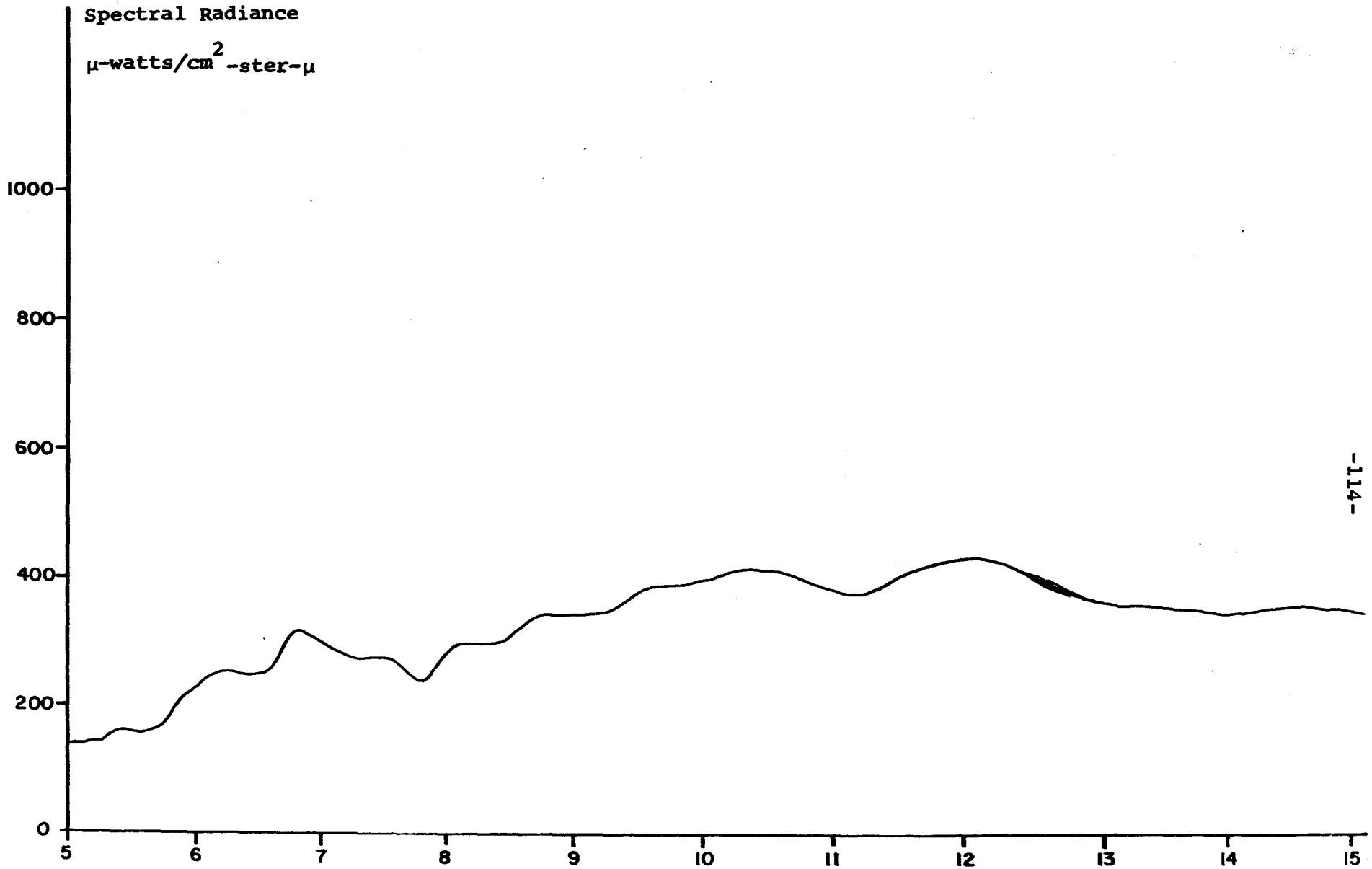

Figure 57
I4T Downward Radiance
at 29,000 feet M.S.L.
2 August 1962

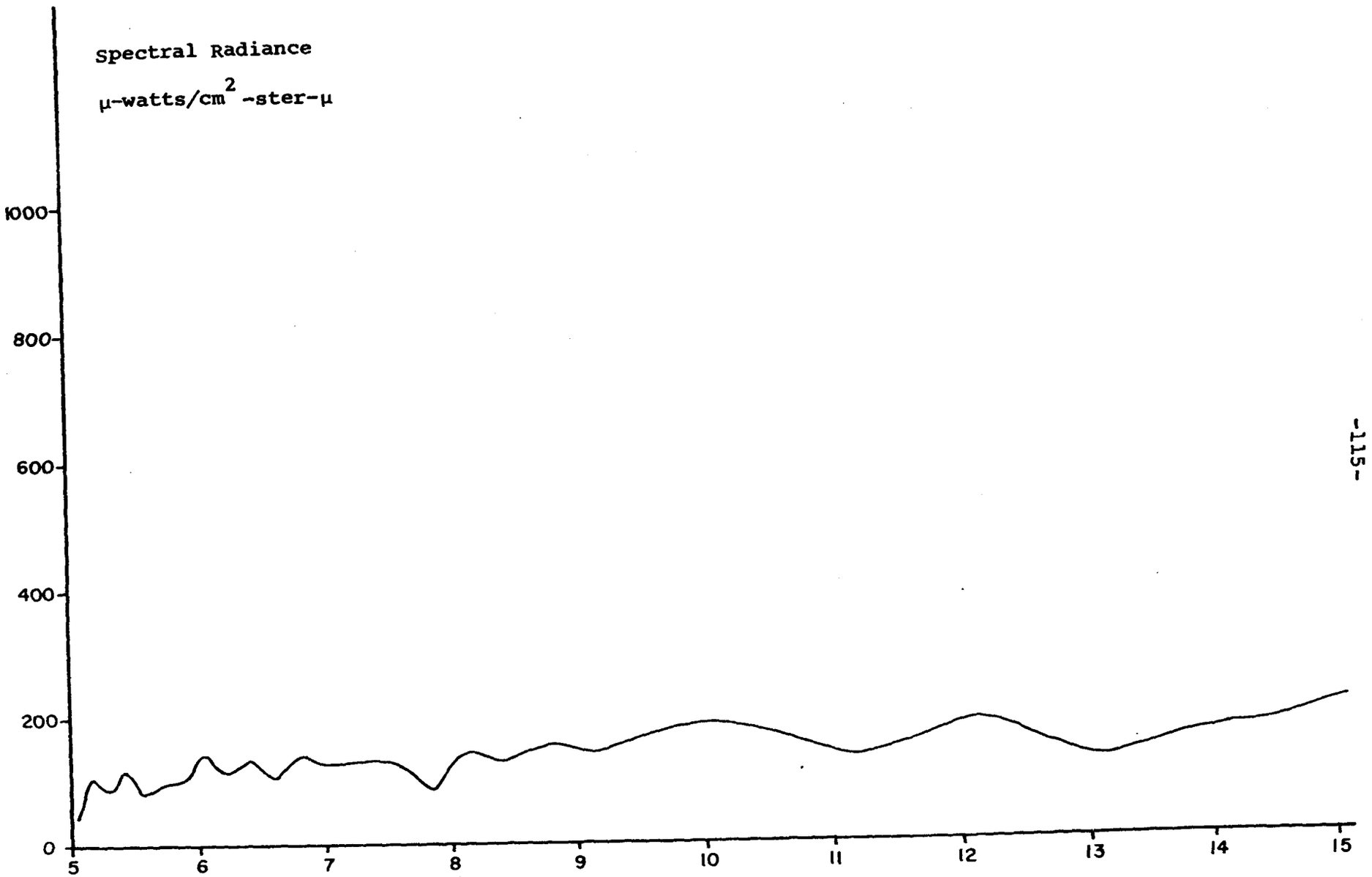

Figure 58
I4T Downward Radiance
at 37,500 feet M.S.L.

7.2.2 Theoretical Analysis

In addition to the experimental measurements, the results of a theoretical analysis of the upward radiance at 21,750 feet M.S.L. and 32,750 feet M.S.L. are presented in Figures 45 and 48, respectively, along with the measured radiance values.

The theoretical results were obtained by applying the one-dimensional transfer equation for a layered gray atmosphere in thermal equilibrium. The transfer equation was evaluated using estimates (from Ref. 5 - see footnote page 121) of H_2O and CO_2 absorption (emission) obtained from published laboratory data and from empirical transmission equations (Ref. 2 - see footnote page 120) derived from laboratory data (Ref. 1 - see footnote page 120).

Available data indicates that the atmosphere below the 50 km level is locally in thermodynamic equilibrium. That is, the relaxation time of the energy absorbed in molecular transitions is short compared to the lifetimes of the excited molecular states, so that a single temperature is characteristic of all the energy states of the gas as a whole (absorbing plus non-absorbing species). The local conditions approximate those within an adiabatic enclosure and hence Kirchoff's Law relating the absorption and emission coefficients may be applied. In this case, the fractional emissivity, ϵ, of an infinitesimally thin layer, dh, at temperature, T, is equal to the absorptivity, α, or the complement of the transmissivity, τ, of the layer. The radiation emitted by the layer is given by:

$$\epsilon_\lambda N_{BB_\lambda} = \alpha_\lambda N_{BB_\lambda} = (1-\tau_\lambda) N_{BB_\lambda} \qquad (1)$$

At any wavelength, λ, where $N_{BB_\lambda} = N_{BB_\lambda}(\lambda,T)$ represents the Planck function. The factors, ϵ_λ, α_λ, and τ_λ depend on the optical properties of the layer, e.g., optical mass, w, and mean

pressure, p, as well as on λ and T. Temperature usually has a much smaller effect than the other variables, and, for this analysis, ϵ_λ, α_λ, and τ_λ are assumed independent of T.

With these assumptions, the transfer equation is derived as follows. Consider a typical atmospheric layer of thickness, dh, at altitude, h, which emits energy at the temperature, T(h), (See Figure 59). From the definition of absorption coefficient, k_λ, the spectral (monochromatic) emissivity or absorptivity of the layer is,

$$\epsilon_\lambda(dh) = \alpha_\lambda(dh) = k_\lambda dw_1 \tag{2}$$

where dw is the optical thickness of the layer. Similarly, the transmissivity between h and some higher level, h_o ("observer" altitude) is,

$$\tau_\lambda\ (h_o - h) = e^{-\int_{w(h)}^{w(h_o)} k_\lambda dw} \tag{3}$$

where w(h) denotes the optical thickness of the atmosphere between the ground and level, h. Thus, the contribution of the typical layer to the upward radiation observed (for the vertical direction) at h_o is,

$$dN_\lambda(h_o) = N_{BB_\lambda}\left[\lambda, T(h)\right] \cdot k_\lambda\, dw \cdot e^{-\int_{w(h)}^{w(h_o)} k_\lambda dw}$$

$$= N_{BB_\lambda}\left[\lambda, T(h)\right] \cdot d\left[e^{-\int_{w(h)}^{w(h_o)} k_\lambda dw}\right] \tag{4}$$

$$= N_{BB_\lambda}\left[\lambda, T(h)\right] \cdot d\tau_\lambda\left[h_o - h\right]$$

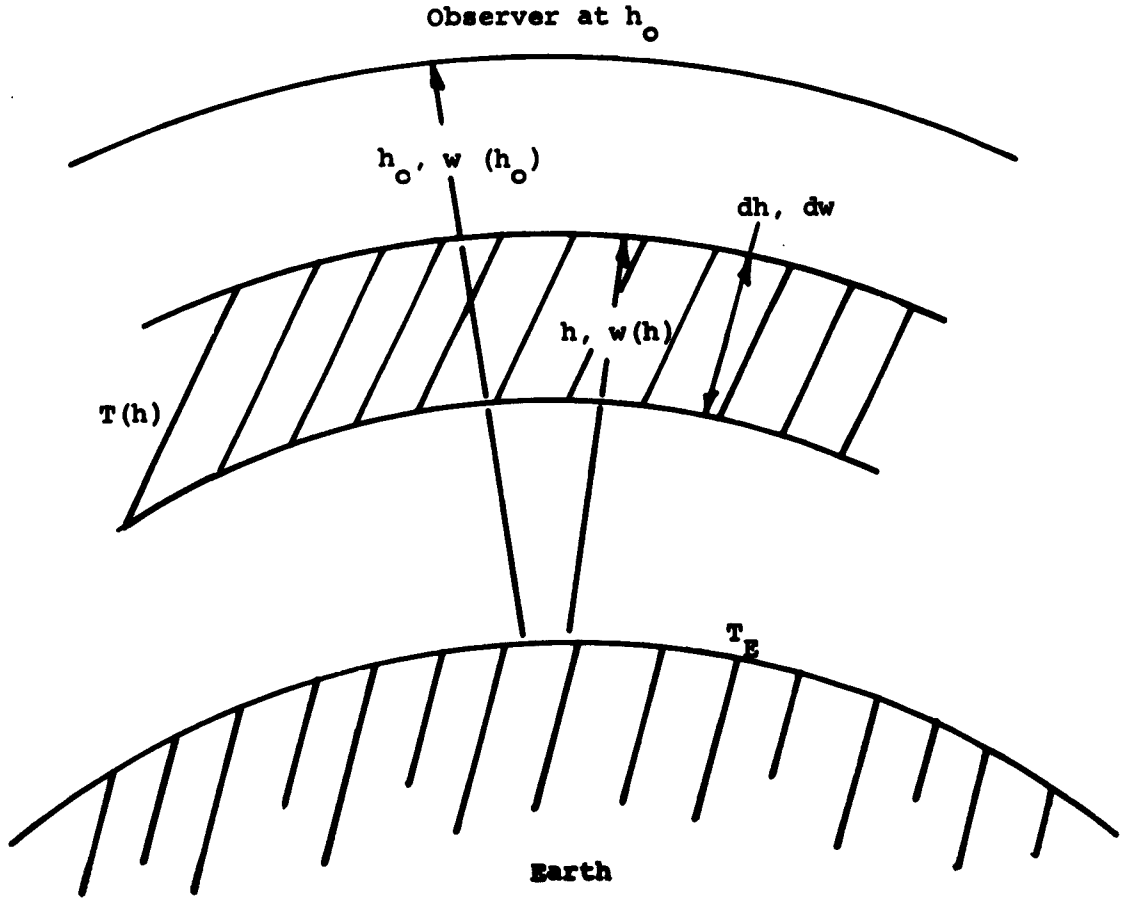

Figure 59.
Illustration of Symbols.

where

$$d\tau_\lambda(h-h_o) \equiv \left[\frac{d\tau(h-h_o)}{dh}\right] \cdot dh$$

is understood to mean the change in the vertical transmissivity between the levels h and h_o due to the change, $h \longrightarrow h + dh$. Adding the contributions from all such layers, dh, to the radiation which is emitted by the earth, we obtain for the total vertical radiation at h_o,

$$N_\lambda(h_o) = N_{BB_\lambda}(\lambda, T_E)\ \tau(h_o) + \int_{\tau(h_o)}^{1} N_{BB_\lambda}[\lambda, T_e(h)]\ d\tau\ (h_o-h) \qquad (5)$$

where $\tau(h_o)$ is the transmissivity between the ground and h_o. We have assumed the earth's emission spectrum is that of a blackbody at the temperature, T_E.

To simplify the calculation of $N_\lambda(h_o)$, the atmosphere was divided into concentric isothermal layers. The temperature of each layer was taken approximately equal to an average value which is determined by weighting the actual temperature by the water vapor partial density for the range of altitudes occupied by the layer. For this layered atmosphere, the upward radiation at h_o is given by,

$$N_\lambda(h_o) = N_{BB_\lambda}(\lambda, T_E)\ \tau(h_o) + \sum_i N_{BB_\lambda}(\lambda, T_i)\ \Delta\tau_i \qquad (6)$$

where T_i is the temperature of the i^{th} layer, and $\Delta\tau_i$ is the difference between the transmissivity between h_o and the top and bottom of the i^{th} layer. This procedure is roughly equivalent to evaluating the transfer integral (second term of Equation 5) by the trapezoidal rule.

The calculations were performed for the 5 to 8 micron region, in which the atmospheric absorption and emission is due to the 6.3μ H_2O band, and also for the 11.5μ to 40μ region, which includes the 15μ CO_2 band and a large portion of the pure rotation H_2O spectrum.

For calculating the transmissivity of water vapor over the 6.3μ band, the Howard, Burch and Williams[1] fit of the Goody Model was used. According to this equation, the transmissivity of a uniform sample of H_2O of optical thickness, w, at effective pressure, p (in mm. Hg), is given by

$$\tau = \exp\left\{\frac{-1.97\,\frac{w}{w_o(\lambda)}}{\left[1 + \frac{4860}{p}\left(\frac{w}{w_o}\right)\right]^{1/2}}\right\} \qquad (7)$$

where $w_o(\lambda)$ is the optical thickness which gives the value $\tau = 1/2$ at the wavelength, λ, when the pressure, p, is exactly 125 mm. Hg. The parameter $w_o(\lambda)$ was determined from laboratory data by Howard, Burch, and Williams, and is is presented by them in graphical form as a function of wavenumber. The parameter $w_o(\lambda)$ is also given by Zachor[2] in graphical and tabular form as a function of wavelength.

Equation 7, which is strictly applicable only to homogeneous (i.e., constant pressure and temperature) paths, was used for the vertical atmospheric paths involved in the present calculations by re-defining p as the mean total pressure over the path.

---

1. Howard, J. N., Burch, D. E., and Williams, D. "Near Infrared Transmission through Synthetic Atmospheres". Geophysics Research Paper No. 40, AFCRC, November, 1955. Also, J. Opt. Soc. Am. Vol. 46, 1956, pp. 186, 237, 243, 334, 452.

2. Zachor, Alex S., "Near Infrared Transmission over Atmospheric Slant Paths". Mithras, Inc., Cambridge, Mass., MC-61-13, July 1961 (reprint).

According to the usual Curtis-Godson[3,4] approximation, the mean pressure is

$$p = \frac{\int P\, dw}{\int w} = \frac{\int P\, dw}{w} \tag{8}$$

for the case in which temperature effects are neglected. Here P is the air pressure at any point along the path, and dw is the optical thickness of water vapor per unit length of path at the same point.

For the 15μ CO_2 band and for the rotational H_2O bands, the data compiled by Elsasser[5] were used. Transmissivity values were read directly from Elsasser's Figures 13 and 26, which give the "actual absorption" vs. wavelength for different values of the "reduced optical path" u. For atmospheric paths, the parameter u is defined by

$$u = \int \frac{P}{P_o} \sqrt{\frac{T_o}{T}}\, dw \tag{9}$$

where P and T are the air pressure and temperature along the path, and P_o and T_o are the air pressure and temperature at sea level. If the temperature dependence is neglected, as for the present calculation, Equation 9 is equivalent to

$$u = \frac{p}{P_o} w \tag{10}$$

---

3. Curtis, A. R., Quart. Jour. R.M.S., Vol 78, 1952, p. 638.

4. Godson, W. L., J. of Met., Vol. 12, 1955, p. 272.

5. Elsasser, W. M., Meterological Monographs, Vol. 4, No. 23, p. i - iii, 1 - 41, August 1960.

The parameters u, p, and w are evaluated separately for H_2O and CO_2. At wavelengths where H_2O and CO_2 both have absorption bands, the transmissivity was calculated as the product of the transmissivities due to each alone; i. e.,

$$\tau = \tau_{H_2O}\,(w_{H_2O},\, p_{H_2O}) \cdot \tau_{CO_2}\,(w_{CO_2},\, p_{CO_2}) \qquad (11)$$

The two "observer" altitudes for which the calculations were performed are h_o = 21,750 ft. M.S.L. and h_o = 32,750 ft. M.S.L. These two altitudes were used to define the highest isothermal layer. The atmosphere between the ground (4090 ft. M.S.L.) and 21,750 ft. M.S.L. was divided at 8,000 ft., 12,000 ft., and 16,000 ft. into four additional layers. The radiosonde data of air temperature and relative humidity were converted to H_2O partial densities by using the table for saturated water vapor given in the Smithsonian Meterological Tables[6]. The partial densities, ρ_{H_2O}, were plotted against altitude (see Figure 60) and planimetered to determine w_{H_2O} between the observer altitude h_o and the bottom of each layer. The plotted results were interpolated or extrapolated wherever radiosonde data is missing. Similarly, p_{H_2O} was determined by planimetering a plot of $P\rho_{H_2O}$ (see Figure 61) and dividing the results by w_{H_2O} in each case (according to Equation 8). The parameter w_{CO_2} is proportional to the integral of the air density ρ over the path since the mole fraction of CO_2 (taken as 0.00033) is approximately constant with altitude; thus w_{CO_2} and p_{CO_2} were determined by planimetering ρ (see Figure 62) and $P\rho$ (see Figure 63), respectively. The calculated parameters w_{H_2O}, p_{H_2O}, u_{H_2O}, w_{CO_2}, p_{CO_2}, and u_{CO_2}, for both observer altitudes, and the mean temperatures for each layer are

---

6. Smithsonian Meteorological Tables, Fifth Revised Edition, Lord Baltimore Press, 1939.

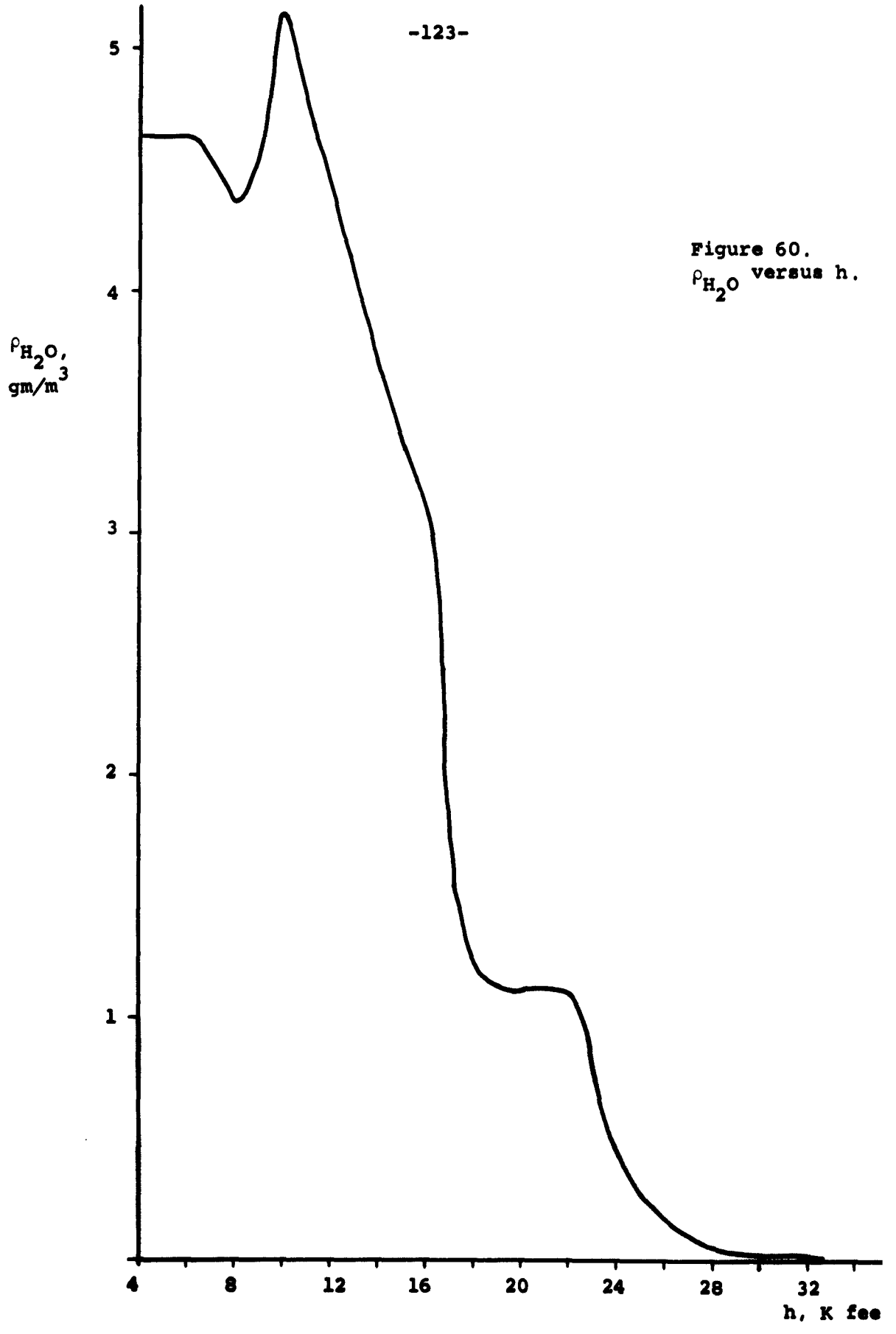

Figure 60.
ρ_{H_2O} versus h.

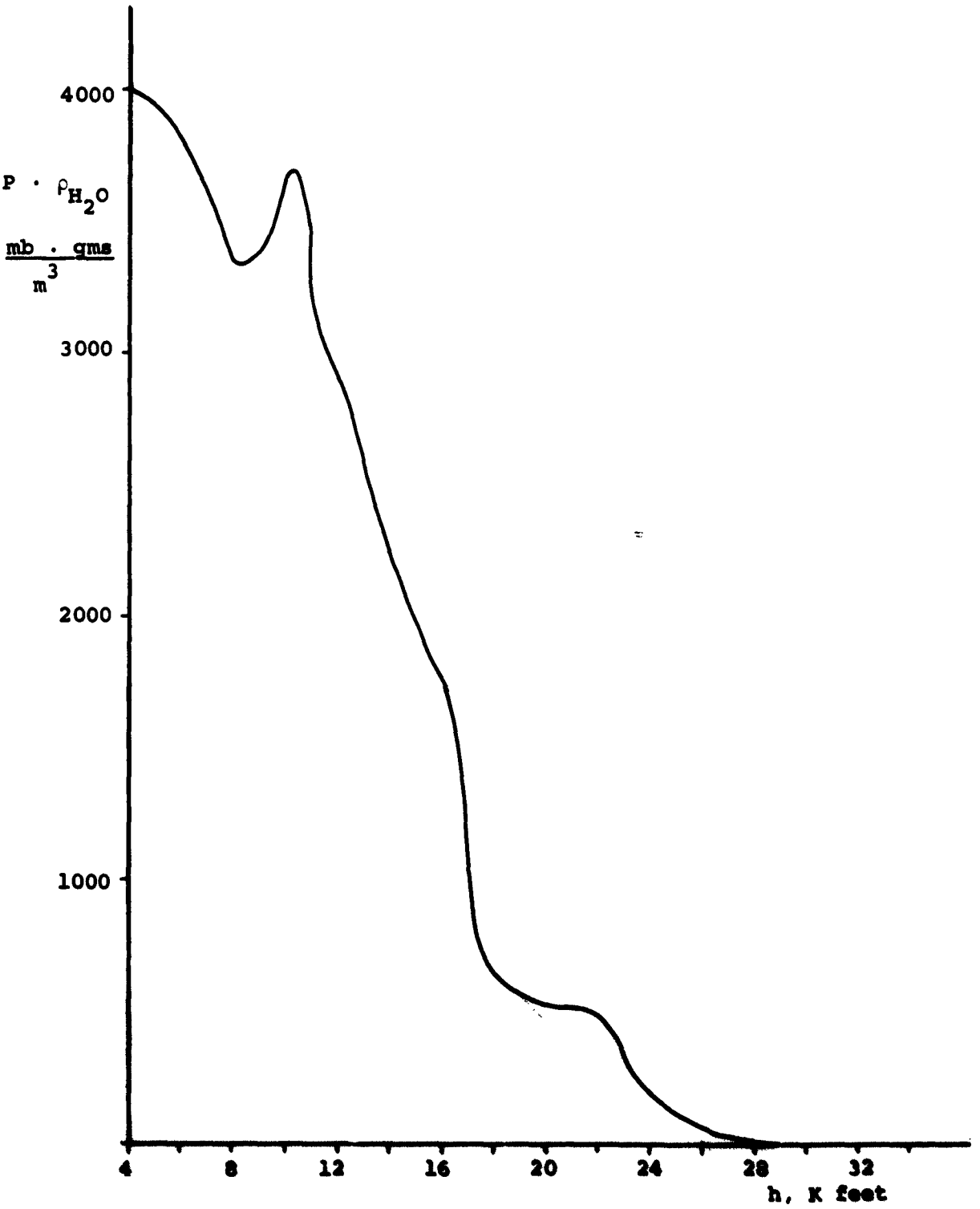

Figure 61.
ρ_{H_2O} versus h

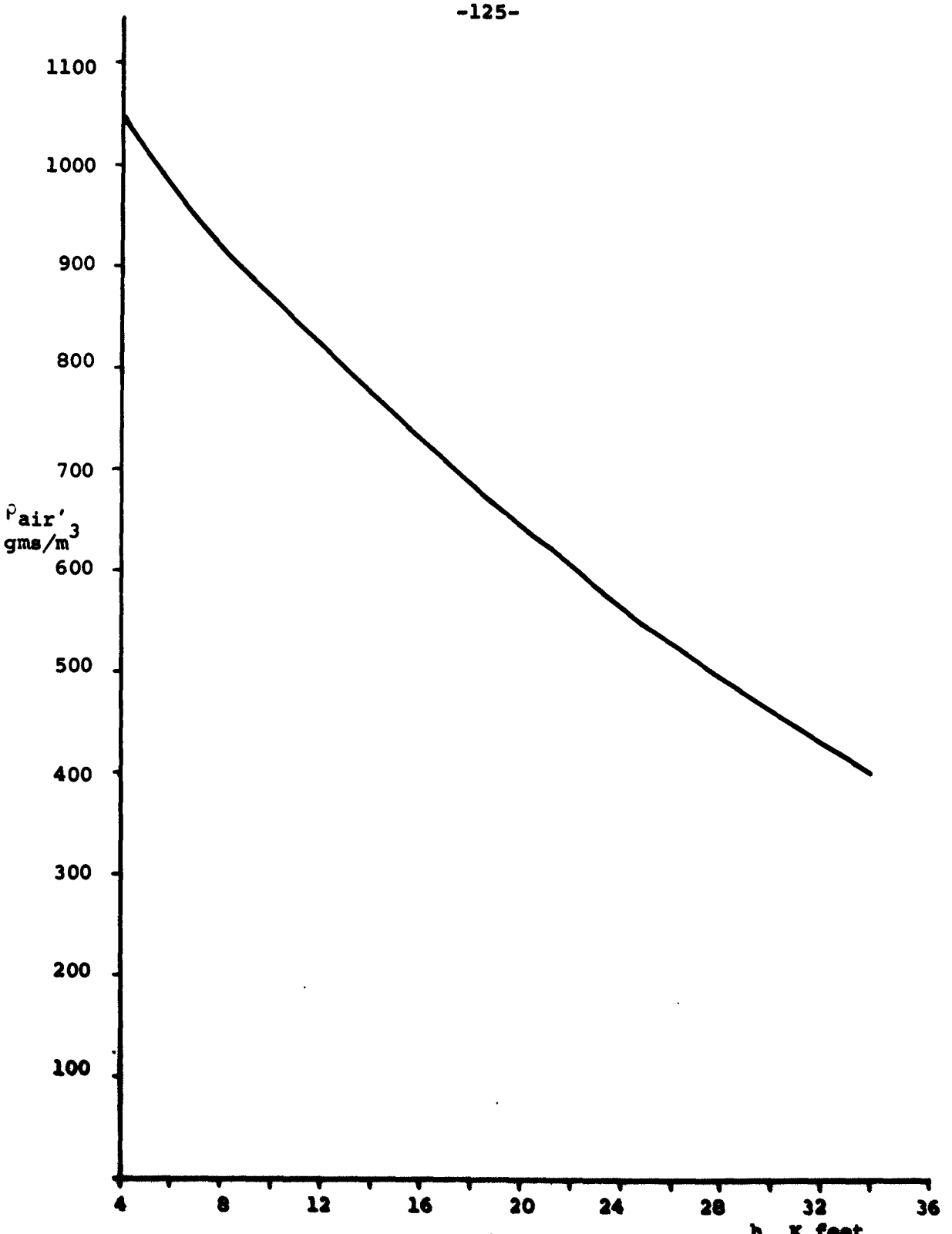

Figure 62.
ρ_{air} versus h

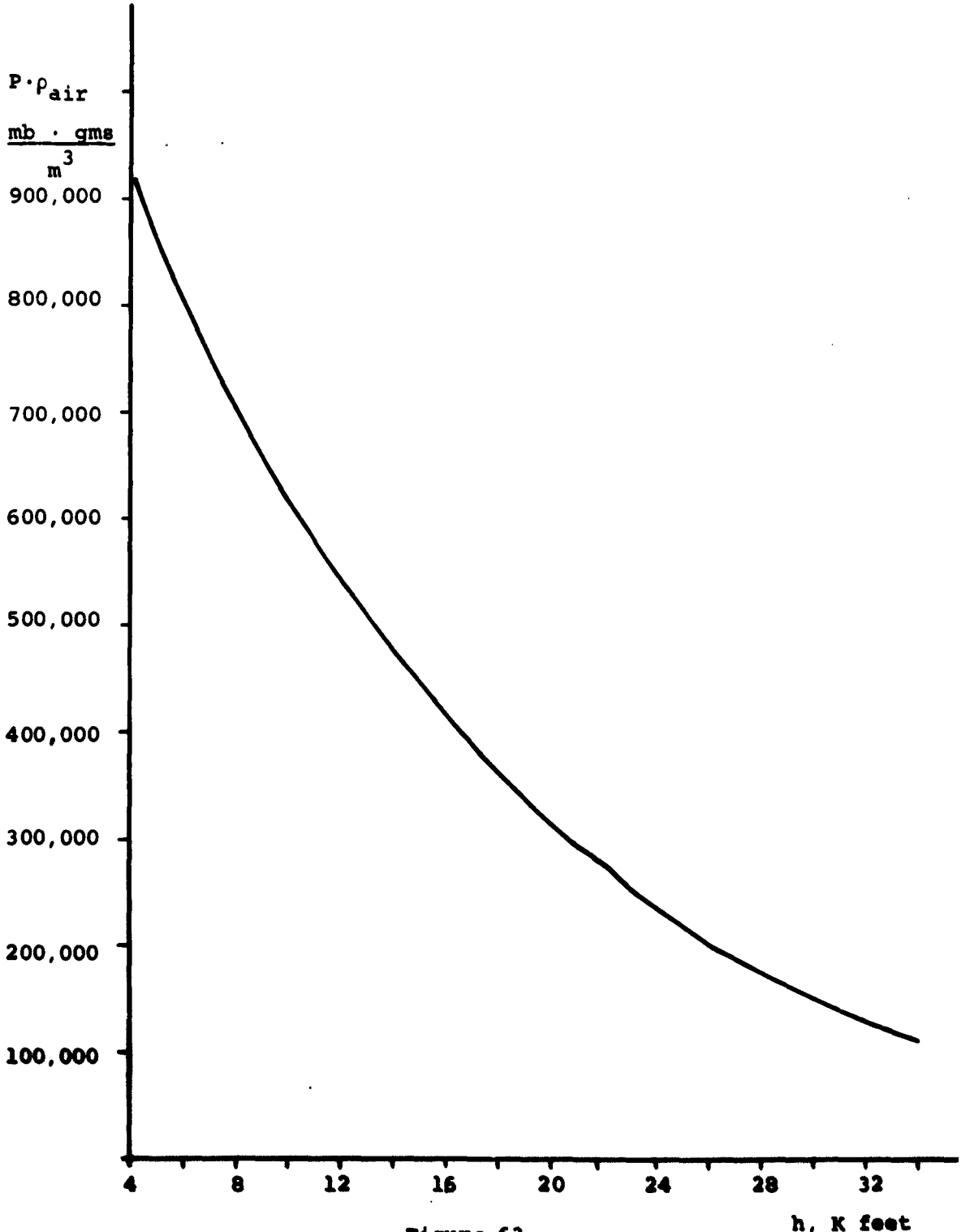

Figure 63.
$P \cdot \rho_{air}$ Versus h.

are listed in Table 1. For h_o = 32,750 ft., only the properties for the 21,750 - 32,750 ft. layer are given, because the radiance at 32,750 ft. was determined from a one-layer model by utilizing the results from the calculation for h_o = 21, 750 ft. This procedure, which is legitimate only when τ has the "weak line" form $e^{-\text{const. x } w}$, actually gives reasonably accurate results in the present case since the 21,750 - 32,750 ft. layer is optically thin over most of the spectral regions considered.

The transmissivity between h_o and the bottom of each layer was evaluated at a large number of carefully selected wavelengths using Equation 7 and References 1 and 2. The black-body spectral radiance corresponding to the temperature of each layer was determined at these same wavelengths using standard tables. Finally, the radiance, N_λ (21,750 feet), was determined from the transfer equation (6). The radiance, N_λ (32,750 feet), was evaluated from

$$N_\lambda\ (32,750) = N_\lambda\ (21,750)\ \tau_{\lambda 5} + N_{BB}(\lambda,\ 259°K)(1 - \tau_{\lambda 5}) \qquad (12)$$

where $\tau_{\lambda 5}$ is the calculated transmissivity of the 21,750 - 32,750 ft. layer.

It is expected that the radiosonde profiles used for the calculations are only approximately the same as the conditions that actually existed during the two observations. The radiosonde data was obtained from weather balloon flights over a period of 4 hours, whereas the conditions that determine the observed or calculated upward radiance are given by the "instantaneous" profiles at the time of the radiance measurements. Obviously, any temporal variations, such as the movement of clouds during

TABLE 1

SUMMARY OF CALCULATED ATMOSPHERIC PROPERTIES

h_o = 21,750 ft. above M.S.L.

h (ft. above M.S.L.)	T(°K)	w_{H_2O} (pr. cm.)	p_{H_2O} (mm. Hg)	u_{H_2O} (pr. cm.)	w_{CO_2} (Atm. cm.)	p_{CO_2} (mm. Hg)	u_{CO_2} (Atm. cm.)
21,750							
	267						
16,000		.251	403	.133	31.0	370	15.1
	276						
12,000		.706	443	.412	55.4	408	29.7
	285						
8,000		1.28	485	.817	82.5	450	48.8
	292						
4,090 (ground)	297.5	1.86	521	1.275	113	494	73.5

h_o = 32,750 ft. above M.S.L.

32,750							
	259						
21,750		.0842	326	.0361	43.6	281	16.1

the radiosonde flights (or at any time between the radiosonde flights and the times of the observations), could cause discrepancies between the measured and calculated spectral radiance. Another source of possible disagreement is the fact that the radiosonde moisture data includes all forms of H_2O (e.g., the ice crystals or water droplets due to clouds) while the theoretical calculations are valid only for pure H_2O vapor.

One would guess that the movements of clouds are the most important temporal variations and also that clouds are the principal sources of spurious water. Moving clouds were, in fact, observed during balloon flight No. 2. Although there is insufficient flight data to include the effects of clouds in the calculated spectral radiance, one can at least determine the relative probability of cloud effects in different wavelength regions. For this purpose, we calculated the altitude, h, for which the transmissivity between h_o and h has some arbitrary small value, δ, as a function of wavelength. The major contribution to $N_\lambda(h_o)$ must come from the atmosphere between h and h_o. Thus, the effects of clouds may be assumed smaller for larger values of h (i.e., closer to h_o) since the probability of finding clouds at a given altitude generally decreases with the altitude. Figure 64 shows h vs. λ for h_o = 21,750 feet and δ = 0.10 and 0.01. Figure 65 shows h vs. λ for h_o = 32,750 feet and δ = 0.01.

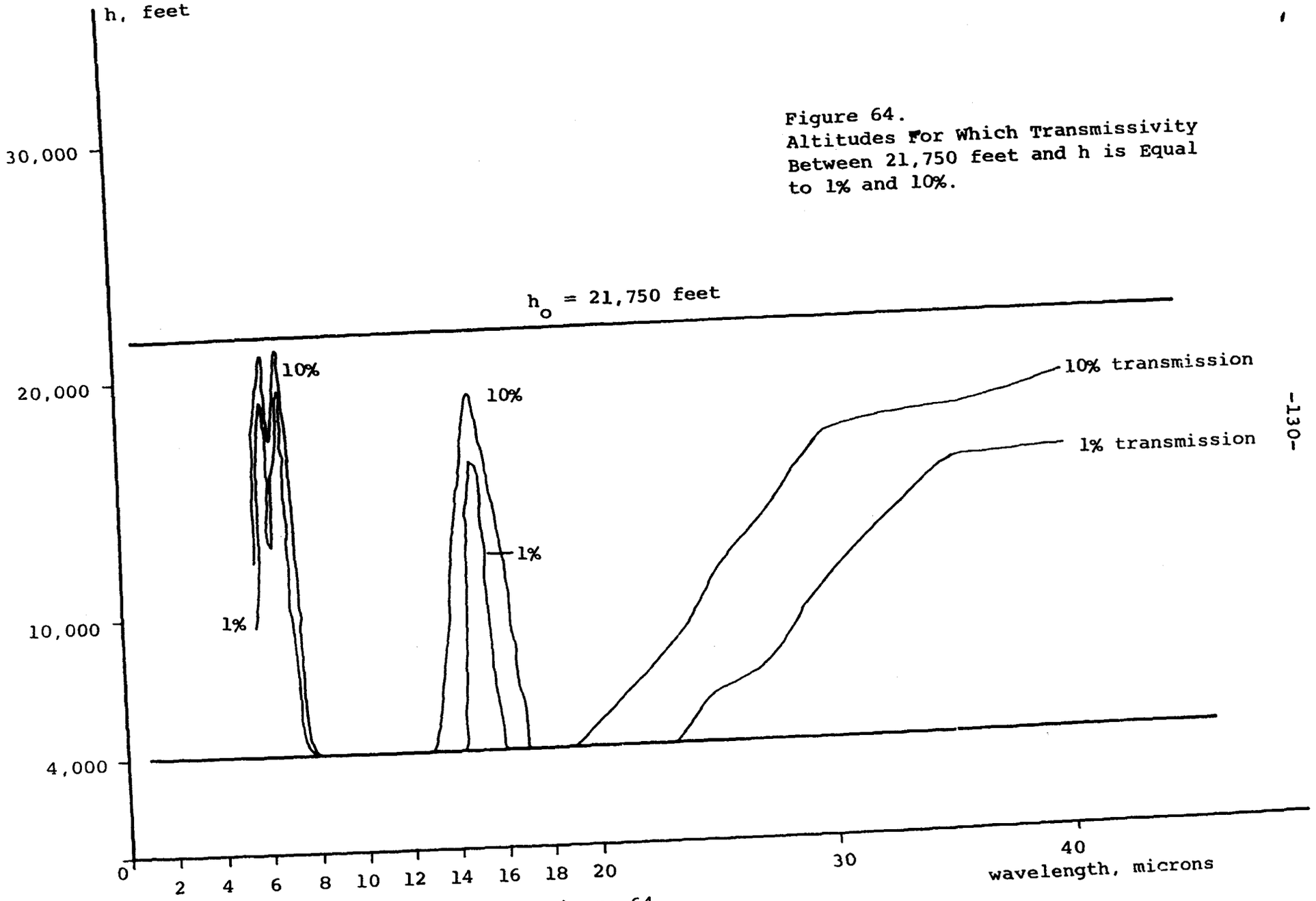

Figure 64.
Altitudes For Which Transmissivity Between 21,750 feet and h is Equal to 1% and 10%.

Figure 64

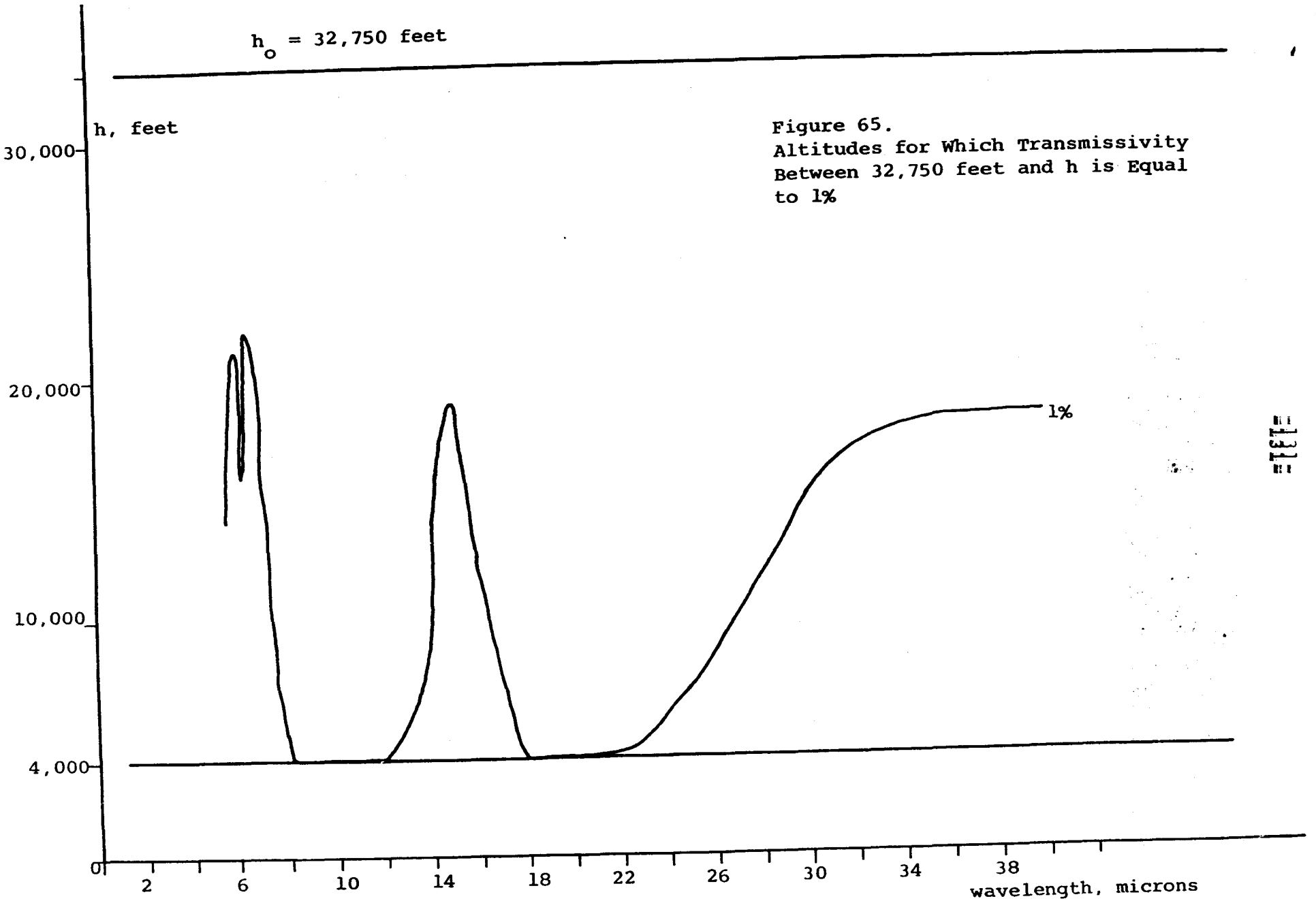

Figure 65.
Altitudes for Which Transmissivity Between 32,750 feet and h is Equal to 1%

Figure 65

7.2.3 Tolerance of Experimental Data

Before analyzing the data, it is important to know what the "tolerance" is on the values presented. In other words, how much would we expect the data to differ from the actual or "real" radiance values.

For the purpose of this discussion, we will consider that there are two factors which combine to determine the overall data tolerance. First is system noise, defined as the noise equivalent spectral radiance, N.E.S.R., which is that spectral radiance which produces a signal just equal to the noise signal. This, then, represents the smallest radiance increment which can be detected and is the ultimate limit on system accuracy. For an optimum system, the N.E.S.R. is determined solely by the detector characteristics. In actual practice, however, this N.E.S.R. is degraded by a combination of instrument inefficiencies such as optical transmission and chopping efficiency as well as electrical noise generated by amplifiers and recording devices.

The N.E.S.R. varies from wavelength to wavelength since many of the parameters which determine it are wavelength dependent and, therefore, we will define the N.E.S.R. at a given wavelength as $N.E.S.R._{\lambda}$.

The $N.E.S.R._{\lambda}$ can be determined experimentally in the laboratory by having the spectrometer view a mirror, thus seeing a source radiance exactly equal to its own radiance, and, therefore, any signal produced is due to noise. In the case of the balloon-borne experiments, however, it was anticipated that the telemetry system would introduce noise; therefore, an additional step was added. The laboratory measurement was considered to represent only the relative N.E.S.R. and the signal levels at wavelengths shorter than 4 microns were used to assign actual values to the

relative $NESR_\lambda$ curve. It should be noted that this method is valid for night flights only since during the day reflected solar radiance could produce signals at the short wavelengths. The signal levels in volts were converted into radiance values by dividing the signal at each wavelength by the appropriate spectral responsivity, R_λ.

Table 1 shows the $NESR_\lambda$ for the I-4T. Column 1 represents the case where the noise is due to the detector only. Column 2 is the $NESR_\lambda$ considering instrument inefficiencies and Columns 3 and 4 represent the NESR values determined from the in-flight balloon data. Two curves, "low noise" and "high noise", are shown since it was noticed that the noise level was not a constant function of altitude due either to variation in the noise characteristics of the on-board equipment, the telemetry reduction equipment, or the spectrometer data processing system. The "leveling off" of the "low noise" curve between 9μ and 15μ is due to the noise characteristics of the Magnecord tape recorder.

The second factor contributing to the tolerance on the data is defined as the error or "inexactness" involved in each of the steps used to determine the spectral radiance. These include errors in responsivity, detector radiance, and signal level, all at a particular wavelength. Errors in wavelength calibration will not be included since what we are concerned with here essentially are ordinate errors, not abscissa errors, in the radiance versus wavelength plots.

The equation by which the source radiance is determined is

$$N_{vs} = \left[N_{vB} - \frac{V_1}{R_v} \right] \qquad (1)$$

where N_{vs} is the source radiance; N_{vB} is the detector radiance, both in μ watts-cm^{-2}-$ster^{-1}$- cm; V_1 is the signal level corrected

TABLE 1

NESR$_\lambda$ VERSUS WAVELENGTH

λ, microns	1	2	3	4
5	6	60	95	300
5.5	5	50	70	230
6	4	40	60	200
6.5	3.5	35	48	140
7	3	30	40	120
7.5	2.3	23	33	110
8	2.2	22	31	100
8.5	1.9	19	30	90
9	1.8	18	30	90
9.5	1.3	13	30	80
10	1.25	12.5	30	75
11	1.1	11	28	70
12	1	10	27	63
13	0.85	8.5	24	60
14	0.65	6.5	23	55
15	0.55	5.5	22	50

All values are μ watts-cm^{-2}-ster^{-1}-μ^{-1}

Column 1: Detector Noise Limit

Column 2: System Efficiency = 10%

Column 3: Experimental Values - Low Noise

Column 4: Experimental Values - High Noise

for noise, in millivolts; and R_ν is the responsivity, in millivolts per μ watt-cm^{-2}-ster^{-1}-cm.

To conform to standard practice, the radiance values are presented as $N_{\lambda S}$, μ watts-cm^{-2}-ster^{-1}-μ^{-1}. The relationship used is,

$$N_{\lambda S} = N_{\nu S} \cdot \nu^2 \times 10^{-4} \tag{2}$$

where ν is the wavenumber in reciprocal centimeters. Combining Equations 1 and 2, we have,

$$N_{\lambda S} = \left[N_{\nu B} - \frac{V_1}{R_\nu}\right] \nu^2 \times 10^{-4} \tag{3}$$

The equation used to determine the error in $N_{\lambda S}$ is derived by first, taking the natural logarithm of both sides of Equation 3.

$$\mathrm{Ln}N_{\lambda S} = \mathrm{Ln}\left[N_{\lambda B} - \frac{V_1}{R_\nu}\right] + 2\mathrm{Ln}\nu + \mathrm{Ln}10^{-4} \tag{4}$$

Differentiating both sides, we have,

$$\frac{dN_{\lambda S}}{N_{\lambda S}} = \frac{1}{N_{\nu B} - \frac{V_1}{R_\nu}} \left[dN_{\nu B} - \left(\frac{1}{R_\nu}\right)(dV_1) + \left(\frac{V_1}{R_\nu^2}\right)(dR_\nu)\right] + \left(\frac{2}{\nu}\right)(d\nu) \tag{5}$$

Substituting Equation 1 into Equation 5,

$$\frac{dN_{\lambda S}}{N_{\lambda S}} = \frac{1}{N_{\nu S}} \left[dN_{\nu B} - \left(\frac{1}{R_\nu}\right)(dV_1) + \left(\frac{V_1}{R_\nu^2}\right)(dR_\nu)\right] + \left(\frac{2}{\nu}\right) d\nu \tag{6}$$

For small increments,

$$\frac{\Delta N_{\lambda S}}{N_{\lambda S}} = \frac{1}{N_{\nu S}} \left[dN_{\nu B} - \left(\frac{1}{R_\nu}\right)(\Delta V_1) + \left(\frac{V_1}{R_\nu^2}\right)(dR_\nu) \right] + \left(\frac{2}{\nu}\right) d\nu \tag{7}$$

where Δ represents the error in each quantity. Since ν as used in Equation 2 is a conversion factor of high accuracy, $\Delta\nu = 0$.

$$\frac{\Delta N_{\lambda S}}{N_{\lambda S}} = \frac{1}{N_{\nu S}} \left[\Delta N_{\nu B} - \left(\frac{1}{R_\nu}\right)(\Delta V_1) + \left(\frac{V_1}{R_\nu^2}\right)(\Delta R_\nu) \right] \tag{8}$$

Substituting Equation 2 into Equation 8,

$$\Delta N_{\lambda S} = \left| 10^{-4}\nu^2 \cdot \Delta N_{\nu B} \right| + \left| 10^{-4} \frac{\nu^2}{R} \cdot \Delta V_1 \right| + \left| 10^{-4} \frac{\nu^2 \cdot V_1}{R_\nu^2} \cdot \Delta R_\nu \right| \tag{9}$$

where the absolute magnitude of each term is used and, thus, $\Delta N_{\lambda S}$ is the maximum possible error.

The first term, $\nu^2 \Delta N_{\nu B}$, represents the error in detector radiance. During the responsivity calibration, a relationship was determined between detector radiance and the signal from a thermistor bead located near the detector. This signal was monitored during the balloon flight by means of the telemetry system; and, therefore, the total error for this term is a combination of the telemetry noise and the radiance versus thermistor bead signal relationship error.

The second term, $\frac{\nu^2 \cdot \Delta V_1}{R_\nu}$, represents the error in signal amplitude read as "units" on the chart recorder. The signal, V_1, at each wavelength is calculated from the relationship,

$$V_1 = \sqrt{\frac{U^2 - U_N^2}{U^2_{G.O.}}} \qquad (10)$$

where U is the chart recorder units of signal including noise, U_N is the chart recorder units of noise, and $U_{G.O.}$ is the chart recorder units of the gain oscillator output (expressed as units per millivolt). The maximum possible error in ΔV_1 is

$$\Delta V_1 = \left| V_1 \frac{U}{U^2-U_N^2} \Delta U \right| + \left| V_1 \frac{U_N}{U^2-U_N^2} \Delta U_N \right| + \left| \frac{V_1}{U_{G.O.}} \Delta U_{G.O.} \right| \qquad (11)$$

The third term, $\frac{\nu^2 . V_1}{R_\nu^2} \cdot \Delta R_\nu$, is the error in responsivity. ΔR_ν was estimated by means of the responsivity plots as shown previously in Figure 24. The line of best fit was used for the value of R_ν. To determine ΔR_ν, the line of <u>poorest</u> fit (which still describes the points) was drawn and the difference between its slope and the best fit is ΔR_ν.

In addition, a portion of the error in ΔN_{ν_B} was determined by using the N_{ν_B} points from the poorest fit lines.

Table 2 shows the values used for the error calculation of a typical spectral observation.

The following is a typical calculation of $\Delta N_{\lambda S}$.

<u>For 10.1 Microns</u>

First, ΔV_1 is calculated by,

$$\Delta V_1 = \left| (1.28) \frac{39}{39^2-2.5^2} 0.5 \right| + \left| (1.28) \frac{2.5}{39^2-2.5^2} 0.5 \right| + \left| (1.28) \frac{1}{30.5} \right.$$

$$= |0.01| + |0.01| + |0.02|$$

$$\Delta V_1 = 0.04$$

TABLE 2

15,000 FEET LOOKING DOWN

λ	$N_{\lambda S}$	U	ΔU	U_N	ΔU_N	$U_{G.O.}$	$\Delta U_{G.O.}$	V_1	V_1	$N_{\nu S}$	R_ν	ΔR_ν	$N_{\nu B}$	$\Delta N_{\nu B}$
15.1	564	44	±0.5	2.5	±0.5	30.5	±0.5	1.45	±.04	12.86	.298	±.007	17.73	±.4
13.2	716	40.5	±0.5	2.5	±0.5	30.5	±0.5	1.33	±.04	12.49	.303	±.007	16.88	±.4
10.1	898	39	±0.5	2.5	±0.5	30.5	±0.5	1.28	±.04	9.16	.357	±.01	12.75	±.5
8.48	777	42	±0.5	2.5	±0.5	30.5	±0.5	1.38	±.04	5.60	.412	±.02	8.95	±.5
7.31	531	36	±0.5	2.5	±0.5	30.5	±0.5	1.18	±.04	2.84	.387	±.02	5.89	±.2
6.06	292	19	±0.5	2.5	±0.5	30.5	±0.5	0.62	±.04	1.07	.338	±.004	2.90	±.05
5.30	238	8	±0.5	2.5	±0.5	30.5	±0.5	0.24	±.03	0.67	.312	±.003	1.44	±.02

λ = microns

$N_{\lambda S}$ = μ watts-cm^{-2}-ster^{-1}-μ^{-1}

$N_{\nu S}$, $N_{\nu B}$, $\Delta N_{\nu B}$ = μ watts-cm^{-2}-ster^{-1}-cm

U, ΔU, U_N, ΔU_N, $U_{G.O.}$, $\Delta U_{G.O.}$ = units

V_1, ΔV_1 = millivolts

R_ν, ΔR_ν = millivolts per μ watts-cm^{-2}-ster^{-1}-cm

Now, $\Delta N_{\lambda S}$ is calculated from Equation 9.

$$\Delta N_{\lambda S} = 10^{-4}(990)^2(0.5) + 10^{-4}(990)^2\left(\frac{1}{.357}\right)(0.04) + 10^{-4}(990)^2\frac{(1.28)}{(.357)^2}(0.0$$

$$= 49 + 11 + 10$$

The total maximum tolerance is the sum of these three terms plus the $NESR_\lambda$ at 10.1μ which was 30 μ watts-cm^{-2}-$ster^{-1}$-μ^{-1}.

$$\Delta N_{\lambda S} = \pm 100\mu \text{ watt-cm}^{-2}\text{-ster}^{-1}\text{-}\mu^{-1} \text{ at } 10.1\mu.$$

The "expected RMS tolerance" is found by using r.m.s. values rather than absolute magnitudes. Thus, for the above example,

$$\Delta N_{\lambda S} = \sqrt{(49)^2 + (11)^2 + (10)^2 + (30)^2}$$

$$\Delta N_{\lambda S} = 60 \text{ } \mu \text{ watts-cm}^{-2}\text{-ster}^{-1}\text{-}\mu^{-1}.$$

The percentage RMS tolerance is

$$\frac{\Delta N_{\lambda S}}{N_{\lambda S}} \times 100 = \frac{60}{898} \times 100 = 6.8\%$$

Table 3 shows the results of this tolerance analysis using the values presented in Tables 1 and 2.

One problem in performing this tolerance analysis was the difficulty in arriving at values for ΔV_1, ΔR_V, ΔN_{V_B}, and $NESR_\lambda$ mutually independent of each other. Therefore, the end result most probably contains some errors included more than once. However, the results do give relative magnitudes and, in addition, indicate the relative contribution of each parameter. For instance,

TABLE 3

EXPECTED RMS TOLERANCE OF FLIGHT DATA

λ, microns	1	2	3	4	5
15.1	18	5.9	5	22	29
13.2	21	7.1	5.4	24	33
10.1	49	11	10	30	60
8.48	69	15.6	17.7	30	79
7.31	37	19.4	29	34	62
6.06	13.6	31	6	60	69
5.30	7.1	45.2	2.7	80	92

Columns 1 $[10^{-4} \cdot \nu^2 \cdot \Delta N_{\nu_B}]$: ($\mu$ watts-cm^{-2}-ster^{-1}-μ^{-1})

2 $\left[\frac{10^{-4} \cdot \nu^2 \cdot \Delta V_1}{R_\nu}\right]$: ($\mu$ watts-cm^{-2}-ster^{-1}-μ^{-1})

3 $\left[\frac{10^{-4} \cdot \nu^2 \cdot \Delta V_1}{R_\nu^2} \cdot \Delta R_\nu\right]$: ($\mu$ watts-cm^{-2}-ster^{-1}-μ^{-1})

4 $[\text{N.E.S.R.}_\lambda]$: ($\mu$ watts-cm^{-2}-ster^{-1}-μ^{-1})

5 Expected RMS Tolerance: (μ watts-cm^{-2}-ster^{-1}-μ^{-1})

Column 1 shows that the error in detector radiance plays a major role in the 8μ to 10μ region which corresponds to the area of its peak value. Signal amplitude errors, shown in Column 2, are significant at the shorter wavelengths due to the low radiance levels from both the detector and the source. Column 3 indicates that errors in the responsivity calibration tend to contribute less than any of the other factors. Column 4 shows that at the extremes of the wavelength region the system noise is the tolerance limit, whereas in the 7μ to 10μ region noise is not as critical as detector radiance.

7.2.4 Discussion of Flight Results

The downward radiance, that is, the radiance seen by looking up, was obtained for the region 5μ to 15μ by the I-4T. Since the I-4TC was not looking up and since no dewpoint data was available for altitudes above 35,000 feet, it is not possible to compare this information with either data from a second instrument or with theoretical values.

Looking up, at launch, the I-4T indicates a black-body temperature in the window region of 259°K, whereas both the 6.3μ H_2O and the 15μ CO_2 indicate a black-body temperature of 291°K. This indicates that the I-4T "saw" to a maximum altitude of 8,000 feet in the absorption regions and to a maximum of 22,000 feet in the window. As the balloon ascended, the radiance in the absorption regions decreased slightly as would be expected since the air temperature is decreasing. However, the black-body temperature in the window region shows an increase possibly due to the presence of clouds between 10,000 feet and 16,000 feet, the temperature of a cloud at these altitudes being warmer than at 22,000 feet.

The decrease in radiance for both the window region and the CO_2 region between 13,000 feet and 20,000 feet followed by an increase at 30,000 feet and a decrease to 38,000 feet may all be as a result of clouds or layers of H_2O continuum moving in and out of the field of view as the balloon ascends into increasingly colder ambient temperatures. The 6.3μ H_2O, however, does not seem to fit into this pattern above 20,000 feet although this may be due to the mixing ratio versus altitude characteristics.

The upward radiance was measured in the 6.3μ water vapor region by the I-4T, in the 2.μ to 40μ portion of the rotational

water vapor region by the I-4TC and the 10μ to 12μ window as well as 15μ CO_2 were measured by both instruments.

Both water vapor regions agree within 20% of the theoretical predictions for the altitudes of 21,750 feet and 32,750 feet. Large discrepancies were noted in the regions of overlap, however. In the window region, especially, the I-4TC was consistently lower in radiance value. Moreover, in the CO_2 region, the I-4TC was consistently lower than both the theoretical and the I-4T which agreed with each other. The exception to the rule was seen at the launch altitude of 4090 feet M.S.L. where both instruments indicated the same radiance values for both the window and CO_2.

Since the I-4T measurement at 6.3μ and the I-4TC measurement in the region from 21μ to 40μ agree with the theoretical for 21,750 feet and 32,750 feet, it appears that the instrumentation was operating satisfactorily. Furthermore, the nature of the interferometer is such that it is difficult to find instrument parameters which could cause errors at one wavelength and not at others. Although the optical alignment is relatively more crucial at short wavelengths, the cyclic nature of the I-4TC data at 15.4μ and 10.6μ tends to preclude a shift in optical alignment after launch. Wavelength calibration is not a factor since the electrical frequency versus wavelength relationship depends upon mirror velocity and, thus, a variation would affect all wavelengths rather than one region alone. Any variation in electronic gain is accounted for in the data reduction process. The two instruments were mounted within 2 feet of each other on the gondola and, although no attempt was made to boresight them together, it is not likely that they were each viewing different atmospheric regions especially since the field of view are identical.

One possible explanation is the effect of system noise since for some unknown reason the I-4TC noise level varied, somewhat in the manner in which the 15.4μ plotted spectra varies. The largest difference between the two instruments for this spectral region occurred at 52,500 feet where the I-4TC noise level was five times what it was at 4090 feet.

Since the responsivity of the I-4TC was low in the 10μ to 15μ region, it is evident that although the noise level is accounted for in the data calculations the combination of low sensitivity and high noise prohibits meaningful interpretation of I4TC data for this region.

The decrease in radiance as a function of altitude seen by the I-4T at 9.64μ and 10.6μ indicates ascension through increasingly colder H_2O continuum as was shown by the downward radiance data. The radiance values at 6.24μ and 15.1μ are also consistent with the atmospheric temperature, pressure, and dew point information.

The radiance values at 34.5μ did not decrease as rapidly as in the other regions mostly due to the fact that at the very long wavelengths it is necessary to have a substantial temperature change in order to have a significant radiance change. The indicated black-body temperatures ranged from 290°K at 4090 feet to 275°K at 20,000 feet and less than 250°K above 30,000 feet.

8.0 Conclusions

The results of the two balloon fligh̄s demonstrate the feasibility and advantages of using the interferometer spectrometer for atmospheric radiance measurements. Moreover, the evaluation of the data reduction system and procedures indicates the direction for improvement, although the equipment and procedures used were adequate.

LIST OF APPENDICES

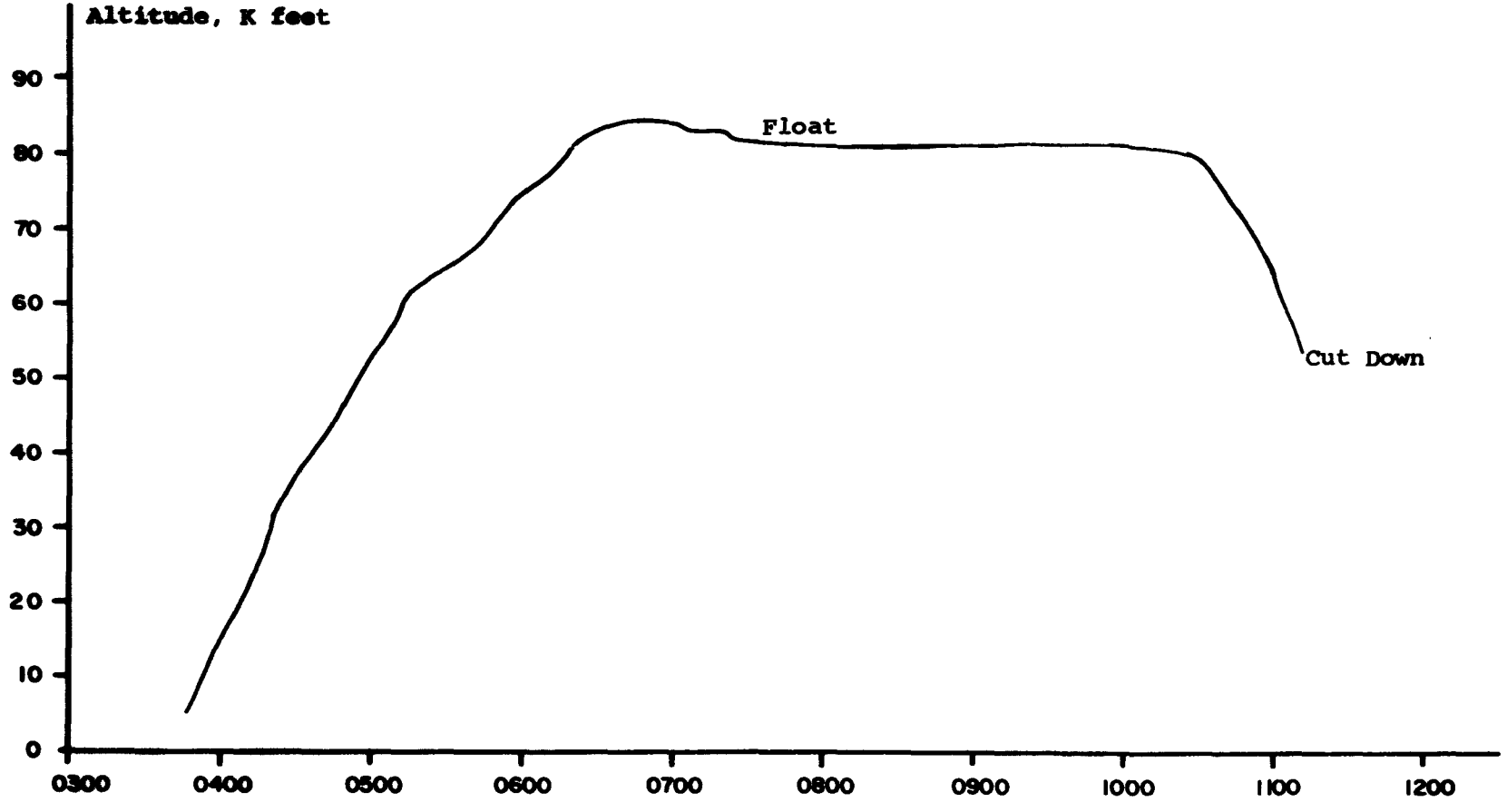

Figure A.
Balloon Flight Trajectory
5 April 1962

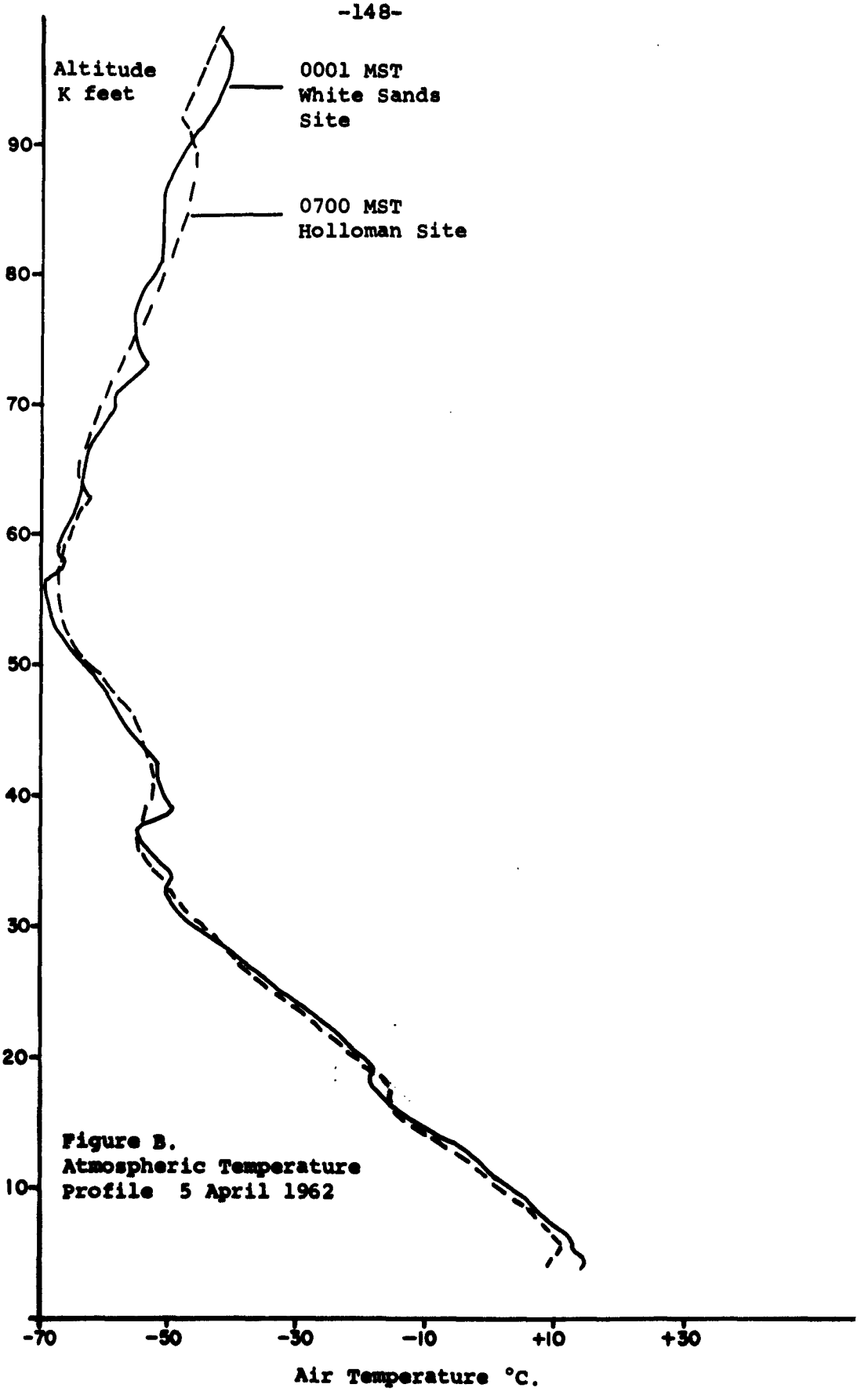

Figure B.
Atmospheric Temperature Profile 5 April 1962

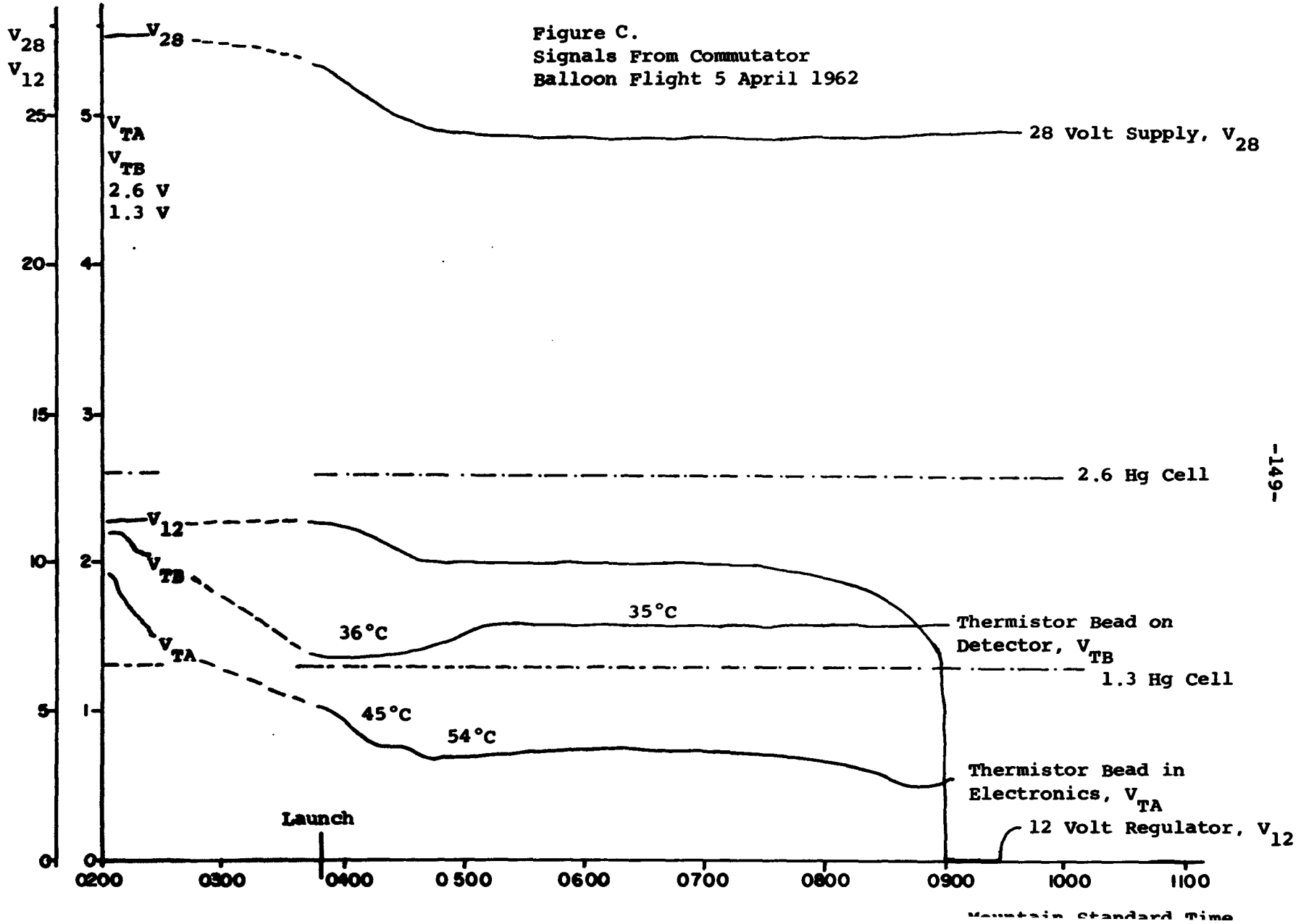

Figure C.
Signals From Commutator
Balloon Flight 5 April 1962

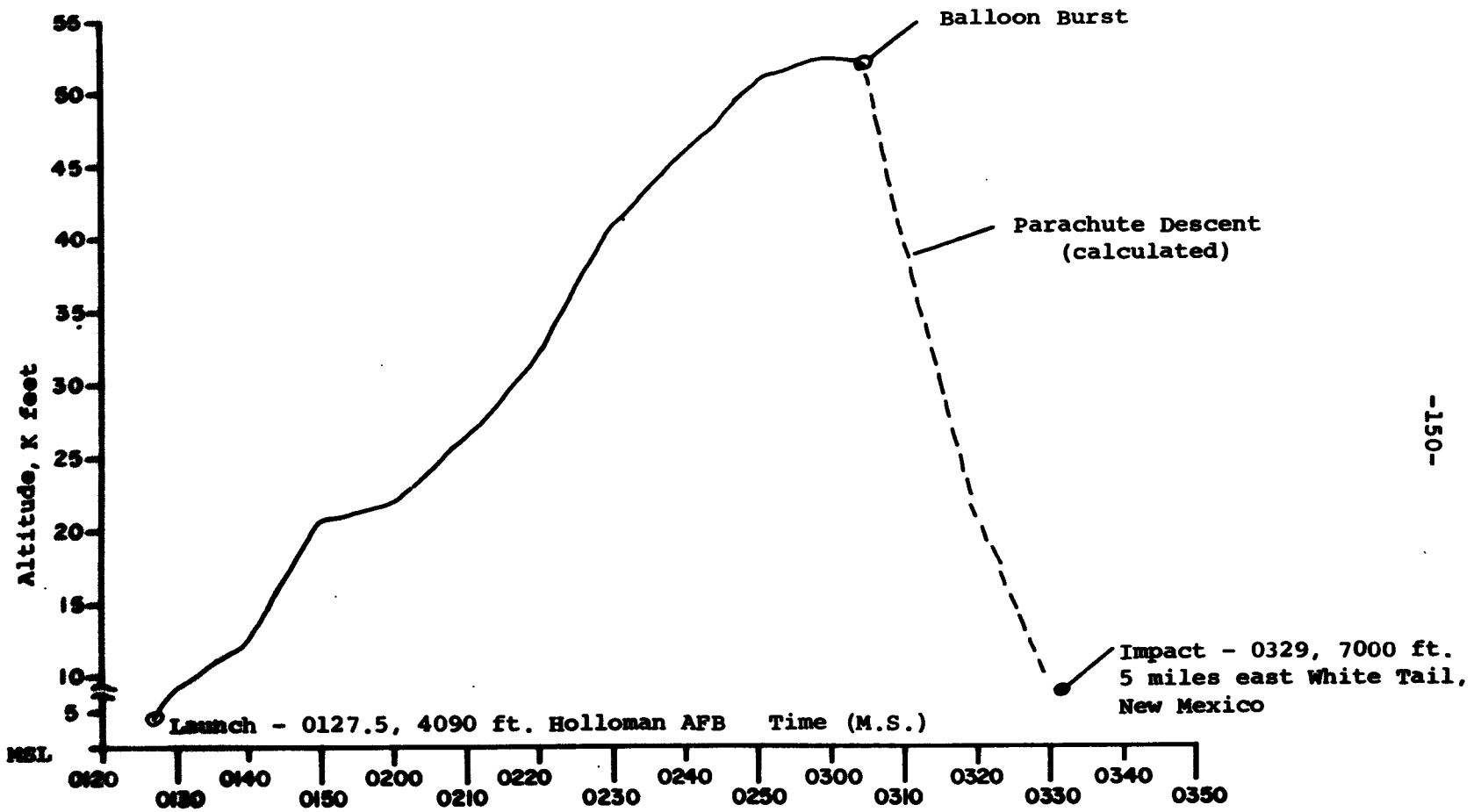

Figure D. Height - Time Data.
2 August 1962

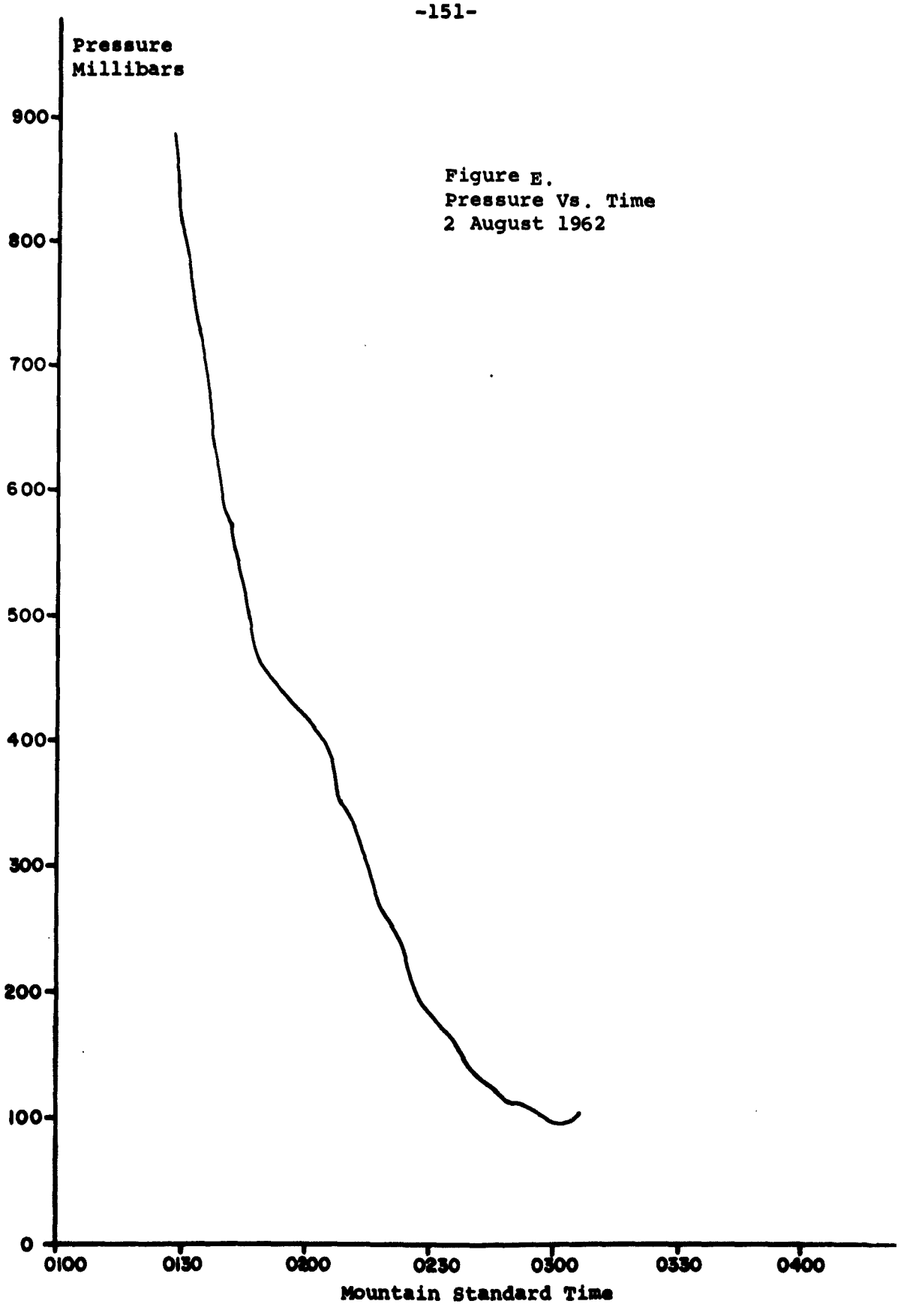

Figure E.
Pressure Vs. Time
2 August 1962

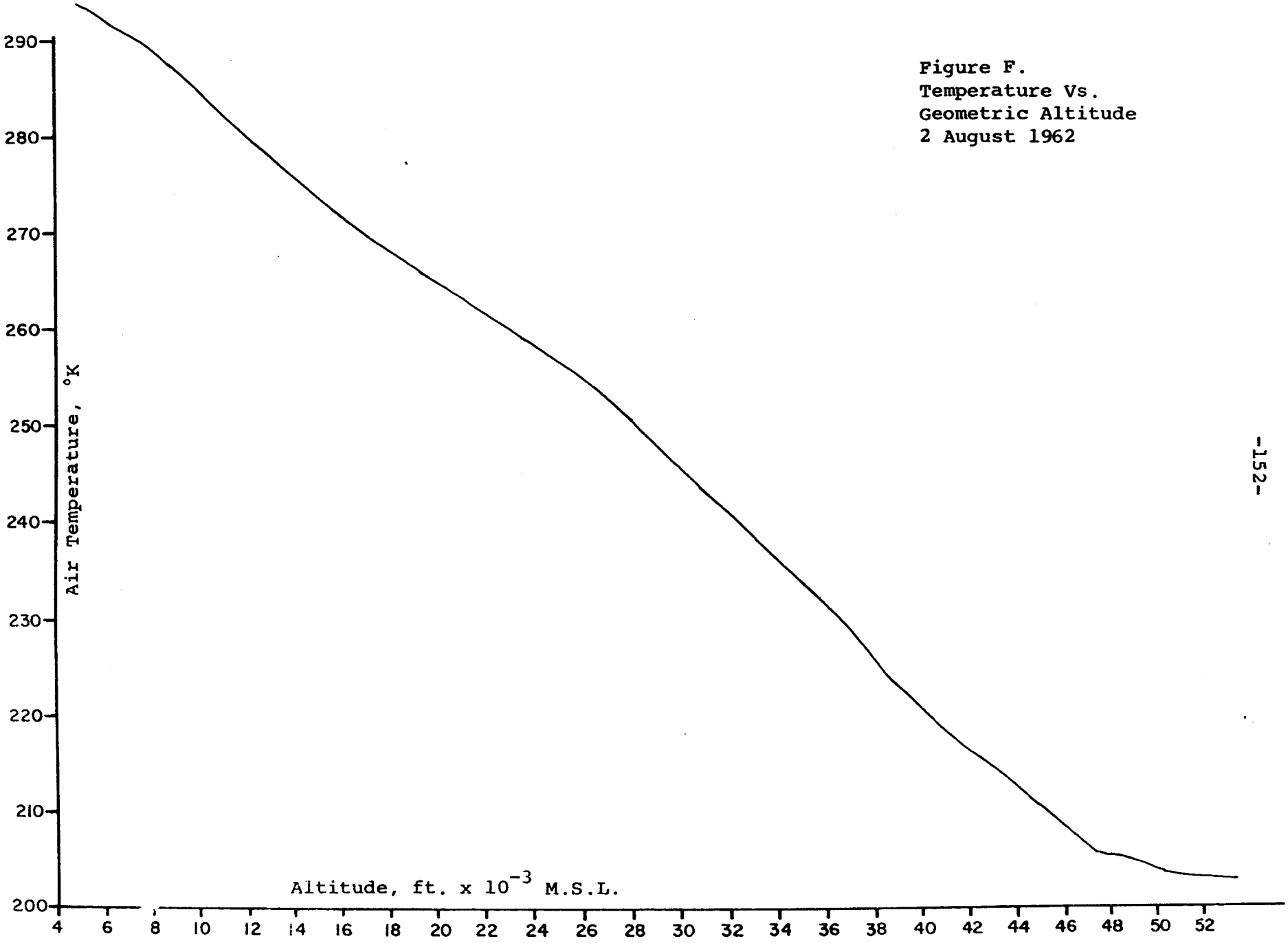

Figure F.
Temperature Vs.
Geometric Altitude
2 August 1962

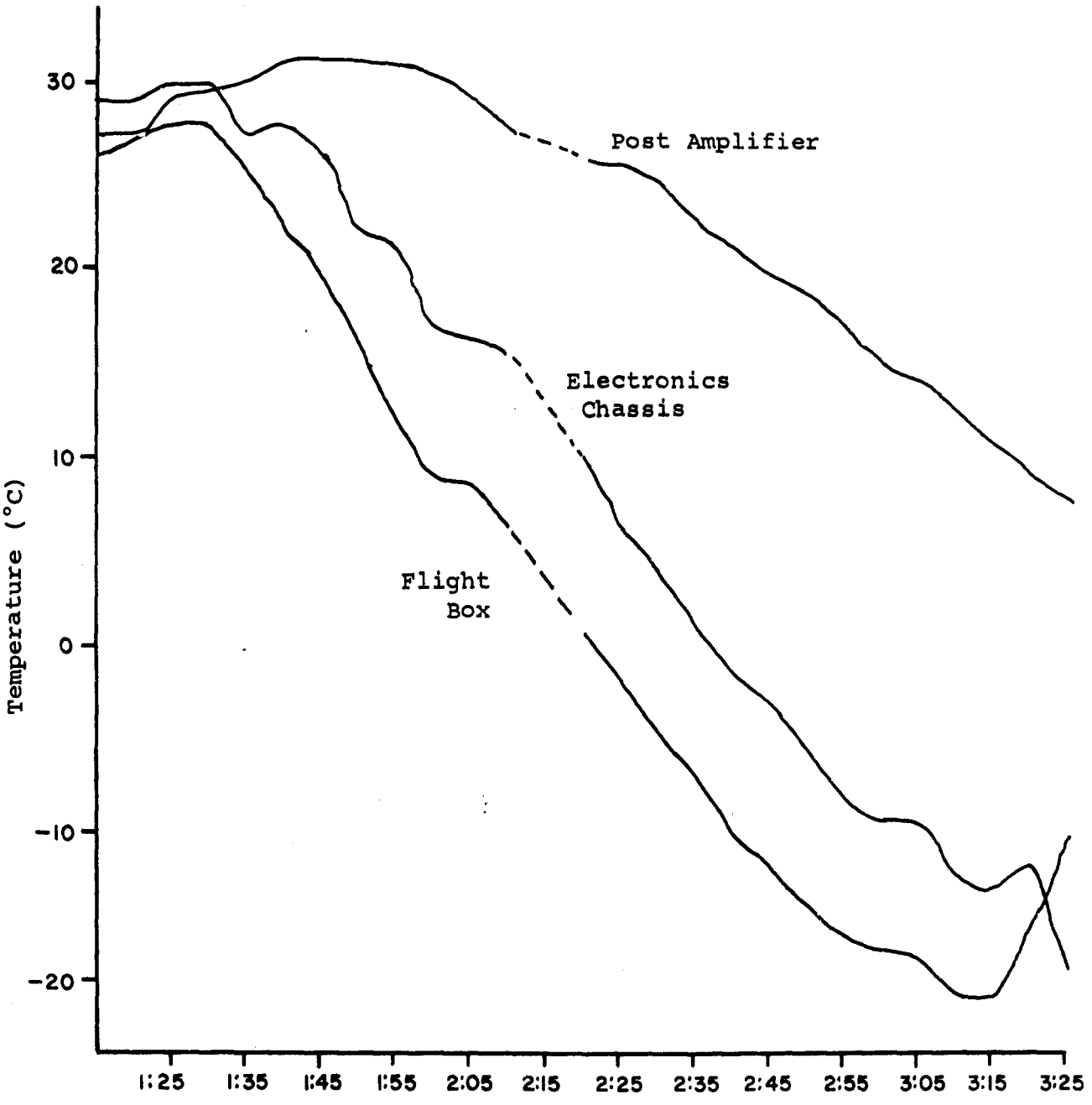

Figure G.
I4T Temperatures.
2 August 1962

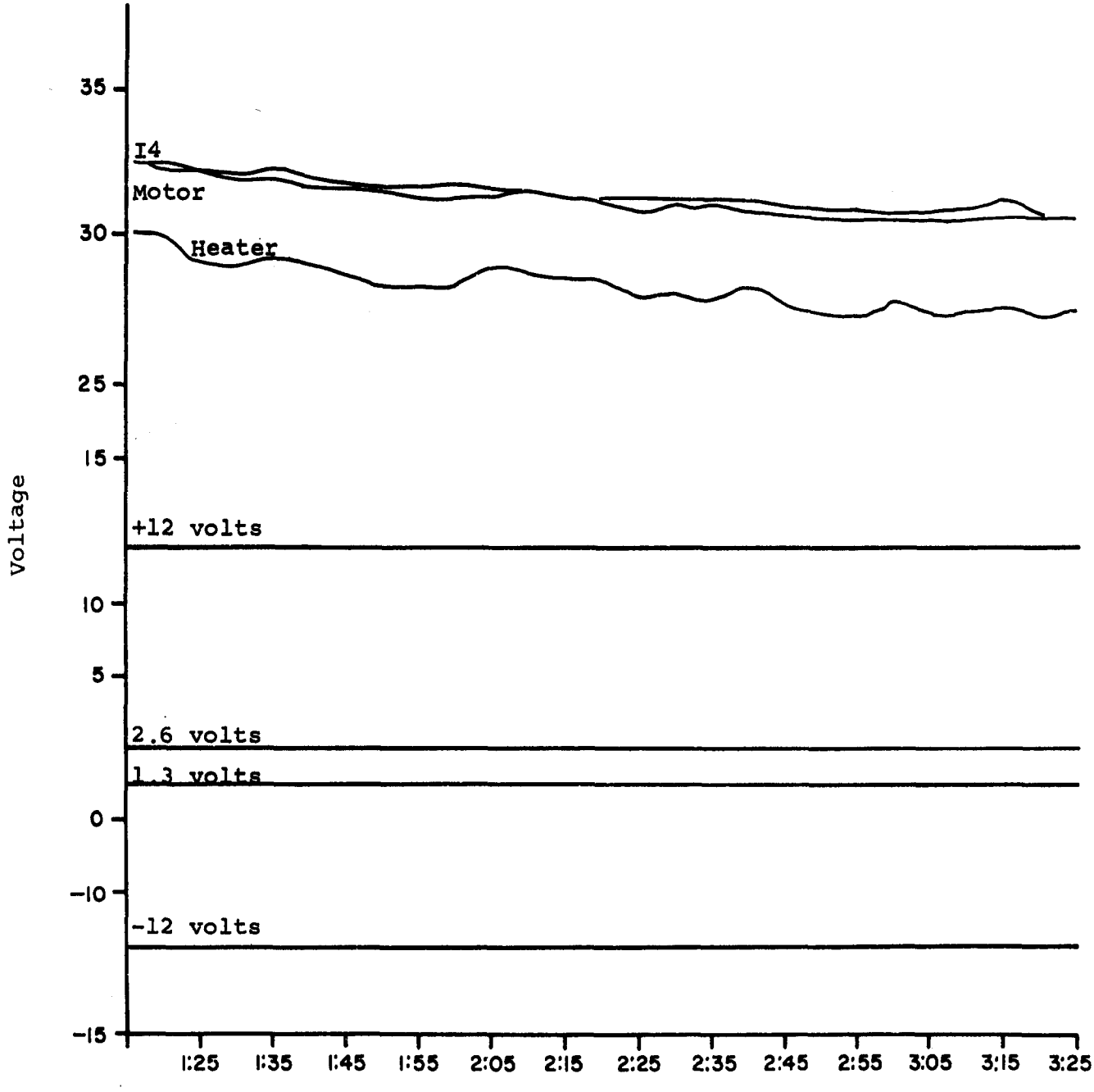

Figure H.
I4T Voltages
2 August 1962

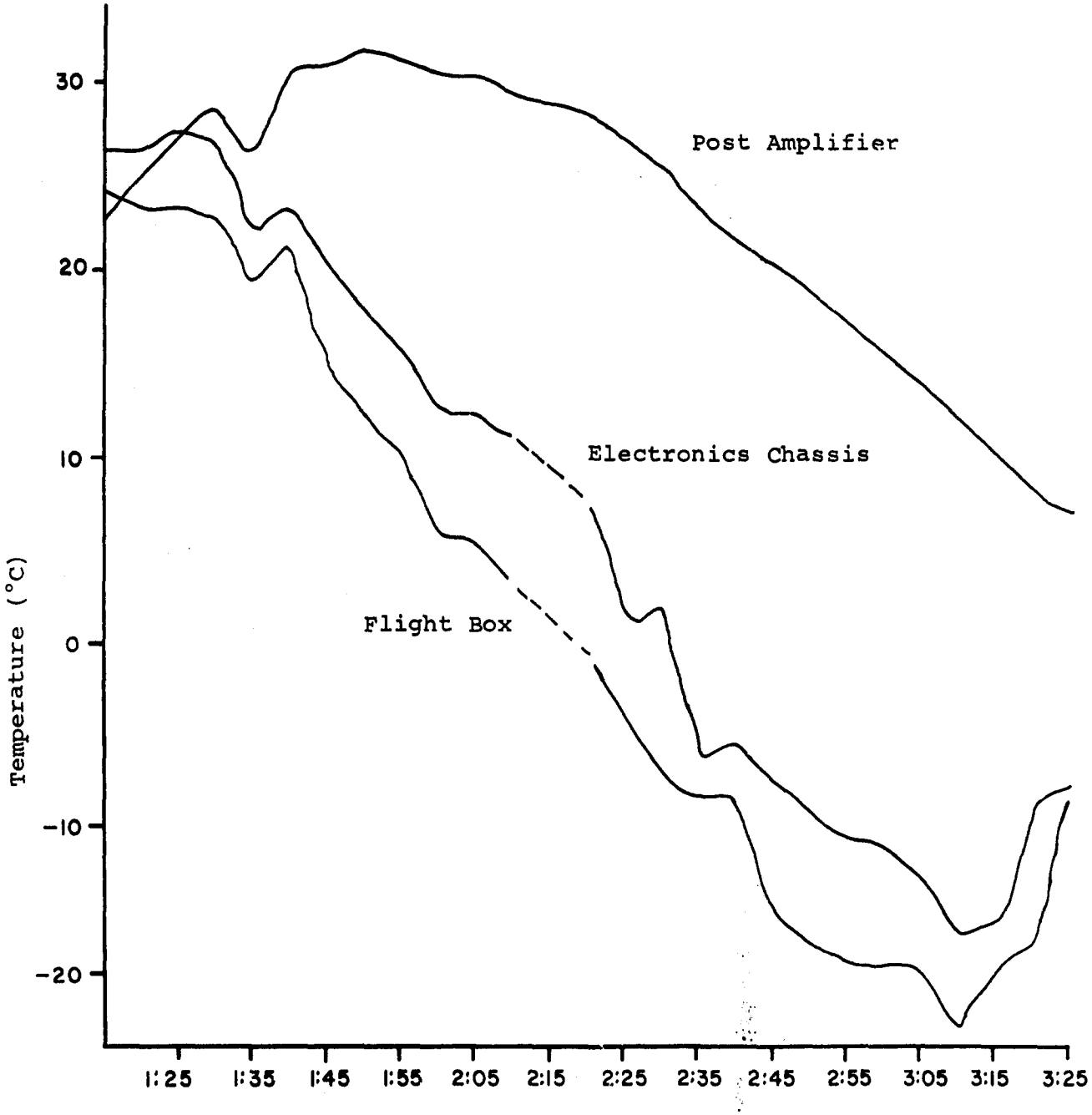

Figure I.
I4TC Temperatures
2 August 1962

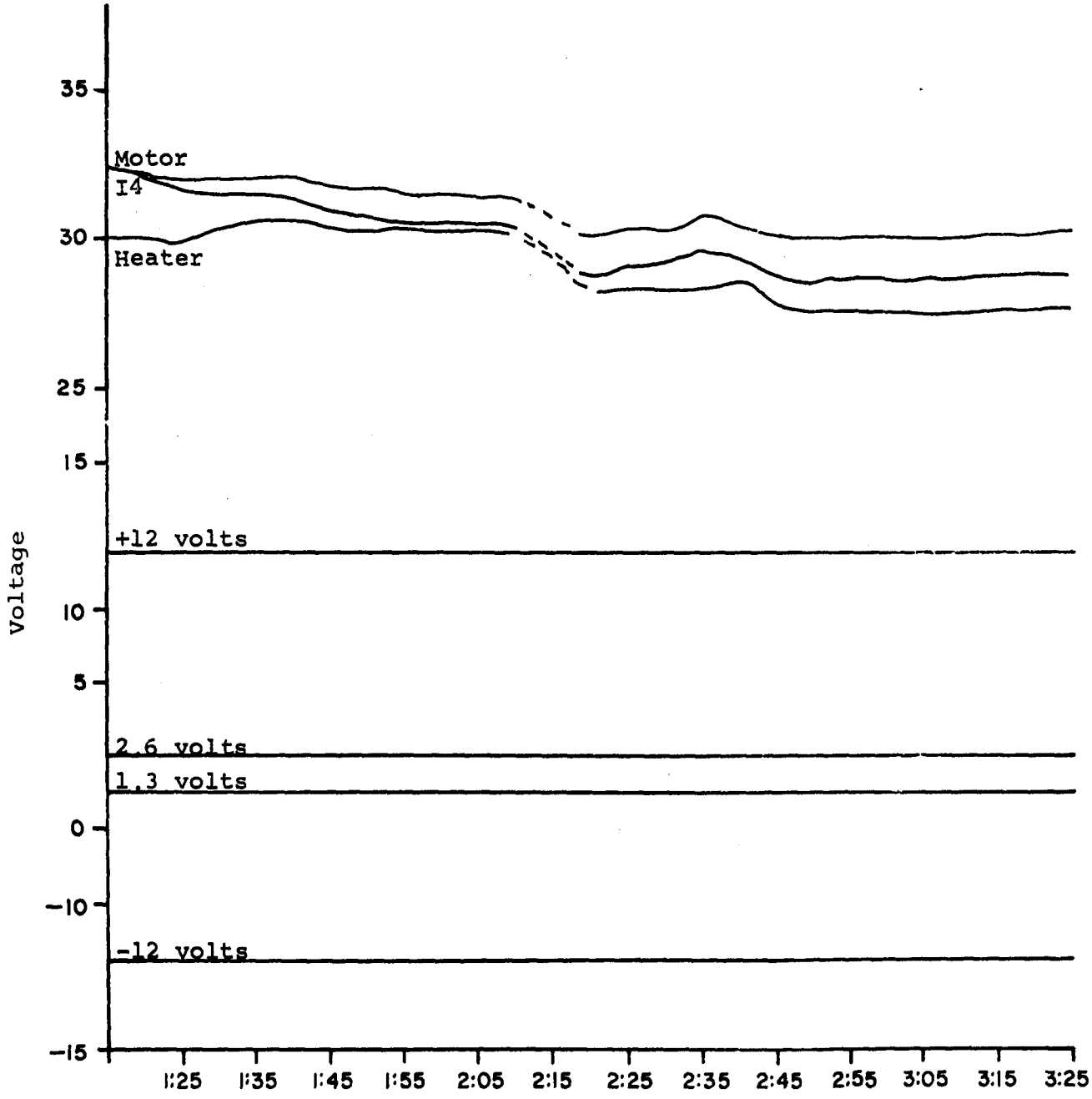

Figure J.
I4TC Voltages
2 August 1962

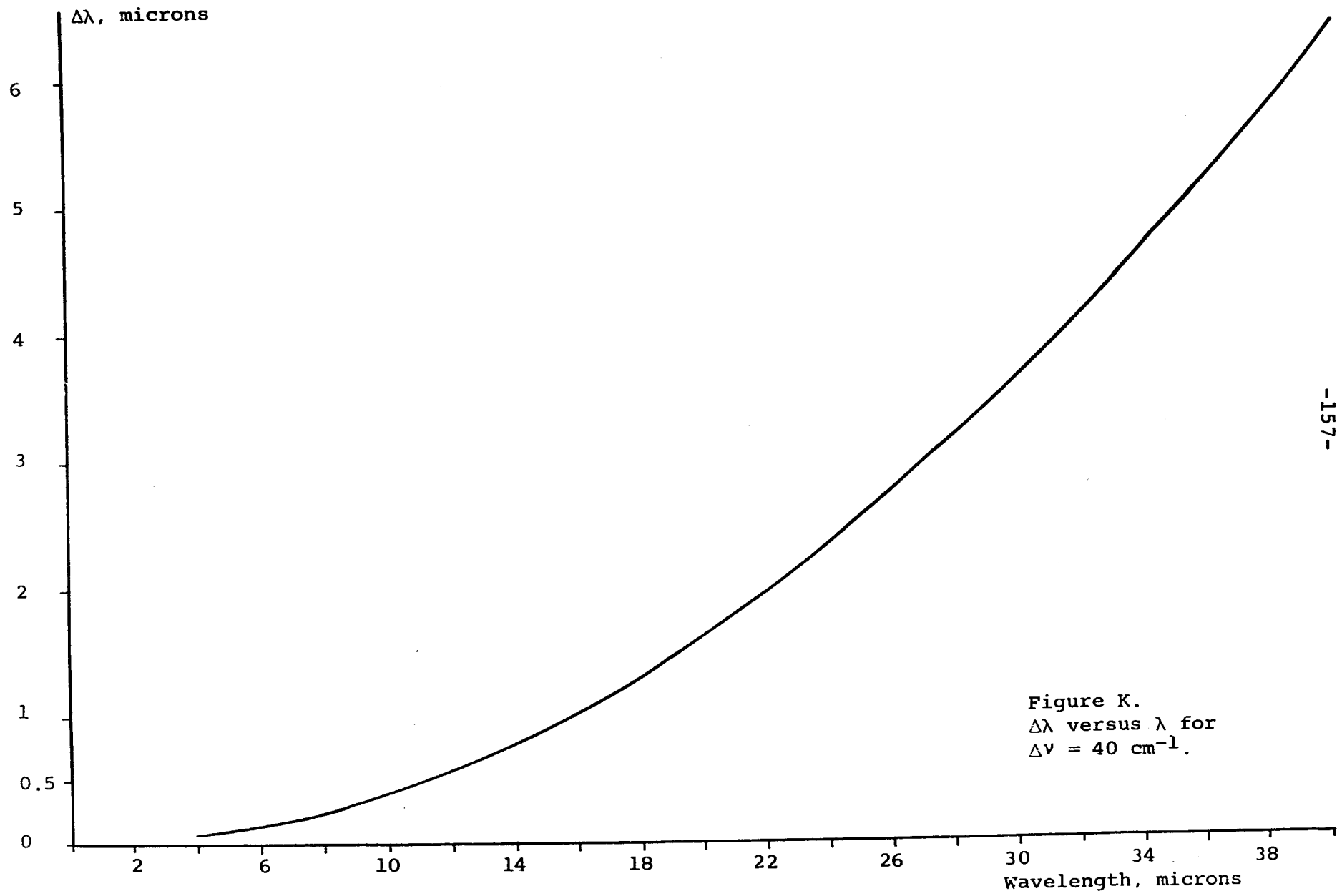

Figure K.
$\Delta\lambda$ versus λ for
$\Delta\nu = 40\ cm^{-1}$.

Appendix L

Reprinted from JOURNAL OF THE OPTICAL SOCIETY OF AMERICA, Vol. 52, No. 12, December, 1962

AN ADVERTISEMENT

A STABLE INTERFEROMETER

The Jamin interferometer shown below has been folded by means of a full mirror, and has worthy properties for multiplex spectrometry or metrology. Its adjustments can be built in and isolated from adversity. Either configuration shown is compensated and adjusted if: 1. the transparent plate has approximately parallel sides (wedge causes shear and loss of compensation) and, 2. each side is optically flat; 3. the separator is approximately parallel (wedge causes shear and loss of compensation); 4. the rocking mirror, is optically flat.

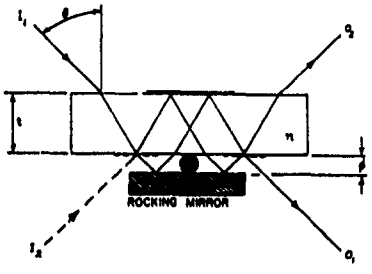

The retardation or difference in pathlength between the two beams is a function of the angle between the transparent plate and the rocking mirror. The location of the tilt axis is unimportant as long as it points normal to the plane of the beams.

By moving the tilt axis toward the centroid of the rocking mirror, mechanical coupling to noisy environments can be arbitrarily reduced. This is important when the tilt drive has a low spring constant.

We have made several interferometers of this type using a convenient construction in which the transparent plate and the rocking mirror are each sprung against a cylindrical separator. Wedge errors using commercial shaft or dowel pins as separators have not exceeded ¼ fringe per cm at $\lambda = 0.5\mu$ for refracting plate thicknesses of about 1 cm.

The retardation δ for a transparent plate of index n and thickness t is the following function of tilt angle ϕ:

$$\delta = 2\phi t \sin 2\theta/(n^2 - \sin^2\theta)^{1/2} = \phi t p,$$

where the parameter θ is the angle from the normal to the refracting plate taken by the central fringe in air. For the case of $n = 1.52$, $p = 1.50$ radian^{-1}. This value of p is its maximum, and occurs at $\theta \simeq 50°$. The values of p and θ are determined by n and t; the derivations are lengthy.[1]

An advantage over a Michelson interferometer is a great reduction of temperature sensitivity. This is because changes of temperature cannot produce significant differential displacements—either through thermal expansions or by differential stress relief of adjustments. Further, note the four accessible apertures. Source radiation is split into two complementary outputs each of which can be collected by a detector. In a Michelson, the second output travels out along the input beam and is usually lost. In this sense, the folded Jamin is a non-degenerate interferometer.

Other configurations are shown below.

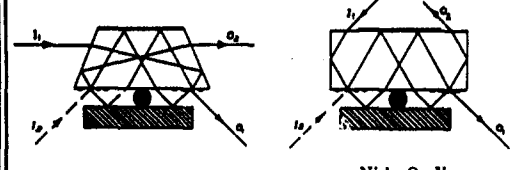

Niels O. Young

1. C. Candler, *Modern Interferometers*, 485 ff., Hilger & Watts Ltd., London, 1951.

Block Associates, Inc.

385 Putnam Ave. Cambridge 39, Mass.

AN ADVERTISEMENT

On Reducing the Dynamic Range of Interferograms

Normally, an interferogram consists of a strong burst of fringes at zero order interference plus much smaller residual fringes extending to large retardations. The large fringes contain the information about the gross characteristics of the spectrum while the residual fringes contain the information on the details in the spectrum. In order to cope with typical spectra, where the gross characteristics have much more intensity than the detail features, it is necessary to have a large dynamic range available for recording the interferograms. Such large dynamic range is frequently not available especially if telemetry must be used. For this reason, it will be desirable to distribute the energy involved in the large central burst over a much larger retardation range in the interferogram so that the fringes will be more uniformly distributed. It is possible to spread them in a manner which will be called "chirping". The low frequency fringes will become concentrated on one side of the interferogram and the high frequency fringes on the other. The shifting of dominant frequency sounds like a rising (or falling) tone, hence the term "chirp".

In essence, the object is to distribute the location of stationary phase of the fringes. Stationary phase is when all the frequencies of fringes have the same phase, thereby adding constructively. We will distribute this location of stationary phase so that its location is on the left for low frequency fringes and shifts to the right for high frequency fringes, or vice-versa. This distribution is tantamount to introducing a fringe phase shift which is a quadratic function of frequency and is similar to "chirp" radar. The introduction of phase

THIS
PAGE
IS
MISSING
IN
ORIGINAL
DOCUMENT

$$= \frac{-\lambda \frac{d^2 n_p}{d\lambda^2} + 2 \frac{\lambda}{n_p} \left(\frac{dn_p}{d\lambda}\right)^2}{\left(1 + \frac{\lambda}{n_p} \frac{dn_p}{d\lambda}\right)^2}$$

Now the group velocity index is not wildly different from n_p so that the denominator will be approximately unity. Also, it will turn out that except for regions close to inflection point on $n_p(\lambda)$ the first term in the numerator dominates so we have

$$\frac{dn_g}{d\lambda} \sim - \lambda \frac{d^2 n_p}{d\lambda^2}$$

In the Willow Run report on IR materials, the dispersion vs. wavelength is graphed in log-log coordinates. For relating to that graph, we can continue the math.

$$\text{Let } n' \equiv \frac{dn_p}{d\lambda}$$

$$\frac{d \log n'}{d \log \lambda} = \frac{\lambda}{n'} \frac{dn'}{d\lambda}$$

$$\text{or } - \frac{dn_g}{d\lambda} \quad \lambda \frac{dn'}{d\lambda} = n' \frac{d \log n'}{d \log \lambda}$$

Thus, we have that the dispersion in the group refractive index is approximately the dispersion in the phase refractive index multiplied by the slope of the graph. This applies when the slope is appreciable, such as to the left of the valleys where the slope is somewhat greater than 2 (absolute value). In that region, we expect the dispersion in group index to be slightly greater than twice the dispersion in phase index. In the valleys, the dispersion in group index will be very small. However, we have not yet achieved the desired result because the simple

insertion of the dispersive plate will drastically reduce the fringe diameters. In order to maintain large throughput, it will be necessary to use two different materials, one in each arm of the interferometer. These materials should be of relative thicknesses such that the fringes remain large diameter and should have very different dispersions in group index so that the "chirping" effect is not cancelled.

The conditions for large fringes is that the apparent path length of the two arms is the same. If we have two materials denoted by subscripts one and two of thickness t, then after insertion of the two materials it will be necessary to shift one of the end mirrors by Δt to reestablish strong fringes for the central wavelength.

$$\Delta t = (n_{g_1} - 1)\, t_1 - (n_{g_2} - 1)\, t_2$$

In addition, we must consider the apparent thickness of the materials, so that for large diameter fringes we have the condition

$$(1 - \frac{1}{n_{p_1}}) - (1 - \frac{1}{n_{p_2}})\, t_2 + \Delta t = 0$$

This reduces to

$$\frac{t_1}{t_2} = \frac{(n_{g_2} n_{p_2} - 1)\, n_{p_1}}{(n_{g_1} n_{p_1} - 1)\, n_{p_2}}$$

or for each material the thickness t will be proportional to

$$t \propto \frac{n_p}{n_g n_p - 1}$$

Since we have available materials with very low group index dispersions (in the valleys), we choose one such material along with a second material of high group index dispersion. Thus, we can neglect the dispersion in the former material and can use that material solely for fringe diameter compensation. Then the distribution range for the fringes in the interferogram is given directly by the dispersion (group index) of the second material times its thickness.

Block Associates, Inc., Cambridge, Mass.
ATMOSPHERIC INFRARED OPTICS — FLUX MEASUREMENTS,
by Merle J. Persky, May 31, 1963. 174 pp.
AFCRL 63-439 Unclassified Report
The preparation and evaluation of two infrared interferometer spectrometers, Block Associates, Inc., Models 14T and 14TC, for the balloon-borne measurement of atmospheric radiance is described. The flights of 5 April 1962 and 2 August 1962 showed agreement with the theoretical data computed from the available temperature, pressure and dewpoint profiles. Auxiliary systems were built, tested and flown in these flights. Comparison spectral runs and evaluations were conducted with independent laboratories. A procedure for calibration was developed and an evaluation of the precision and accuracy of the instrument was undertaken. Several possible improvements for future measurement programs were evaluated and proposed recommendations are included.

UNCLASSIFIED
1. Infrared
2. Atmospheric Radiance
I. Persky, Merle J.

UNCLASSIFIED

Block Associates, Inc., Cambridge, Mass.
ATMOSPHERIC INFRARED OPTICS — FLUX MEASUREMENTS,
by Merle J. Persky, May 31, 1963. 174 pp.
AFCRL 63-439 Unclassified Report
The preparation and evaluation of two infrared interferometer spectrometers, Block Associates, Inc., Models 14T and 14TC, for the balloon-borne measurement of atmospheric radiance is described. The flights of 5 April 1962 and 2 August 1962 showed agreement with the theoretical data computed from the available temperature, pressure, and dewpoint profiles. Auxiliary systems were built, tested and flown in these flights. Comparison spectral runs and evaluations were conducted with independent laboratories. A procedure for calibration was developed and an evaluation of the precision and accuracy of the instrument was undertaken. Several possible improvements for future measurement programs were evaluated and proposed recommendations are included.

UNCLASSIFIED
1. Infrared
2. Atmospheric Radiance
I. Persky, Merle J.

UNCLASSIFIED

Block Associates, Inc., Cambridge, Mass.
ATMOSPHERIC INFRARED OPTICS — FLUX MEASUREMENTS,
by Merle J. Persky, May 31, 1963. 174 pp.
AFCRL 63-439 Unclassified Report
The preparation and evaluation of two infrared interferometer spectrometers, Block Associates, Inc., Models 14T and 14TC, for the balloon-borne measurement of atmospheric radiance is described. The flights of 5 April 1962 and 2 August 1962 showed agreement with the theoretical data computed from the available temperature, pressure, and dewpoint profiles. Auxiliary systems were built, tested and flown in these flights. Comparison spectral runs and evaluations were conducted with independent laboratories. A procedure for calibration was developed and an evaluation of the precision and accuracy of the instrument was undertaken. Several possible improvements for future measurement programs were evaluated and proposed recommendations are included.

UNCLASSIFIED
1. Infrared
2. Atmospheric Radiance
I. Persky, Merle J.

UNCLASSIFIED